Development of a Stream Welding Process

-by-

Christopher Ratliff

B. S. in Mechanical Engineering
University of Arizona
(1992)

Submitted to the
Department of Mechanical Engineering
in Partial Fulfillment of the Requirements
for the Degree of

MASTER OF SCIENCE IN MECHANICAL ENGINEERING

at the
MASSACHUSETTS INSTITUTE OF TECHNOLOGY
(July 1994)

Signature of Author _____
Department of Mechanical Engineering

Certified By _____
David E. Hardt, Professor of Mechanical Engineering

Accepted By _____
Ain A. Sonin, Department of Mechanical Engineering
Chairman, Departmental Committee on Graduate Students

Development of a Stream Welding Process:

-by-
Christopher Ratliff

Submitted to the Department of Mechanical Engineering
July 1994 in partial fulfillment of the requirements for the
Degree of Master of Science in Mechanical Engineering.

Abstract

Improving welding processes through better process control has been the focus of much recent welding research. Past research has shown that consumable electrode welding processes, such as gas metal arc welding, have limited independent controllability over heat and mass transfer into a weld seam. This limitation is the reason for developing a new process called stream welding. With stream welding, the mass flux and heat content of the mass flux are independently controllable, which will lead to better control over the thermal properties and geometry of a weld seam.

The focus of this thesis is developing some of the necessary closed loop control systems for a stream welder as well as analyzing and improving its capabilities. A digital PID temperature controller was designed and implemented to control the temperature of the molten metal stream. In designing this controller the temperature dynamics of the stream welder were modeled and used to tune the controller through simulation.

A closed loop wire feed system was also developed to replenish the molten metal supply as it is ejected out of the furnace. The control scheme for this wire feeder is essentially an on/off type with the feed magnitude being related to the molten metal temperature to maximize replenishing rates in different regimes of operation.

Experimentation has shown that a number of problems with this process need to be solved before it can be a viable welding process. One such problem is the erosion of the exit orifice where the stream emanates. This causes inconsistent stream size which is intolerable since one of the objectives of this welder is to have a high degree of control over mass flow into a weld seam. It was also observed that the weld beads made thus far produced very little penetration. Because of this, a finite difference model is presented that predicts the penetration achievable with the stream welding process under different conditions. The model indicates that to achieve the penetration of conventional welding processes, the stream welding process cannot rely solely on the heat content of the molten metal stream.

Thesis Advisor: David E. Hardt
Professor of Mechanical Engineering

Acknowledgments

I would like to thank Professor Dave Hardt for his guidance in conducting this research. Also, I would like to thank Benny Budiman and the rest of the students and staff at MIT who gave valuable input and helped me complete this work.
Lastly, I would like to thank Monica and my family.

This project was supported by the U.S. Department of Energy under contract number DE-FG02-85ER13331.

Table of Contents

Chapter 1: Introduction

A. Motivation

Gas Metal Arc Welding (GMAW) is one of the most widely used welding processes in industry today and is still gaining in popularity. Hundreds of millions of dollars are spent each year on GMAW processes [U.S. Department of Commerce, 1993] to help fabricate products such as ships, automobiles, aircraft, and buildings. Since it is such an essential manufacturing process to so many different industries, there has been substantial effort to automate the process to improve quality and reduce costs. The ultimate goal of GMAW, or any other welding process, is to be able to make welds that are indistinguishable from the workpiece(s) being welded; the weld should have the same metallurgical properties as the workpiece and have an appropriate geometry.

To achieve this ideal weld quality under varying conditions, it is necessary to have a high degree of controllability over both the metallurgical properties and geometry of a weld seam. Controlling metallurgical properties is primarily a problem of controlling spatial and temporal temperature distributions in and around the weld, especially distributions characterizing cooling rate and heat affected zone (HAZ). Controlling weld bead geometry is also a matter of controlling spatial temperature distributions when it comes to depth of penetration. Filler metal deposition also plays a major role in determining weld bead width and height. Refer to Figure 1 to see these output parameters of interest.

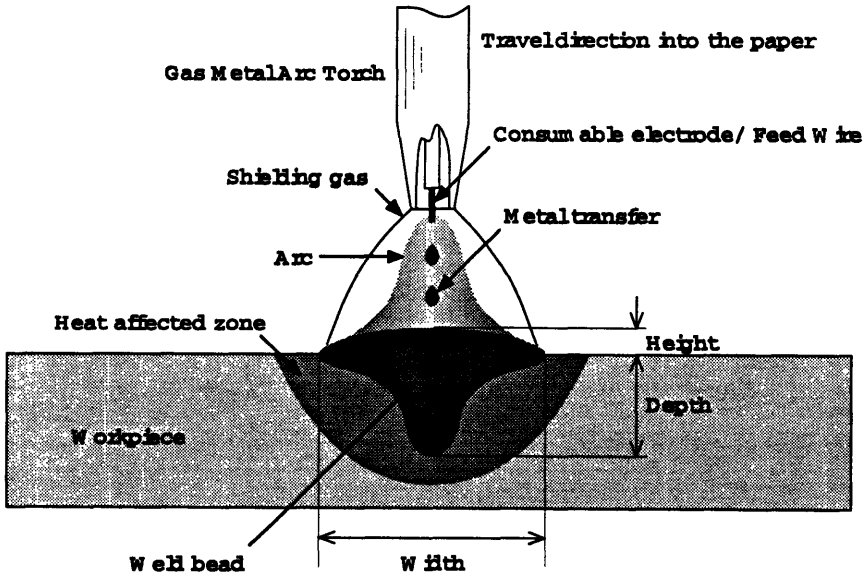

Figure 1: Output Parameters for Consumable Electrode Arc Welding

Controlling these parameters is largely a problem of controlling the heat and mass flux into a weld seam. However for consumable electrode welding like GMAW, it has been found that heat flux and filler metal flux into a weld seam are coupled such that there is very limited independent control over bead geometry and heat input to a weld. The mass deposition rate is typically given by the following equation:

$$WFR=aI+bLI^2$$

where

WFR = the wire feed rate (mm^3/sec)

a = a constant of proportionality for anode or cathode heating. Its magnitude is dependent on polarity, feed wire composition and other factors [mm/(sec A)].

b = proportionality constant reflecting arc resistance[$1/sec\ A^2$]

L = electrode extension or stickout [mm]

I = welding current [A]

The heat input is given by

$$P_{input}=\eta IV$$

where

P_{input} = Power transferred to weld

η = arc efficiency, percentage of heat input transferred into weld.

I = welding current [A]

V = arc voltage [V]

There is limited range for manipulating a, b, and L in a real time fashion. The value of V must also be kept within narrow limits to ensure good weld quality. This means that I is the main variable with a broad range of manipulation, and this variable has a strong effect on both mass input and heat input. To have an increased mass flux means an increase in heat input. It is impossible to GMA weld certain workpiece geometries like thin sheets of steel because, in order to get the appropriate filler metal rate, the heat input rate is high enough to melt the workpiece[O'Brien, 1991].

Since different workpiece geometries and material properties require different amounts of heat and mass input, one would want complete and independent control over both heat and mass transfer into a weld seam. The range of independent control over heat

and mass input for GMAW into a weld was determined experimentally by Hale [Hale, 1989], and the extent of this range is given in Figure 2.

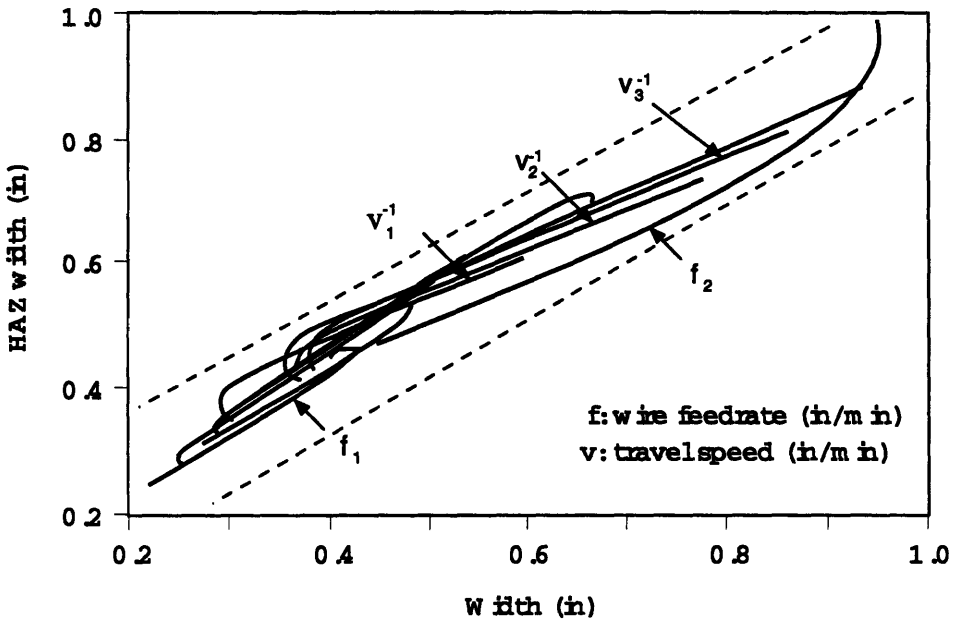

Figure 2: Controllability Over Both Heat Affected Zone and Bead Width

Here the heat affected zone is proportional to the heat input while the width is proportional to the mass input. The dashed lines represents the estimated limits of control. Ideally, one would want the largest control range possible which would mean having the dashed lines as far apart as possible.

Another important problem with GMAW is the difficulty of manipulating the mode of mass transfer into the weld. There are a number of different mass transfer modes which are dictated by operating conditions such as weld current. The more common modes of mass transfer are shown in Figure 3. These different flow characteristics have substantial impact on the weld bead geometry and, in some cases, the amount of molten metal spatter.

These modes of mass transfer are governed by a number of forces which include: 1) pressure generated by the evolution of gas at the electrode tip: 2) electrostatic attraction between electrodes: 3) electromagnetic forces on the tip of the electrode due to geometry of the current flow through the workpiece: 4) gravity: 5) viscous and momentum forces from the shielding argon flow and: 6) surface tension.

Having so many significant forces that are difficult or impossible to control means that it is difficult to control characteristics of mass transfer. Globular transfer modes are

typically observed at low current levels, and in this situation, gravity and surface tension are the most significant forces. Projected and streaming modes are typically observed at welding currents above 270 A, and the dominating forces are electromagnetic [Norrish, 1992]. At very high welding currents, the rotating mass transfer mode is observed.

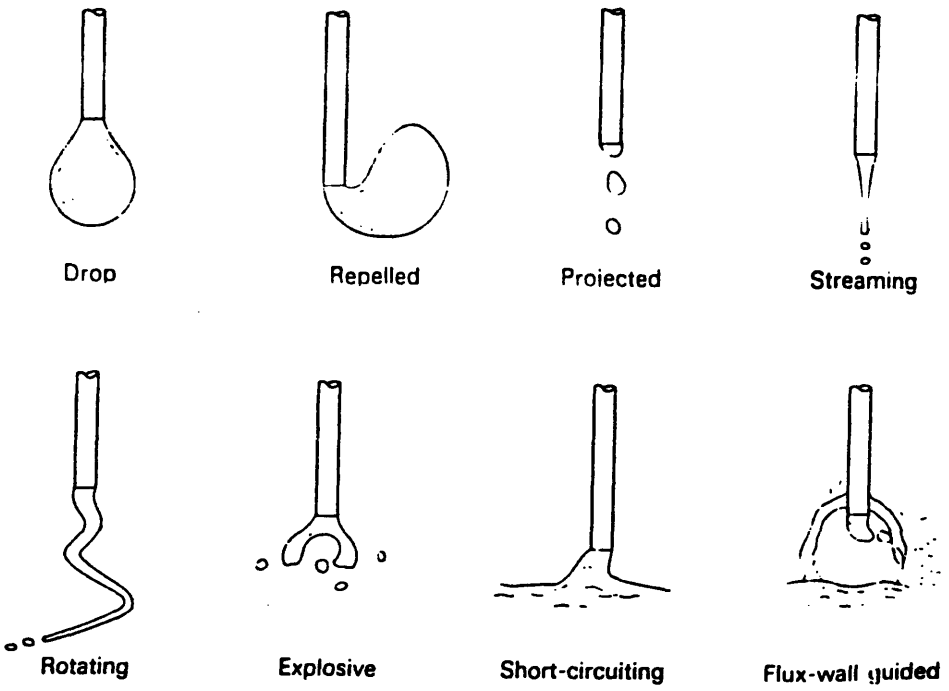

Figure 3: Metal Transfer Modes for Consumable Arc Welding Processes

Another drawback to GMAW is that the transition from globular transfer to spray transfer is very abrupt as shown in Figure 4. If it is necessary to weld a seam at or near this transition current, a very erratic weld bead could result. Some research is currently being carried out to expand the range of the spray transfer mode [Jones et al, 1993] since it is generally a more desirable mode of mass transfer. By vibrating the feed wire the transition current can be reduced by as much as 20%, but a transition current still exists, and globular transfer occurs below this transition current.

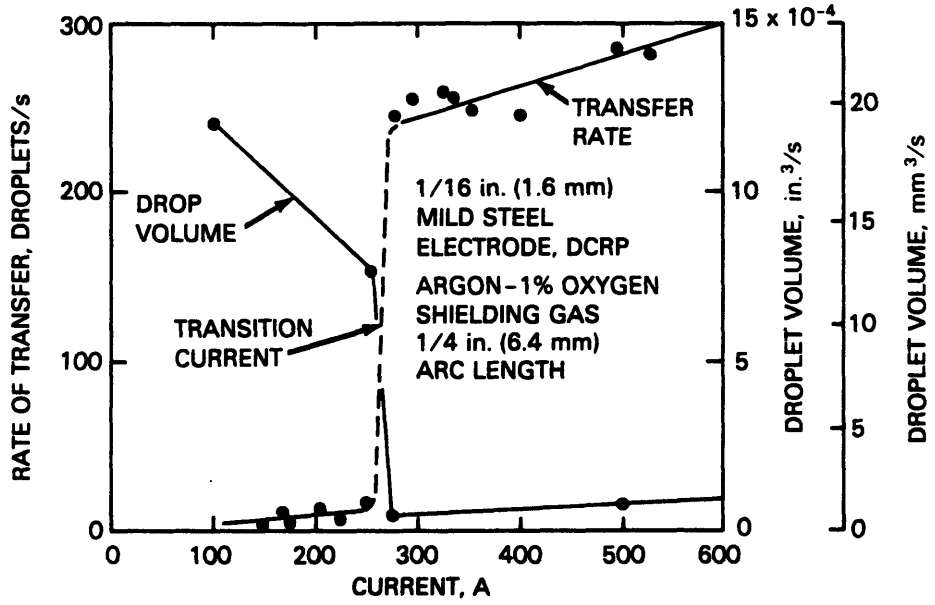

Figure 4: Variation in Volume and Transfer Rate of Drops With Welding Current for GMAW
[O'Brien, 1991]

A larger scale negative effect sometimes experienced in all kinds of arc welding processes, including GMAW, is a phenomenon known as 'arc blow' which is when the arc and filler metal being deposited are deflected by magnetic forces induced by the current within the workpiece. In Figure 5 one can see that magnetic forces can be induced that vary with position of the torch. In the diagram below, there would be no deflection of the arc when the torch is directly above the workpiece lead and an increasing deflection as the torch is moved away from the workpiece lead.

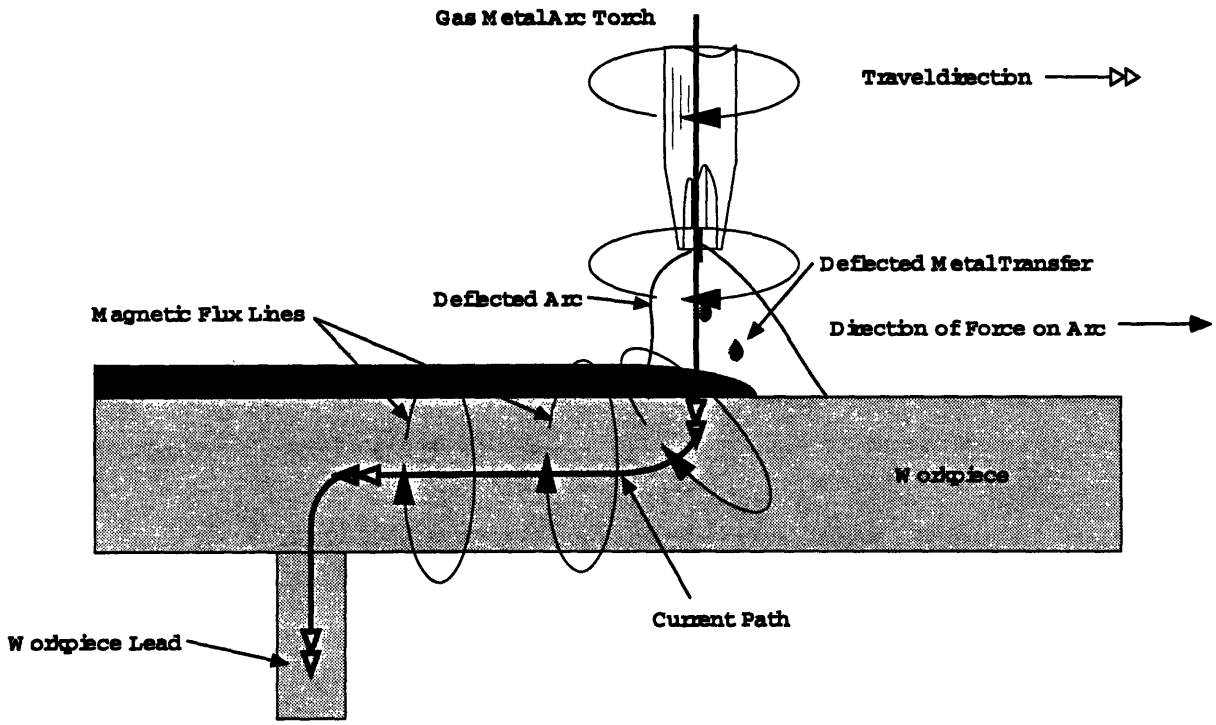

Figure 5: Deflection of Arc and Filler Metal From Induced Magnetic Forces

The limitations of GMAW typically apply to other forms of consumable electrode welding also. Although the mass transfer is stable and predictable in some operating conditions, it is erratic and hard to control in others. The lack of controllability over characteristics of the mass transfer and the limited independent controllability over both heat and mass flux into a weld seam is what motivated the development of the stream welding device described here.

B. Description of Stream Welder

A diagram depicting the process of stream welding in comparison to GMAW is given in Figure 6. This stream welder is essentially a small scale arc furnace with an exit orifice at the bottom of a crucible containing molten metal. During welding conditions, a molten metal stream emanates from this exit orifice due to the pressure in the molten metal chamber. By modulating the pressure within the molten metal chamber, one can control the velocity of the molten metal stream and hence, the mass deposition rate. To stop the molten metal flow, the pressure in the molten metal chamber is reduced below some critical value where surface tension forces stop the flow.

Modulating the arc power in the molten metal chamber allows control of the temperature of the molten metal stream. Since the pressure in the molten metal chamber and the arc power are independent, it is possible to control the temperature of the molten metal stream and the flow velocity independently.

With Stream Welding, not only are the temperature and rate of mass transfer independent, but the forces acting on the molten metal stream are few in comparison to consumable electrode processes such as GMAW. Surface tension, gravity, and fluid forces of the shielding flow (momentum and viscosity) are still present, but electromagnetic, electrostatic, and pressure forces generated by the evolution of gas at the electrode tip, have all been eliminated. The main factors affecting flow are the pressure driving the molten metal stream and the exit orifice geometry. This should lead to accurate control of both the rate of deposition as well as the location of deposition.

It is yet to be fully determined if modulating the temperature of molten metal stream will provide the necessary range of heat input to the weld. In chapter 4, this issue will be analyzed with both a mathematical model and through experimentation.

a. Control Systems

For precision operation of the stream welder it is necessary to develop a molten metal temperature controller, a molten metal replenishing system, and a stream flow rate controller. The former two have been designed and implemented as shown in Figure 7 and will be presented in detail in chapters 2 and 3.

The closed loop temperature control system uses a high temperature pyrometer for temperature sensing. The analog output from the pyrometry unit is digitized and incorporated into a PID control algorithm. The resulting digital control action from the control algorithm is turned into an analog signal with a 12-bit D/A converter. This

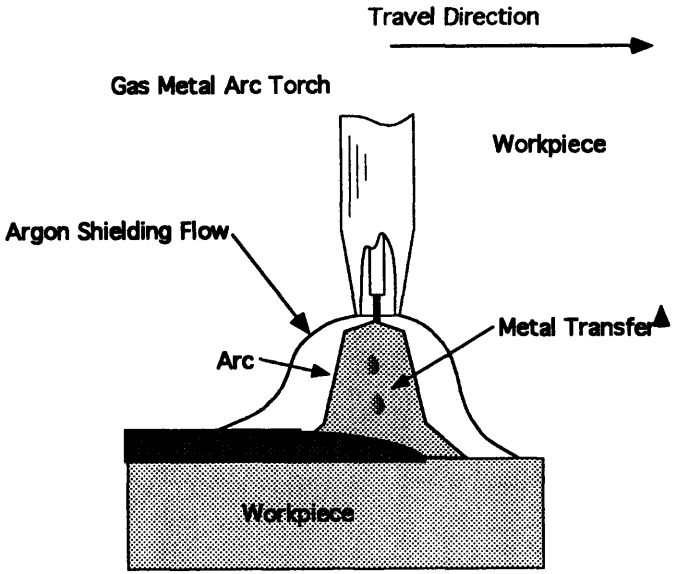

Figure 6a: Gas Metal Arc Welding

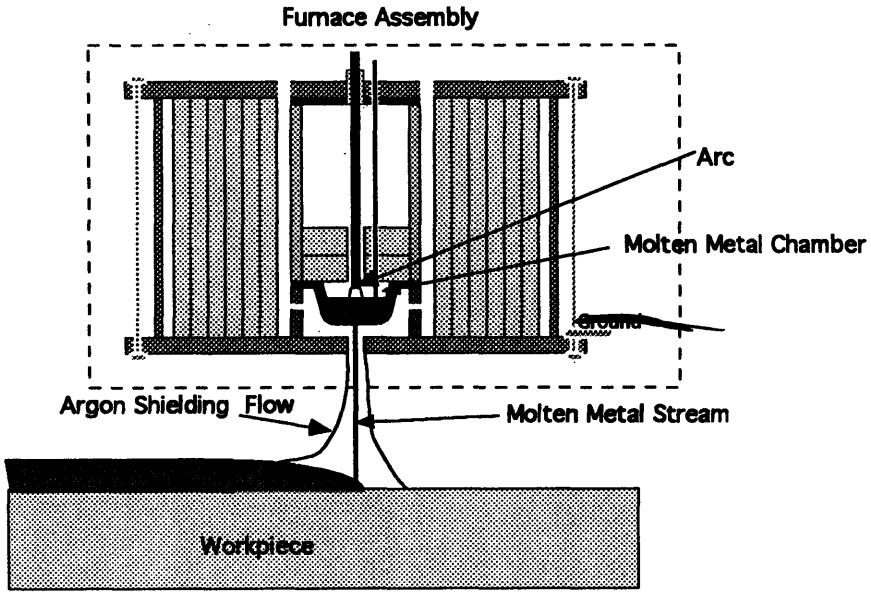

Figure 6b: Stream Welding

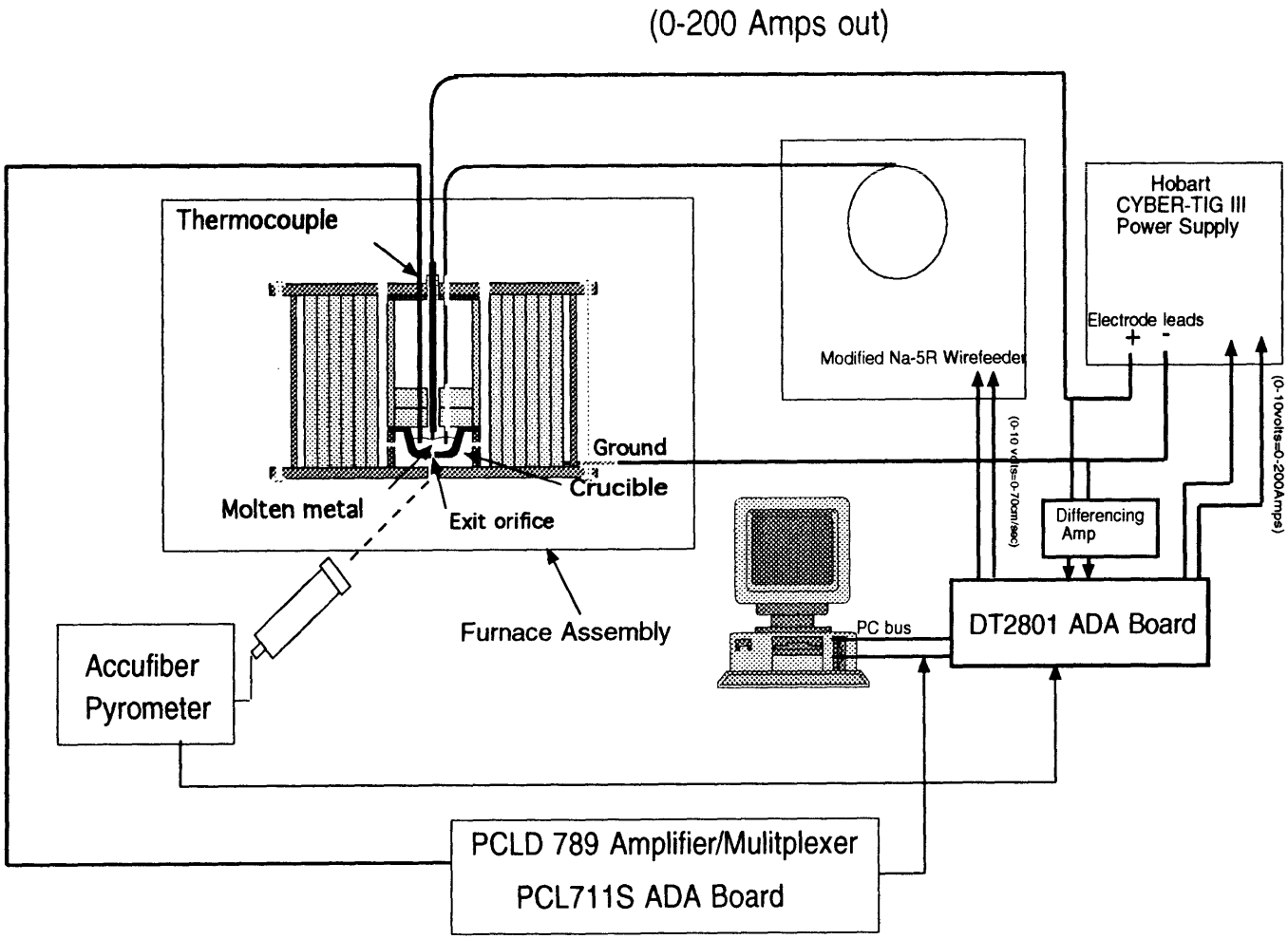

Figure 7: Components of Stream Welding System

analog signal dictates the current and hence the power into the furnace from the high bandwidth Hobart CyberTIG III power supply.

The closed loop wire feed system is necessary to replenish the molten metal supply as it is ejected out of the furnace onto the weld seam. One of the most difficult aspects of this system is a means of sensing the molten metal level in the crucible. Presently the level is sensed by measuring the arc voltage which is proportional to the arc length. So if the molten metal level is low, the arc voltage is high. However, the voltage is also a function of the arc current that is being modulated by the temperature controller. Hence the voltage fluctuates with arc current. Another means of sensing molten metal level that was tried was measuring arc resistance, which is known since the arc voltage and current are known. It turned out that the arc resistivity is an even stronger function of arc current than the arc voltage which is why arc voltage is still the means of measuring molten metal level height: it has proven to do a satisfactory job for this stage in prototype development.

The arc voltage is preprocessed with a differencing amplifier and digitized. The digitized arc voltage is then incorporated into an on/off control scheme. If the voltage is higher than the reference voltage, wire is fed into the molten metal chamber where it melts from the heat of the surrounding metal. One of the main problems hindering the performance of this closed loop replenishing system is that the replenishing rate is relatively low. The wire cannot be fed any faster than the melting rate of the wire or it will eventually puncture a hole in the bottom of the crucible. The fact that the wire will melt faster at higher temperatures is accounted for in the on/off controller, at higher temperatures the wire is fed faster than at lower temperatures to improve performance where possible. The relationship between wirefeed rate and temperature is discussed in more detail in the molten metal level control chapter.

Before the flow control system can be developed, it is necessary to find an exit orifice material that can withstand the mechanical and thermal wear of a high temperature molten steel flow. This problem is addressed in chapter 5 where two new furnace designs are presented.

b. Furnace Assembly

Most of the furnace assembly design was done by Steve Lee and a working description of the first prototype is given in his thesis [Lee, 1993]. However, there have been a number of changes in this design to improve the performance of the furnace and to

cater to the molten metal temperature and replenishing control systems. AutoCAD drawings of the present state of the furnace assembly are given in Appendix A2.

As mentioned earlier, a high temperature pyrometer is used to sense temperature rather than a high temperature thermocouple (C type). There were problems with the noise as well as melting of the thermocouple at sensed temperatures above 1700 C. The pyrometer is capable of reading temperatures up to 2000 C and can be upgraded to read up to 2700 C. To focus the pyrometer on a spot near the exit orifice, the opening in the base plate had to be enlarged. It was decide to have a "keyhole" geometry rather than a large circular hole to minimize heat transfer from the crucible to the surroundings. This keyhole shape allowed the pyrometer to focus on the crucible from an angle where it was less likely to be damaged from stray molten metal.

Additional insulation was added inside the furnace to help improve the maximum achievable temperature. Alumina felt insulation was added around the lower half of the molten metal chamber as shown in the cross section schematic. The felt is porous enough to allow the argon shielding gas to flow and perhaps even distribute the flow more evenly around the molten metal chamber causing a more uniform shielding flow around the molten metal stream. Additional insulation was also added below the crucible to reduce the effect of heat loss through the large keyhole opening in the base plate.

The wirefeed guide tube was angled to achieve higher wire melting rates which means better molten metal replenishing capabilities. The angled wirefeed improved wire melting rates by more than 20%. This modification will be elaborated on in the molten metal replenishing system in chapter 3.

One significant operating characteristic that was changed was the operating arc voltage. This voltage was increased from 14-16V to 17-21V. The increased arc voltage increased the power input to the furnace which helped improve thermal performance. With the additional insulation mentioned above and the additional power input, the furnace was able to achieve temperatures well over 2000 C. The magnitude above 2000 C is unknown since the pyrometer cannot presently sense temperatures above this temperature.

The argon pressurization and shielding flow system was redesigned to improve control over the shielding flow. Initially, the Argon used to pressurize the molten metal chamber was also used as the shielding gas with the flow pattern shown in Figure 8a. The reasoning behind this design was two-fold: the first reason was to ensure that the shielding flow was thoroughly preheated so it would not cool the molten metal stream. The second reason was to reduce heat loss from the furnace by reducing the net argon flow through the furnace. The present design is given in Figure 8b. With this design

there is negligibly more heat transfer away from the furnace and stream, but the shielding flow is now independent of the pressure within the molten metal chamber.

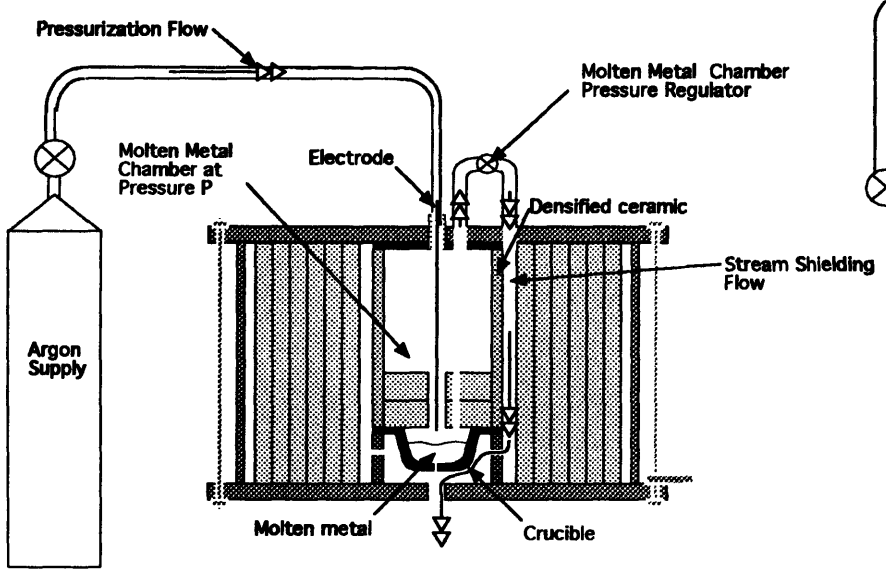

Figure 8a: Previous Pressurization and Shielding Flow Configuration

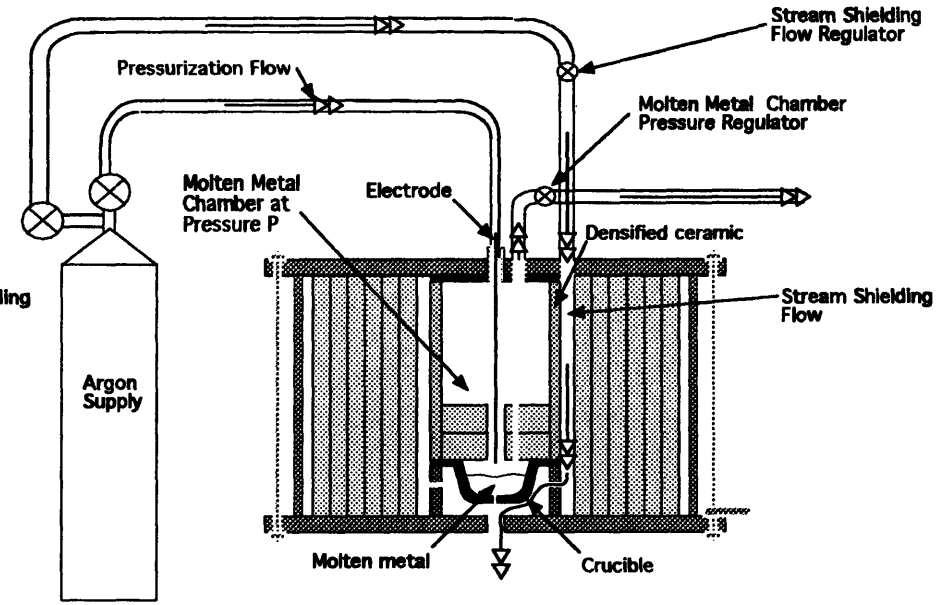

Figure 8b: Present Pressurization and Shielding Flow Configuration

Chapter 2: Closed Loop Temperature Control System

A. Overview

Controlling the temperature of the molten metal being ejected from the stream welder is one of the primary objectives in developing this device. By controlling the temperature of the ejected molten metal, we control the heat flux into the weld seam; this, in turn, determines certain properties of the weld seam (i.e. penetration depth, heat affected zone, etc.). A schematic of components of the temperature control system is shown in Figure 9.

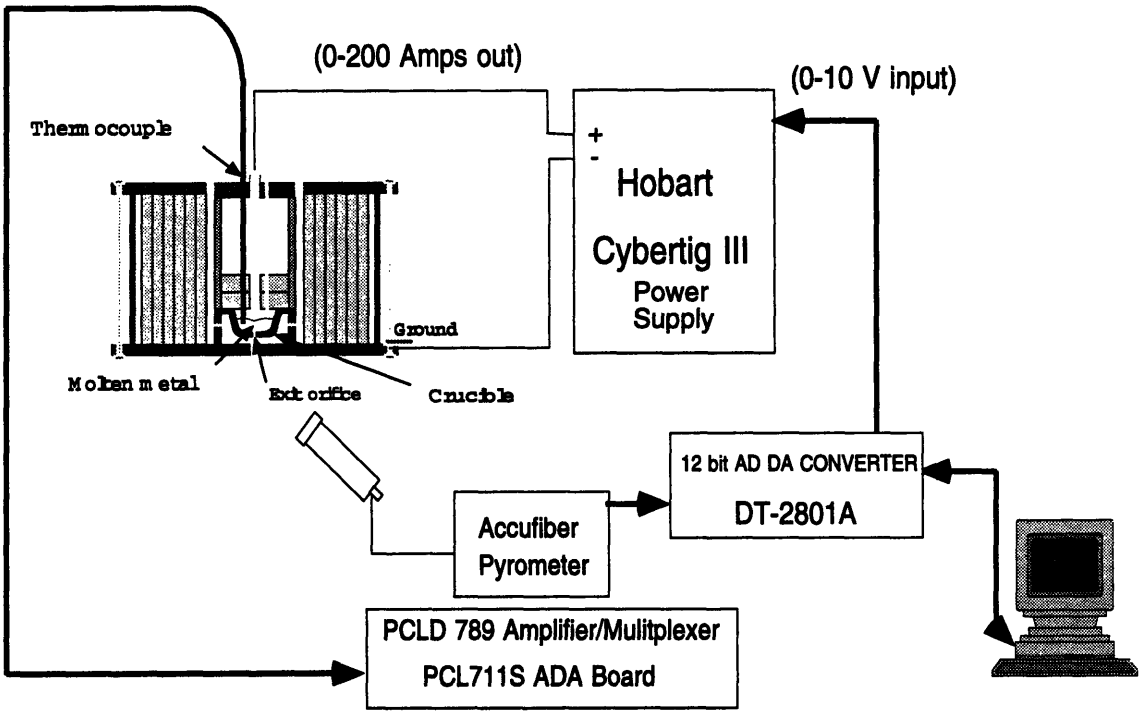

Figure 9: Schematic of Temperature Control System Components

Nomenclature:

T	- Temperature [C]
t	- Time [seconds]
V_{pyro}	- Pyrometer output voltage[V]
I_{out}	- Current output of Hobart Power Supply[A}
V_{arc}	- Arc voltage[V]
P_{in}	- Power input from Hobart power supply [W]
η	- Arc efficiency
V_{input}	- Voltage input to Hobart Power Supply[V]
K_1	- Generalized thermal mass coefficient[J/C]
K_2	- Generalized convective heat transfer coefficient[W/C]
K_a	- Steady state relationship between P_{in} and T[C/W]
τ_a	- Time constant for the first order approximation of plant[seconds]

To implement a digital control system with a PC, the analog temperature information from the thermocouple or pyrometer must be digitized. The signal from the pyrometer is 0-10 volts and is related to the sensed temperature by the following function:

$$T = 500C + \frac{V_{pyro}}{10[V]} \cdot 1500C$$

The 0-10 volt signal is digitized by a 12-bit DT-2801 A/D D/A board and read by the program pyropid.c. To filter out some of the noise in the pyrometer signal, this program acquires 10 voltages and averages them over a time interval of about 0.03 seconds. When accounting for the execution time of the rest of the code, which also controls the wire feed rate, the resulting sample period is 0.1 seconds. The filtered temperature is then used to compute the closed loop control action with a PID control algorithm. The digital control action is then converted to an analog signal (0-10volts) with a D/A channel on the DT2801. This analog signal (0-10 volts) is sent to the Hobart CyberTIG III power supply where it dictates the current and hence the power into the furnace. The current out of the Hobart is related to the input signal by

$$I_{out} = 200A \cdot \frac{V_{input}}{10volts}$$

And the resulting power input is:

$$P_{in} = \eta \cdot I_{out} \cdot V_{arc}$$

Here η is defined as the arc efficiency. The time constant of the Hobart power supply is roughly 0.001 seconds, negligibly small relative to the plant thermal time constant which is why its input/output relationships are treated as static as given in the above equation.

B. Temperature Sensing: Thermocouple Versus Pyrometer

Temperature information can be acquired using either a high temperature thermocouple immersed in the molten metal chamber, or a high temperature pyrometer focused near the crucible exit orifice. There are advantages and disadvantages to both methods. The obvious benefit of using thermocouples is the relatively low initial cost, the tungsten rhenium thermocouples cost approximately $100 each (including lead extensions etc.) and the amplifier mulitplexer board (Omega PCLD 789) for processing the thermocouple signals is about $250. The Accufiber 100C pyrometer unit, on the other hand, costs roughly $6000. Neither of these prices include the A/D boards.

Since both were readily available in the LMP, both were initially incorporated in the temperature control design to see which would work best. The tungsten rhenium thermocouples worked well until the furnace was improved to a point where it could achieve temperatures in excess of 1700 C, the thermocouples started to melt at these high temperatures. These C type thermocouples are rated for a temperatures in excess of 2400 C, but this is only in an ideal inert atmosphere. Although argon is used as the pressurizing gas, other materials such as carbon, molten steel and trace amounts of oxygen may be reacting with the tungsten rhenium alloy. Putting the thermocouple in a zirconia test tube to keep it isolated from some of these substances did not help, the thermocouple still melted within the test tube. It is yet to be determined if the thermocouples are faulty or if a significant amount of oxygen is in the test tube. In any case, this meant that the thermocouples could not be used for closed loop control above 1700 C.

The main advantage of the pyrometer is that it is non-intrusive and hence is not directly exposed to the high temperatures within the furnace. It relies only on the infra-red radiation collected from the object on which it is focused to measure temperature. The focal length of the Accufiber 100C is 30cm and the desired focal point is the base of the crucible, next to the exit orifice. The temperature at this location is less than the

temperature within the molten metal chamber, the difference between the molten metal chamber temperature and the sensed temperature can be approximated using the following closed loop temperature response.

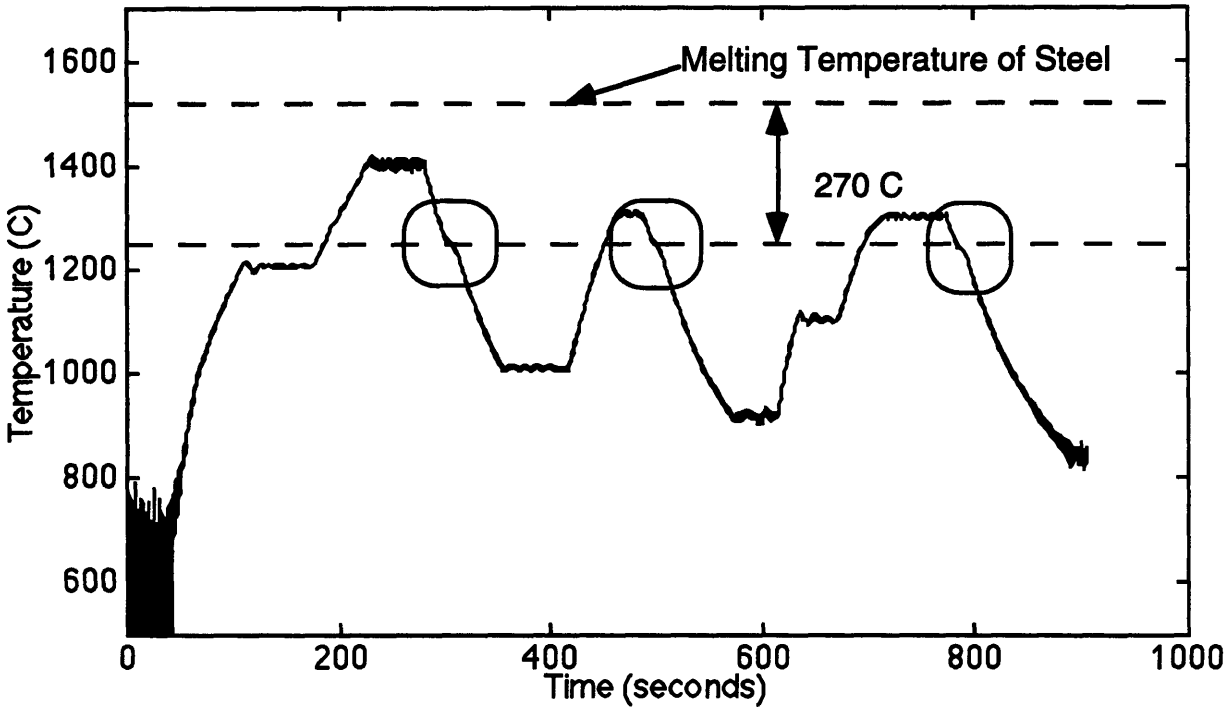

Figure 10: Determination of Difference between Pyrometer Sensed Temperature and Actual Temperature within Molten Metal Chamber
(from step4894.dat)

The three circled parts of the plot most likely represent the solidification of the molten metal. Since the solidification temperature of the steel is about 1530 C it appears that the difference is about 270 C. At higher temperatures this difference between the molten metal temperature and the sensed temperature is likely to increase since temperature gradients would expectedly increase with temperature.

The reason the pyrometer is not focused directly at the exit orifice is because of the difference in emissivities of the molten steel and graphite. To sense the temperature accurately, the emissivity of the material must be known and programmed into the pyrometer unit for it to compute for temperature. The emissivity of molten steel is 0.45 and for graphite it is 0.8. If the pyrometer were focused directly on the exit orifice, the

temperature measurement would change depending on whether or not molten steel was flowing.

Presently, the Accufiber Pyrometer can accurately read temperatures between 750 C and 2000 C, the upper limit on this range can be increased to 2700 C with a $1000 upgrade. Between 500 C and 750 C, the signal is extremely noisy, but this temperature range is of little interest.

Because of its higher temperature capabilities and upgradability, the Accufiber Pyrometer, rather than tungsten rhenium thermocouples, is used for the closed loop temperature control system. The thermocouples are sometimes used for lower temperature (less than 1700 C) data acquisition.

C. Temperature Dynamics of the Furnace

a. Defining the Plant

Ultimately it is desired to control the temperature of the molten metal stream by modulating the power input from the arc. In this section the focus is to determine a suitable input output relationship that accurately describes the thermal dynamics of the stream temperature in relation to the power input.

The stream temperature will be directly related to the crucible and molten metal temperatures. Figure 10 in the previous section indicates the temperature in the molten metal chamber might be significantly higher than the sensed temperature of the exterior of the crucible, and the temperature of the stream will likely be between these two temperatures. Before entering the exit orifice, the molten metal will be the same temperature as the surrounding molten metal, but while passing through the exit orifice, there will be some cooling of the molten metal. The resulting temperature of the emanating metal will be a function of relevant states such as flow rate, as well as temperature of the molten metal chamber and the temperature of the crucible. It should be noted here that there will be some heat transfer away from the molten stream after exiting the exit orifice and before it hits the workpiece due to both radiation and convective heat transfer. These effects will be minimized by minimizing the distance the stream has to travel and hence, will presently be neglected.

Ideally, an estimator could be formulated to predict the emanating stream temperature given the relevant furnace states. However, formulating this estimator would lead to complicated analysis and experimentation, so as a first attempt, a more simplistic approach will be taken. The approach will be to control the sensed temperature, that of

the base of the crucible, rather than the stream. From initial observations of open loop temperature responses to steps in input power, it appears that the system behaves much like a first order system, which indicates that it is possible to use the following equation to describe the plant dynamics:

$$K_1 \frac{\partial T}{\partial t} = -K_2 T + P_{in} \quad (1)$$

Here K_1 is a generalized thermal mass coefficient and K_2 is a generalized convective heat transfer coefficient. Both of these coefficients will be functions of temperature but for now are treated as constants. Taking the Laplace transform of eq. 1 gives the continuous transfer function describing the simplified furnace dynamics:

$$H(s) = \frac{T(s)}{P_{in}(s)} = \frac{K_a}{\tau_a s + 1} \quad (2)$$

Both K_a and τ_a can be determined experimentally from open loop responses to various step inputs of power. One such response is shown in Figure 11. The dashed line, which is a first order exponential with a time constant of 70 seconds, fits the response reasonably well. However, such large step responses are not of as much concern as small steps at elevated temperatures, since this will more closely resemble an actual stream welding situation. These types of open loop responses are looked at later in this chapter.

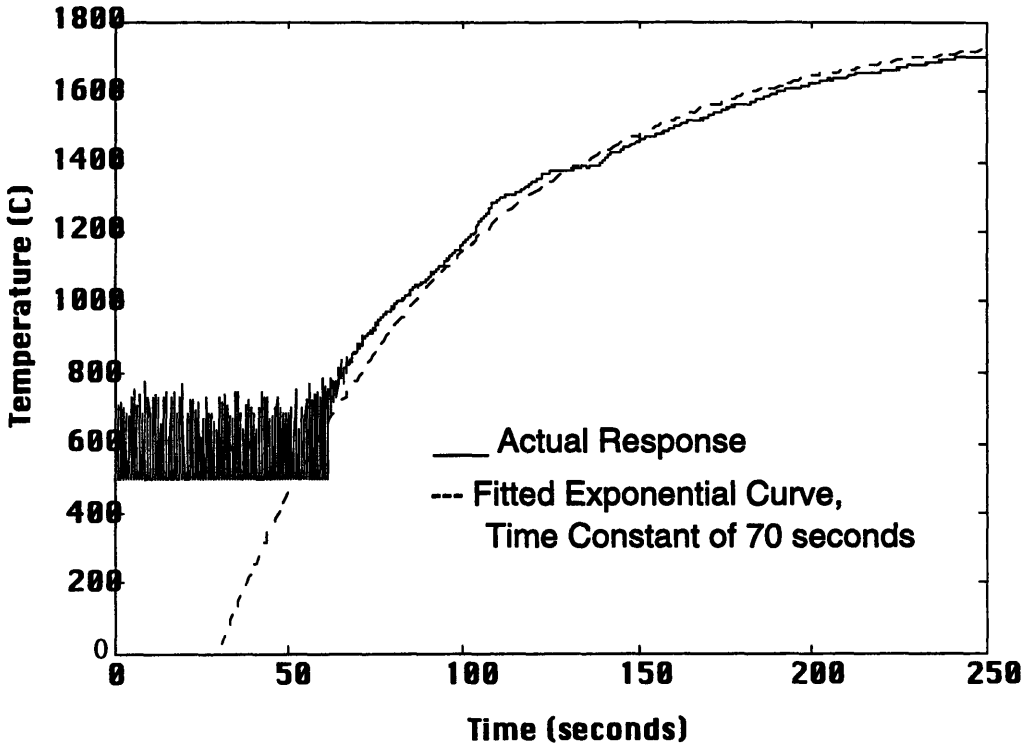

Figure 11: Open Loop Temperature Response Depicting First Order Furnace Dynamics (from feed512.dat)

b. Variations in the Plant Dynamics

The open loop responses do not always display the almost ideal first order behavior shown in Figure 11. It has been found that there is variation in open loop responses obtained under the same experimental conditions. Figure 12a shows two responses that are subject to the same experimental conditions. The power input as a function of time for both responses is given in Figure 12b. Both experiments are carried out using the same mass of molten metal, approximately 60 g. Although these responses are similar, there are some definite differences. These differences, such as the one that occurs for the dashed line response at about 520 seconds, are not easy to explain. It could be nature of the heat source, the resistivity of the arc may fluctuate in an unpredictable manner or it could be problems with the pyrometry unit.

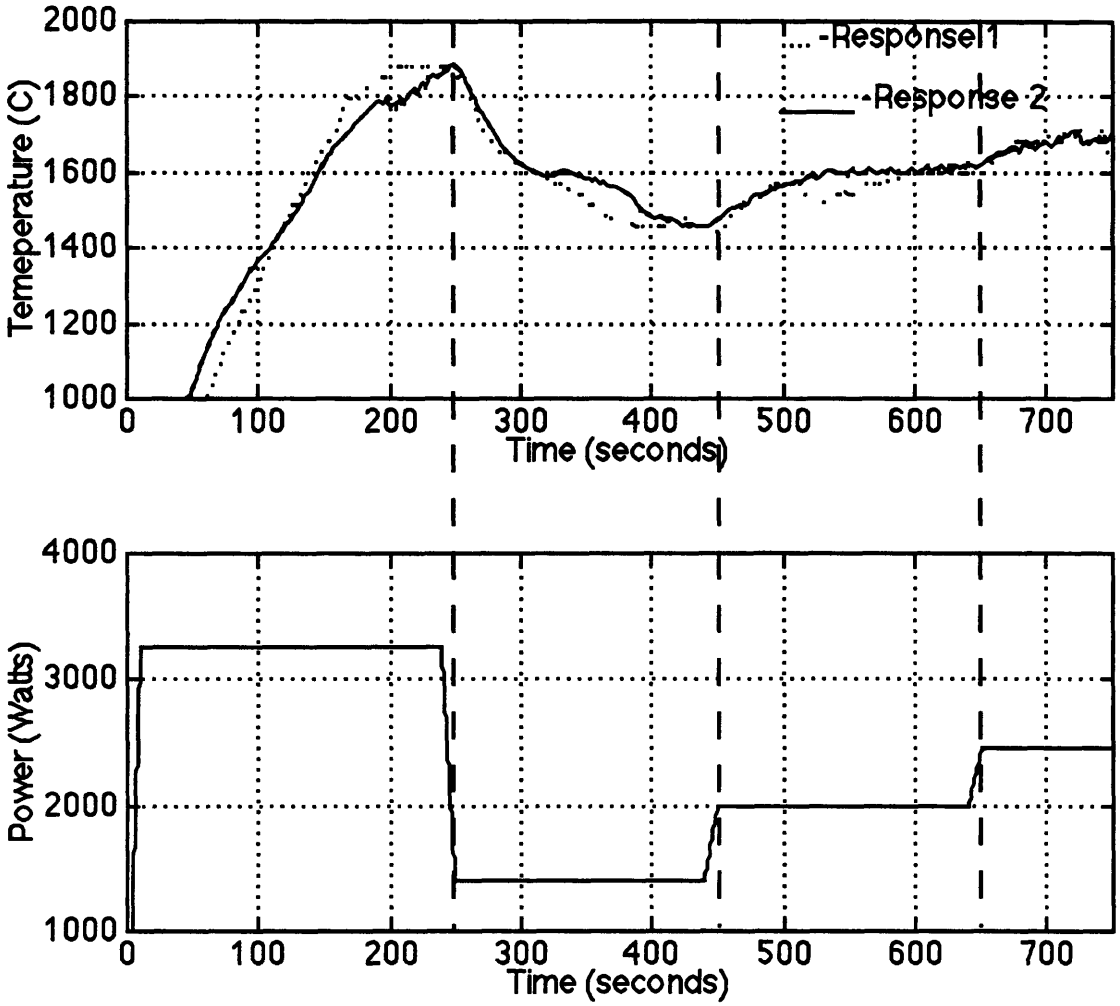

Figure 12(a) Two Open Loop Temperature Responses Carried Out Under the Same Circumstances with a Molten Steel Charge of 60g, Temperature Sensed from Base of Crucible with Pyrometer
12(b) Power Input as a Function of Time
(from weld712.dat and weld714.dat)

Both K_a and τ_a were found experimentally from open loop step responses in power input, like the ones shown in Figures 13 and 14. As expected, K_a and τ_a varied under different operating conditions such as different molten metal masses and temperature ranges. However, some of this variability can be attributed to the erratic behavior previously described. The value of τ_a was found by fitting exponential curves to open loop responses as done in Figure 11. The value of K_a was found by dividing the

approximated steady state temperature by the steady state power input as given by the equation below.

$$K_a = \lim_{s\to 0} \frac{K_a}{\tau_a s + 1} = \lim_{t\to\infty} \frac{T_{ref}(t)}{P_{in}(t)}$$

It was found that τ_a varied from 30 seconds to 90 seconds depending on the operating temperature and amount of metal within the molten metal chamber. The value of K_a also varied anywhere from .6C/W to .89C/W. Two open loop responses are given in Figures 13 and 14. An exponential response is fitted to each response at t = 250 seconds. In Figure 13 the amount of molten metal is 50g and in Figure 14 the amount of molten metal is 80g. The value of τ_a in Figure 13 is 30 seconds and for Figure 14 it is 80 seconds.

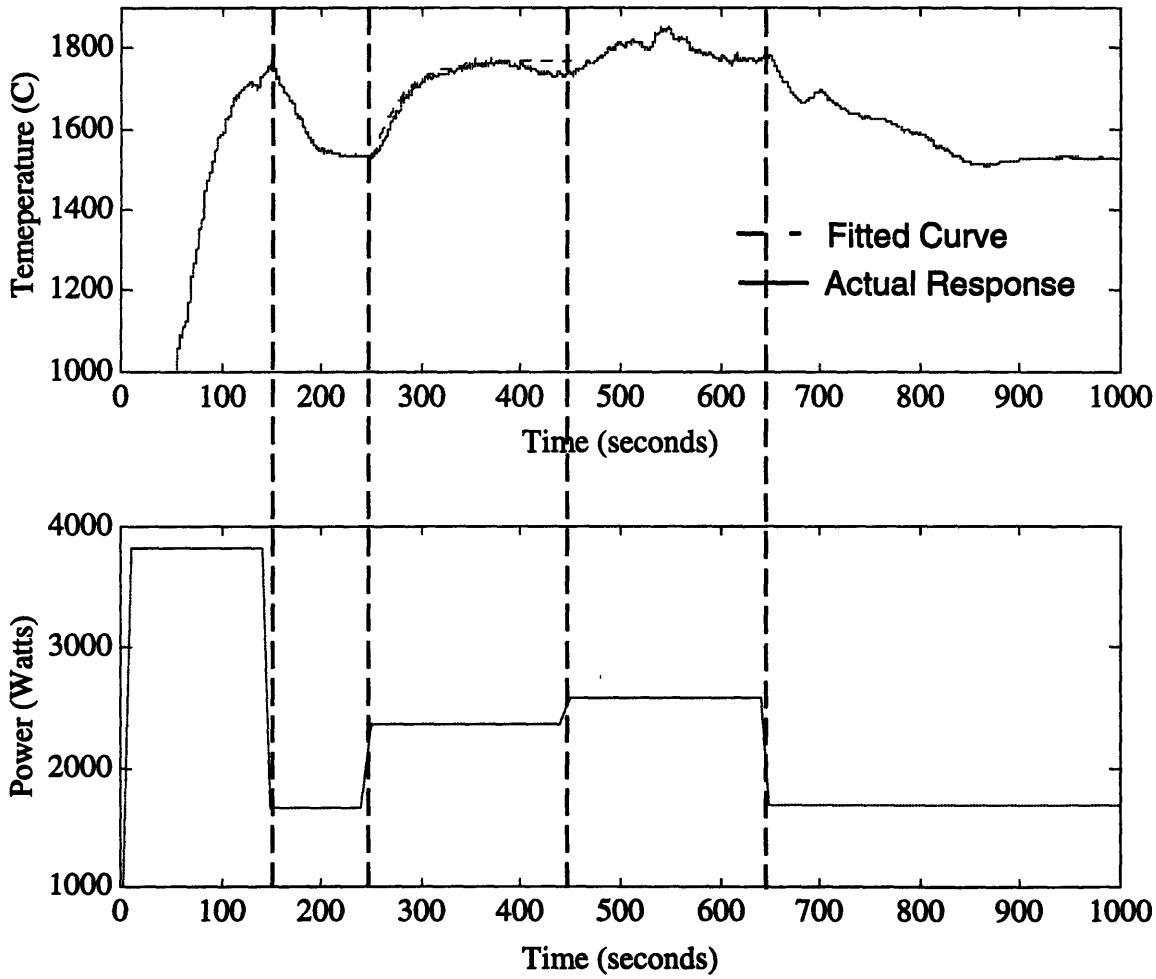

Figure 13 (a) Open Loop Temperature Response to Steps in Power Input, Molten Metal Charge is 50g, Temperature Sensed from Base of Crucible with Pyrometer;
(b) Input Power vs. Time (from weld617.dat)

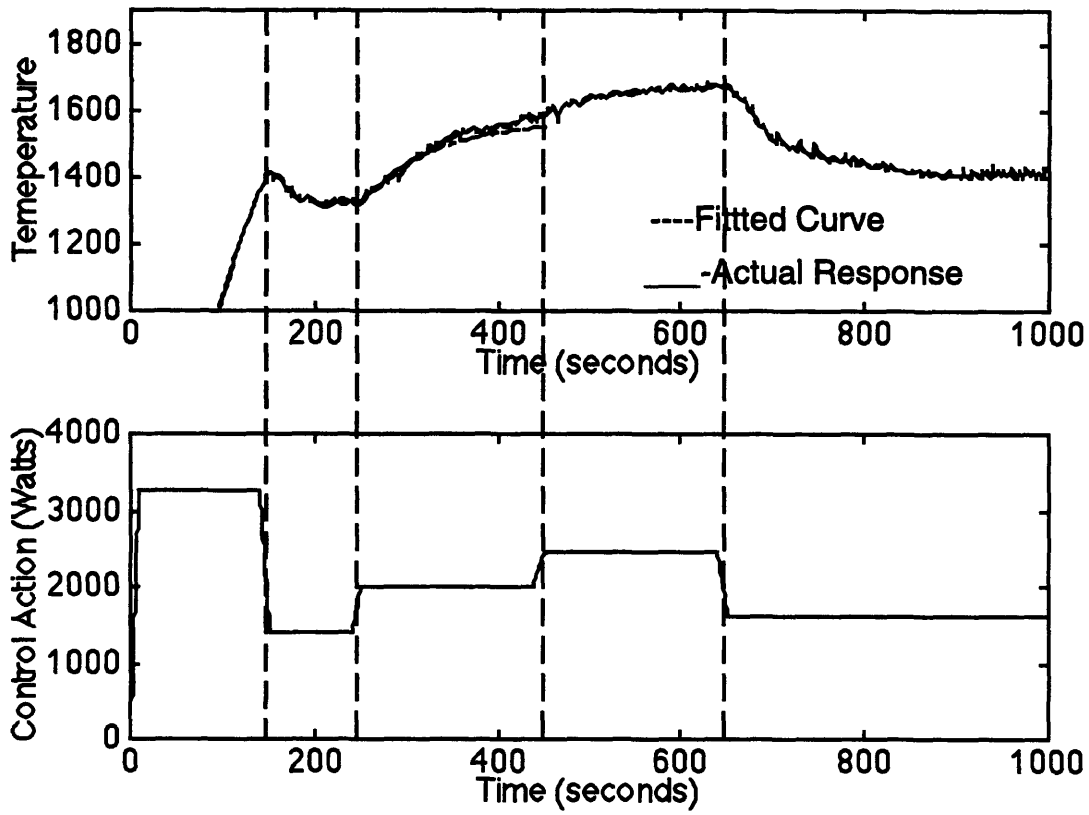

Figure 14 (a) Open Loop Response to Steps in Power Input, Molten Metal Charge is 80g Temperature Sensed from Base of Crucible with Pyrometer;
(b) Input Power vs. Time
(from weld6172.dat)

Although there is substantial variation in both K_a and τ_a both are initially given nominal values of τ_a=50 seconds and K_a = 0.6 C/W. Appendix E analyzes of the effects of operating conditions on K_a and τ_a. The transfer function that will be used to describe the temperature dynamics of the stream welder is as follows:

$$H(s) = \frac{T(s)}{P_{in}(s)} = \frac{.6}{50s+1}$$

It turns out that these nominal values work well in designing the closed loop temperature control system as will be shown near the end of this chapter where an actual closed loop response is compared to a simulated closed loop response.

D. Control System Design

With the plant description from above it is possible to begin designing a controller. In choosing a control scheme it is necessary to eliminate any steady state error. To achieve this, integral control action must be used since this is essentially a type 0 system (no poles at the origin of s plane). With these criteria and simplicity in mind, either a proportion plus integral (PI) controller or a proportional plus integral plus derivative (PID) controller will be used. Ideally, a PID controller would not be necessary since a PI controller can arbitrarily place the closed loop pole for a first order system. However, derivative control action may help to minimize temperature disturbances.

a. PI Controller

First the option of a PI controller will be analyzed using root locus analysis and then simulation. To carry out the discrete root locus analysis we must first find the discrete equivalent (using zero-order hold reconstruction) of the continuous plant transfer function. The equivalent is given as follows:

$$H_{eq}(z) = \frac{z-1}{z} Z\{\frac{H(s)}{s}\} = \frac{.0012}{(z-.998)} \tag{1.6}$$

The PI controller is of the following form:

$$G_{cPI}(z) = K_p(1 + \frac{Tz}{T_i(z-1)}) \tag{1.7}$$

The sampling period T may range from 1 second to 0.01 seconds in the future. The sampling period will never by any faster than 0.01 seconds with the present pyrometer because its maximum sampling frequency is 100 Hz. Ultimately the sampling period will depend largely on the other tasks required of the C program controlling the whole system which will have to cater to the other control systems as well. Presently, the program is doing free running A/D D/A conversion that results in a sampling period of approximately .1 second. The value of T_i was initially chosen to be 2 seconds since a lesser value would make the system very sensitive to the sample period. With the z transforms of the plant and the controller defined, one can perform some root locus analysis to find the best Kp given T and T_i above. The characteristic equation of the closed loop system is

$$G_{cPI}H_{eq}(z) = 1 + Kp\frac{.0012(1.05z-1)}{(z-.998)(z-1)}$$

The resulting root locus is shown in Figure 15

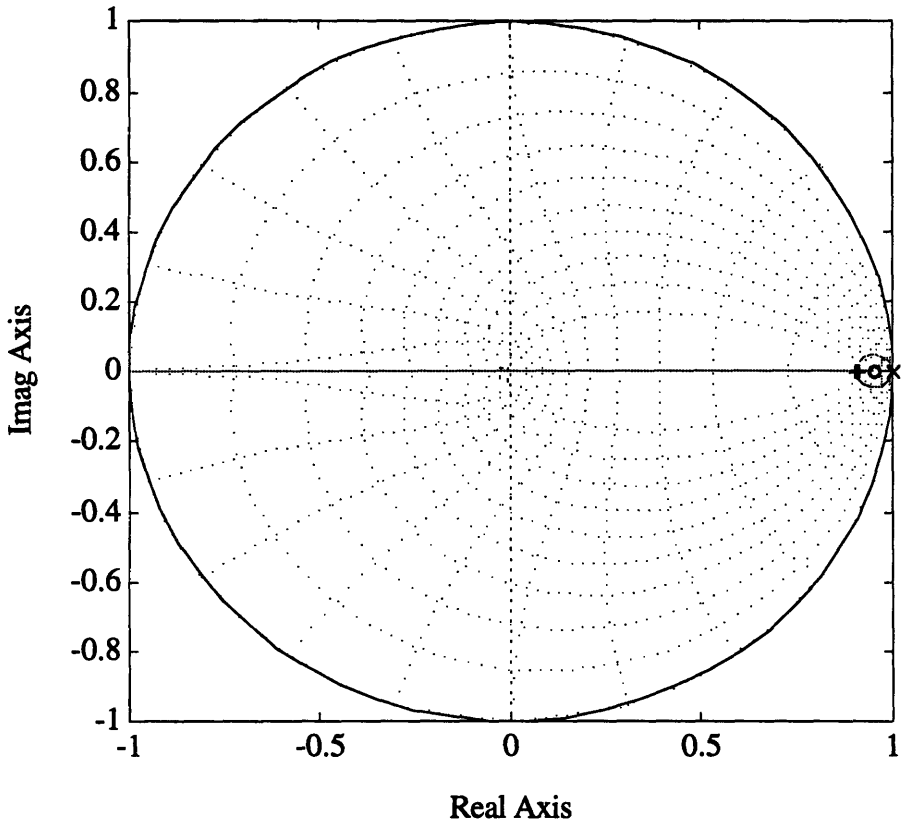

Figure 15: Discrete Root Locus for PI Controller

Kp=148 corresponds to the break-in point on the real axis at z=.909. Ideally, from the standpoint of root locus, we would choose a T_i that is slightly more than T which would result in a break-in point close to the origin with the appropriate Kp, giving a very fast response with no overshoot. Designing this control system would be unrealistic though, it would require an enormous amount of power and the maximum available from the Hobart is only 4000 Watts.

A better means of design in this case is through simulation, a block diagram of the system to be simulated in Simulink is shown in Figure 16.

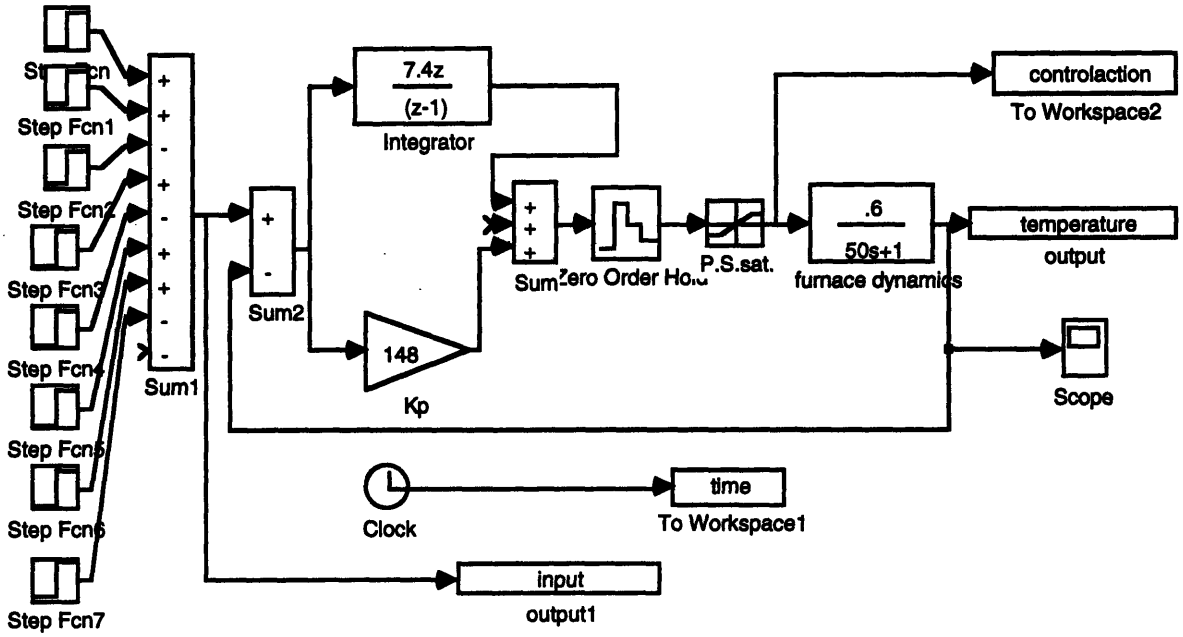

Figure 16: Block Diagram of PI Controller

All of the simulations have multiple step inputs since this will be similar to the anticipated mode of operation when welding.

Some important features of the system should be noted here. One feature is that we are only able to put heat into the furnace and cannot take it out, this characteristic is accounted for in the saturation block. The minimum heat input is 40 W while the maximum is 4000W. The minimum is 40 rather than 0 because it is necessary to sustain the arc throughout the process; a current of 0 would extinguish the arc and require restarting it with the high frequency arc starter which can sometimes cause the computer to lock up. To obtain a controlled negative energy input, one could incorporate a cooling system, but this is presently deemed unnecessary since the furnace dissipates a substantial amount of heat at operating temperatures. The simulated step response of the system is shown in Figure 17. The reference input is given by the dashed line and the simulated response is given by the solid line. This response shows substantial percent overshoot even though the chosen gain value placed the closed loop root locus poles on the real axis. This discrepancy can be attributed to the saturation of the power supply which cannot be accounted for using root locus analysis.

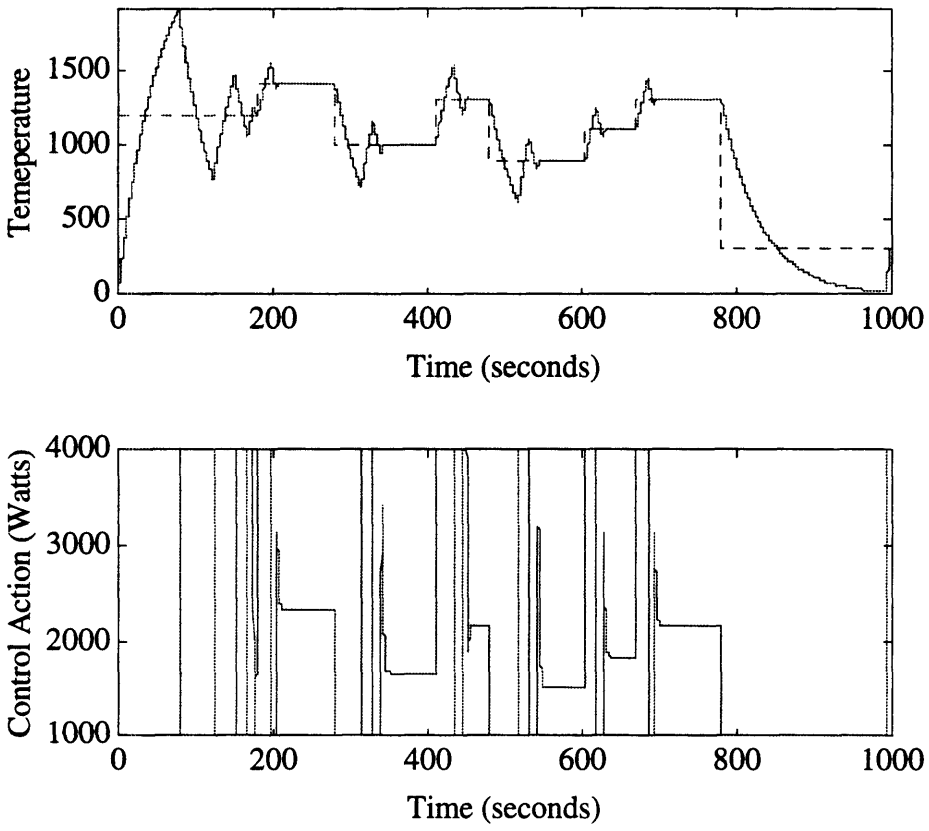

Figure 17: Simulated Response of Root Locus Designed PI Controller

There are a number of ways to improve this response. One would be to pick a larger Kp and a larger T_i, this would place less emphasis on the integral control action which is causing the overshoot. Another way that would have a similar effect, is to incorporate an anti-windup feature which limits the magnitude of the error within the integral. In other words, it would limit the magnitude of e' in the following equation representing the control action

$$u_c(t) = K_p(e(t)) + \frac{K_p}{T_i}\int e'(t)dt$$

Both of these options are incorporated into the PI control scheme and tuned iteratively. The closed loop response improved substantially as shown in Figure 18 below. The value of T_i was increased to equal Kp and Kp was increased to 1300. The anti windup limits were fixed at (+/-)100 C.

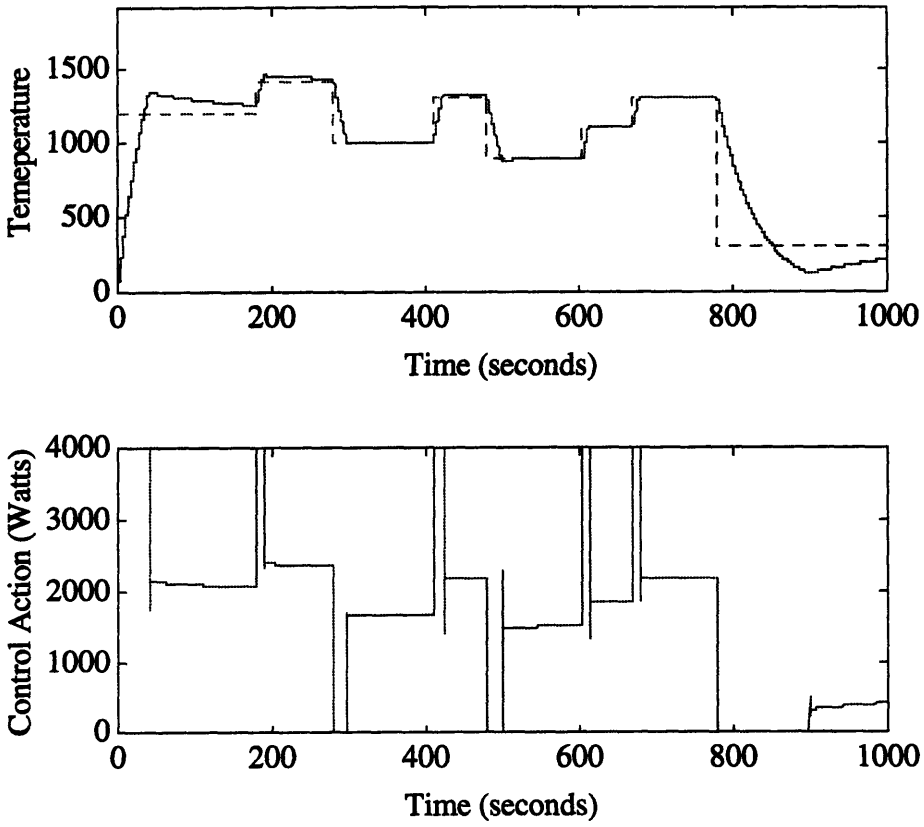

Figure 18: Simulated Response of Refined PI Controller

b. Design of PID Temperature Controller with Anti-windup

Even though this PI controller performs well, the control system might be further improved with respect to temperature disturbance rejection by using a PID controller while retaining the anti-windup feature. Disturbance rejection will likely be important to the control system given the slightly erratic nature of the open loop temperature responses given in Figure 12. The PID control law is of the following form

$$G_c(z) = K_p(1 + \frac{Tz}{T_i(z-1)} + \frac{T_D(z-1)}{Tz})$$
$$= K_p + \frac{K_i z}{(z-1)} + \frac{K_D(z-1)}{z}$$

The first approach in tuning this controller was to use the Ziegler-Nichols method which uses an open loop transient response to determine initial values for K_p, T_i, and T_d (or K_p, K_d, and K_i). The method is depicted in Figure 19

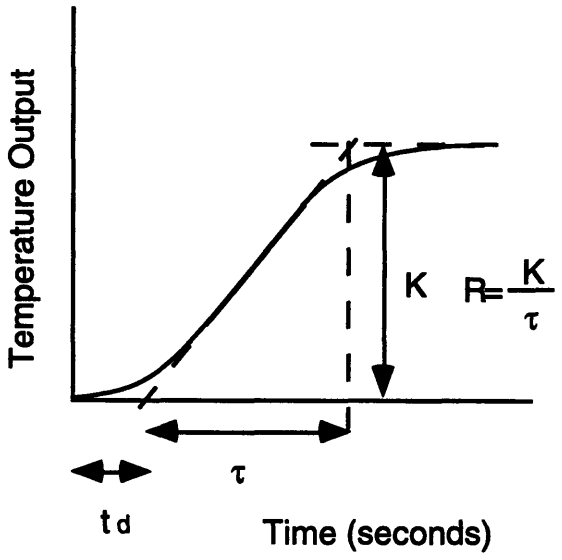

Figure 19: Necessary Parameters for Ziegler-Nichols Tuning of PID Controller

How to calculate K_p,K_i and K_d, given the parameters described in the previous figure, is shown on the following table [Ogata, 1990]:

Controller Parameter	K_p	K_i	K_d
Parameter Formula	1.2/(R*t_d)	(Kp*T)/(2*t_d)	(Kp*.5*t_d)/T
Resulting Parameter Values	1333	667	667

It should be noted here that t_d is actually 0 since the behavior of the system is first order but here it was assigned to be 0.1 seconds, a very small value relative to the plant time constant. This was done since it is necessary that t_d be some finite value to use this method, and no alternative methods were found. The value of R was obtained from open loop responses and is 66.7 C/sec. Given these values of t_d and R, the resulting values of K_p , K_i, and K_d are shown in the table above. These values serve merely as starting points in determining the best values of K_p,K_i,and K_d. Taking K_i and K_d from above, the resulting root locus as a function of K_p is shown in Figure 20.

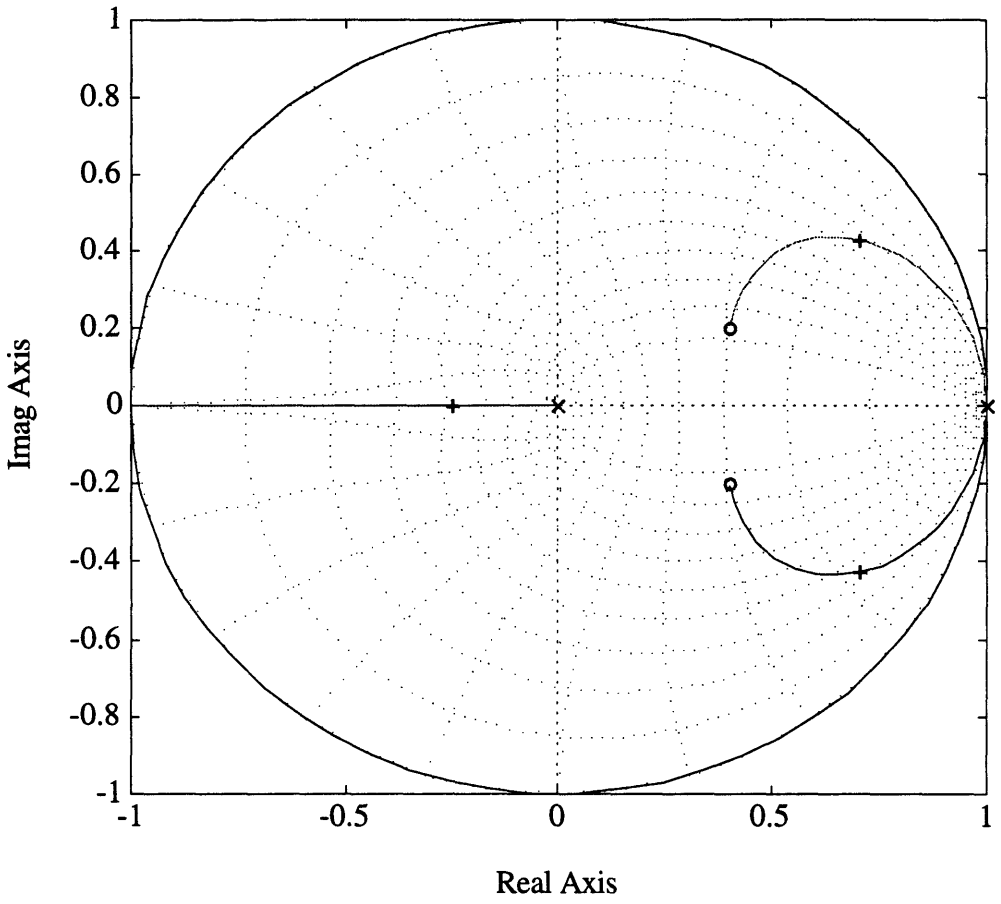

Figure 20: Initial Root Locus for PID Controller

One can see that the root locus predicts a oscillatory response which turns out to be the case as shown in simulated response in Figure 21

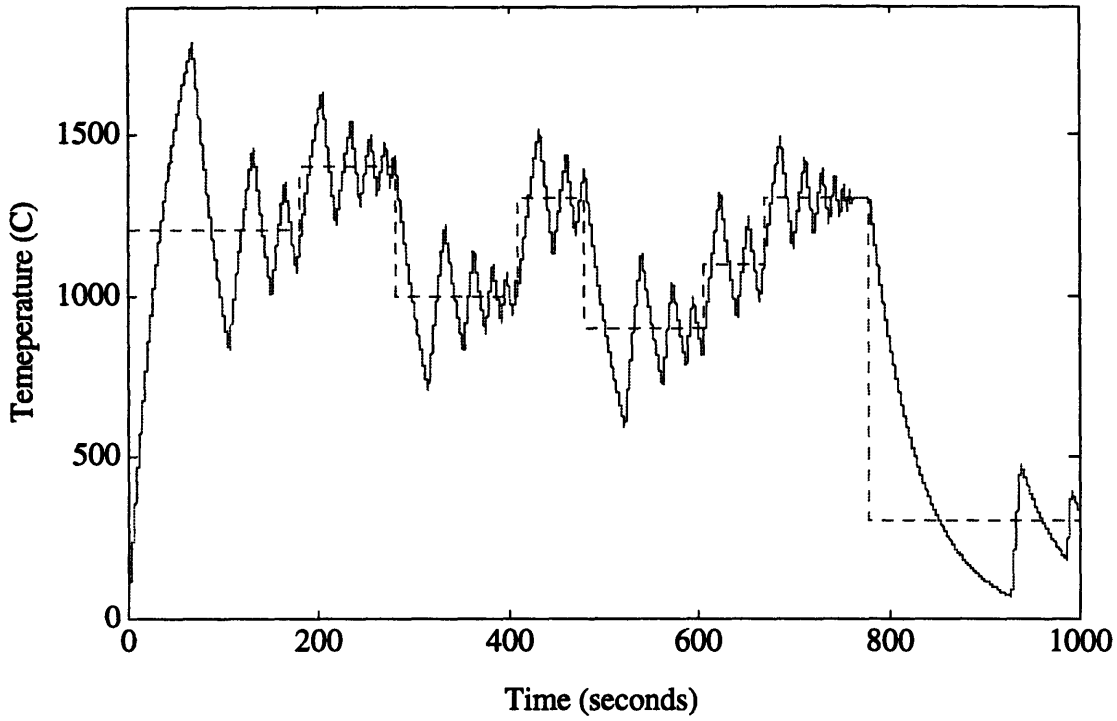

Figure 21: Simulated Response with Initial Values for Kp, Ki and Kd

Using root locus analysis, the value for K_i was decreased to bring the closed loop zeros onto the real axis and dampen the response. K_i was further tuned iteratively using simulation, until a value was found that gave a suitable response (K_i=1). Better values for K_p and K_d were found in a similar fashion (K_p=1300 and K_d=500). The block diagram of the final system is shown in Figure 22.

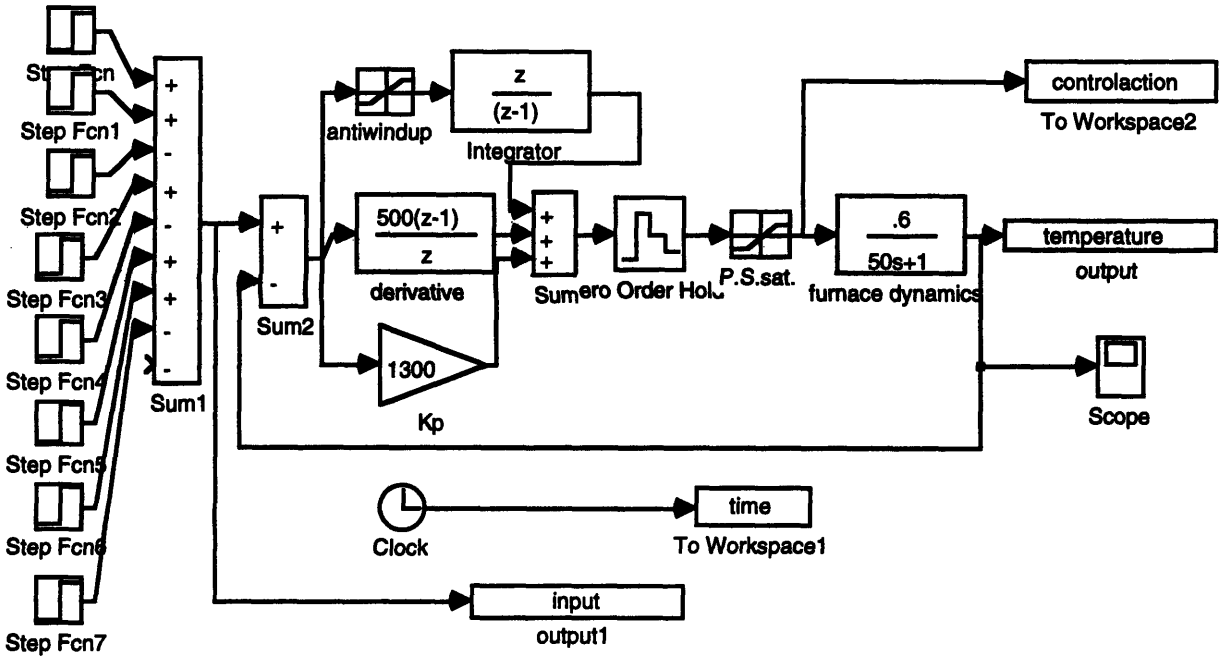

Figure 22: Block Diagram of Final Design of Temperature Control System

The performance was greatly improved from the response shown in Figure 21, as shown in Figure 23. The overshoot appears to be less than 10% for even the large initial step to 1200 C where there is some integral wind-up. The main concern, however, will be the smaller steps like the one from 1200 C to 1400 C since this will be the more likely magnitude of control steps when welding.

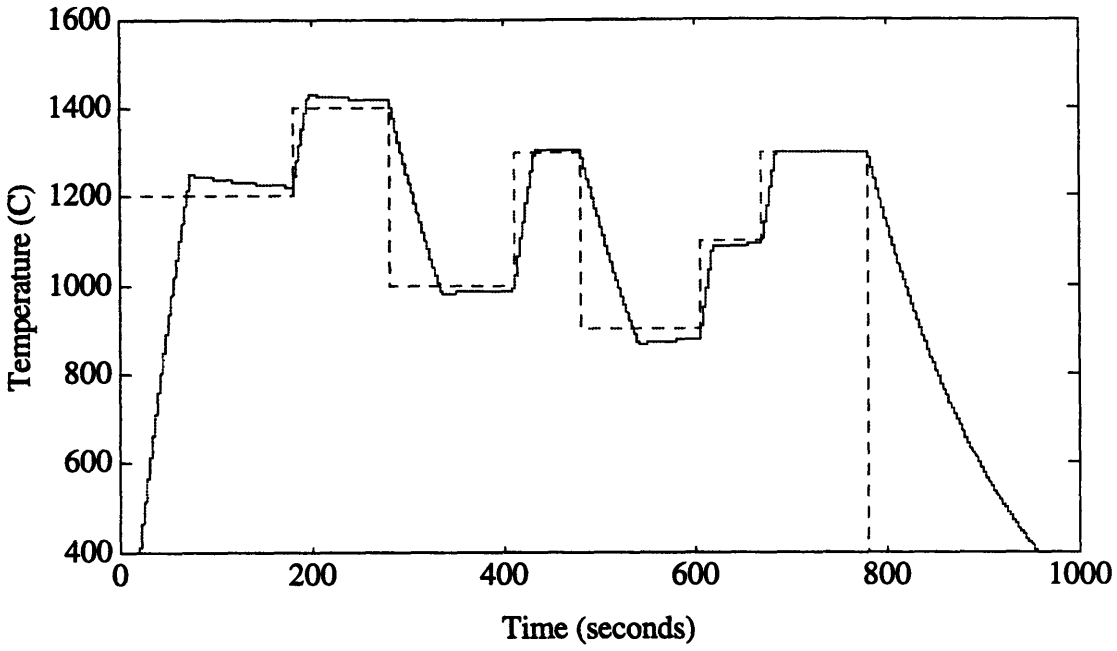

Figure 23 Simulated Response of PID Controller with Anti Wind-up Feature

In comparing the performance of this PID controller with the previous PI controller, it turned out that there was little, if any, benefit in adding the derivative control. In many situations derivative control action is incorporated in furnace temperature control systems to help reduce disturbances, but in this case it had no apparent effect on disturbance rejection. Both controllers were subject to simulation with both white noise and step temperature disturbances at the output, and there was no observable difference between the two controllers. However, the PID controller will continue to be used since it has no negative effect on the system.

c. Performance of Actual Controller

We now compare this simulated response with reality, implementing the same values of K_p, K_i, and K_d in the c code, pyropid.c, that were determined from the simulation. The actual response is shown in Figure 24.

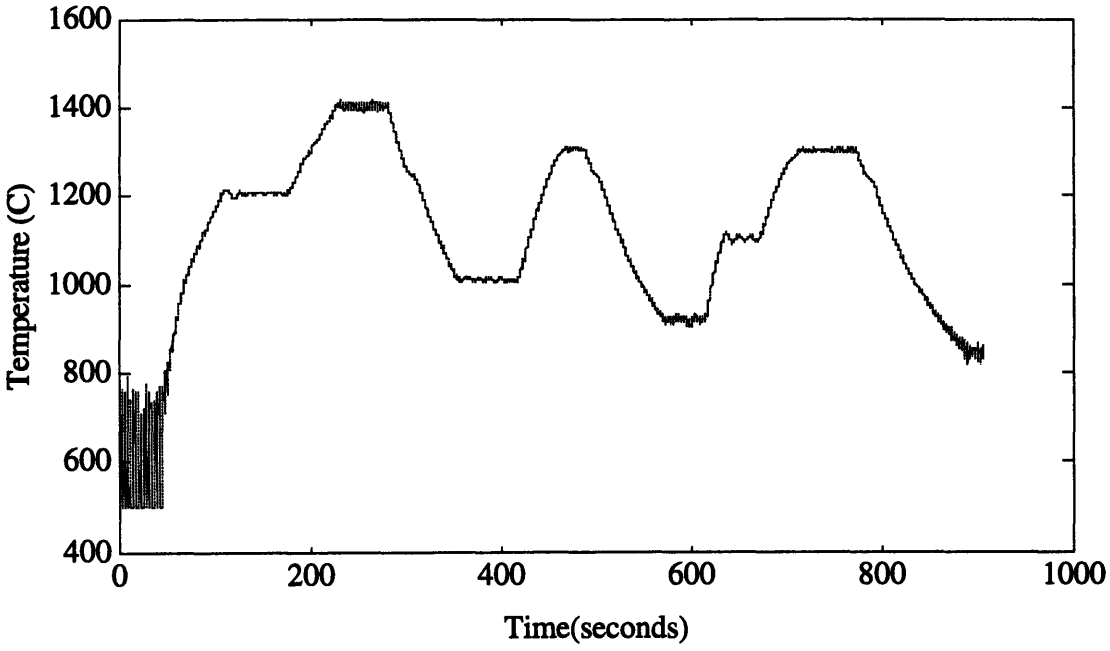

Figure 24: Actual Response of Closed Loop PID Temperature Controller with Anti Wind Up Feature (from step4894.dat)

The actual response is similar in to the response predicted by simulation in many respects. It appears that the actual response has a larger time constant than the simulation which can be attributed to more molten metal within the crucible. The actual response appears well dampened with very little overshoot. There is some negligibly small steady state oscillations in the response, but the system can be fine tuned when a high degree of temperature precision becomes an issue. Overall the performance of the PID temperature controller is good at this stage in development of the steam welder.

Chapter 3: Closed Loop Molten Metal Level Control System

A. Overview

For the stream welding process to run continuously, it is necessary to replenish the molten metal supply as it is ejected out of the furnace and onto the weld seam. Another reason to maintain the molten metal at a constant level is to ensure a consistent thermal mass for the temperature control system. The method used to accomplish a constant level is a wire feed system. Solid wire is fed into the crucible where it melts from the heat of the surrounding molten metal. A schematic of the components of the molten metal level control system is shown in Figure 25:

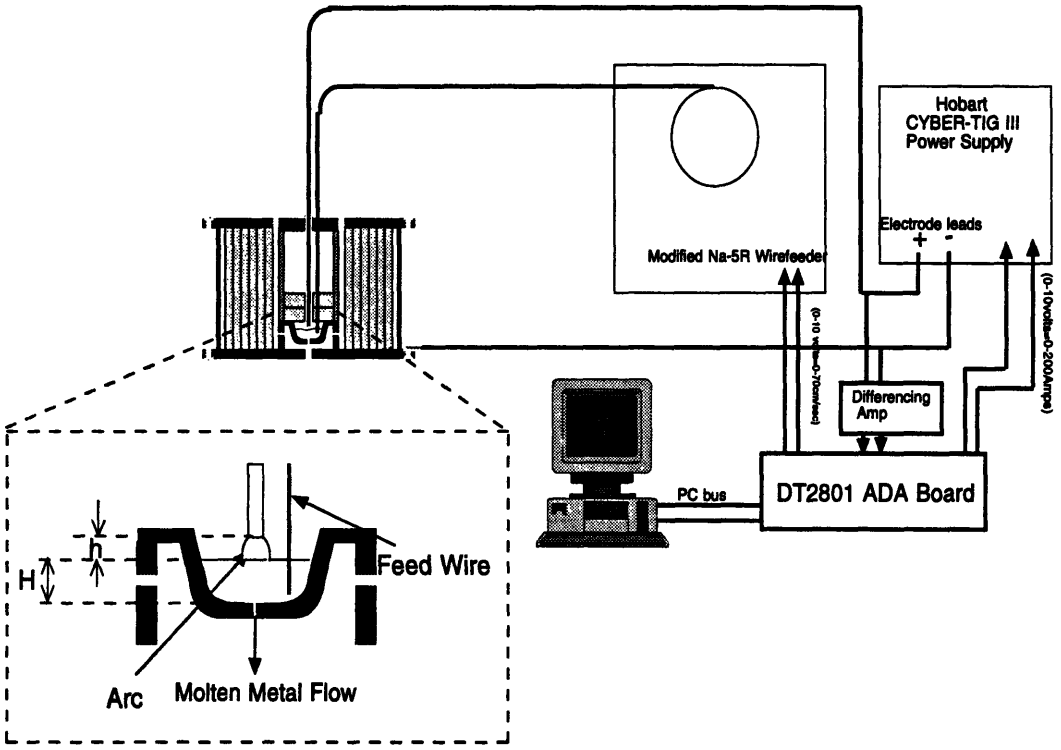

Figure 25: Components of Closed-Loop Wirefeed System

The variable of interest is the height of the molten metal in the crucible, H, which should be maintained at a constant level. The state of this variable is sensed indirectly by measuring the arc voltage V. The arc voltage is proportional to the arc length h. Since the length H+h is fixed, the arc voltage is inversely proportional to H (in other words, if the arc voltage is large, H is small). The arc voltage is measured directly from the positive

and negative electrodes of the power supply. Since the arc voltage will range anywhere from 10 to 25 volts, it is necessary to preprocess this signal to get it in a range that the DT 2801 A/D board can handle (0-10 volts). This is accomplished with a simple differencing amplifier with a gain of 0.24. The signal from the differencing amplifier is digitized by the DT2801A board. This digitized value of the arc voltage is then divided by 0.24 and incorporated into the control scheme.

The control scheme is essentially an on/off type that is implemented with the C program pyropid.c. One important aspect of the system is that the maximum wirefeed rate is limited by the melting rate of the wire being fed into the crucible. It is important not to feed faster than the wire can melt to avoid damaging the graphite crucible from steel wire poking into it. To prevent this kind of damage, the control scheme uses the sensed temperature in determining the magnitude of the 'on' control action, higher sensed temperatures mean that a higher wire feed rate can be used without damaging the crucible.

The control action is computed every 0.1 seconds and sent to the DAC. The analog signal from the DAC is sent to the modified NA-5R wire feeder. Here the DAC input voltage is directly proportional to the steady state wirefeed rate (0-10 volts=0-70cm/sec). The fed wire then melts in the crucible, replenishing the molten metal supply.

B. Modeling the Dynamics of the Wirefeed System:

Before coming up with a suitable control strategy it was necessary to understand the dynamics of the system components mentioned above as well as the nature of the disturbances to the system. A continuous block diagram of all of the main system components is shown in Figure 26.

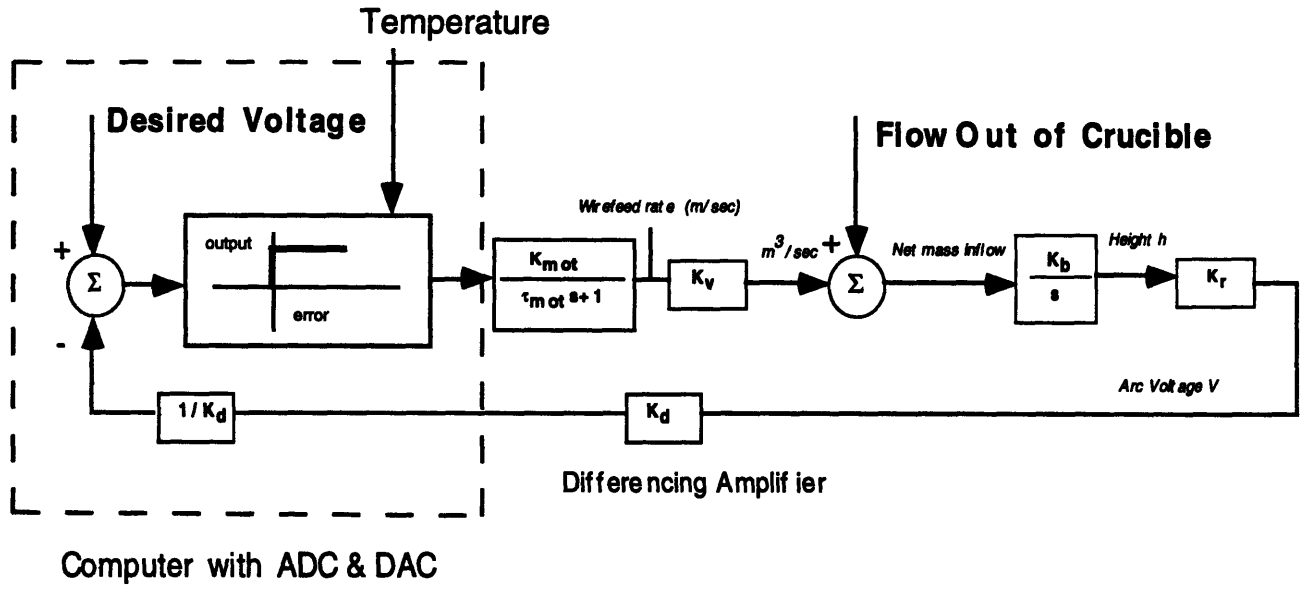

Figure 26: Block Diagram of Closed Loop Wirefeed System

Here an explanation is given of how the transfer functions for each component was obtained. Most are simple static functions.

The transfer function for the wire feeder is essentially that of a typical velocity controller. It was obtained from an open loop response to a step input in voltage and observing the wirefeed velocity response. This had already been done by Hale [8] who used the same wire feeder (but less modified) for some of GMA Welding research. Both the motor time constant of 0.1 seconds and gain of 70.4mm/sec/volt, determined by Hale, were verified.

K_V will be dependent on the diameter of the wire fed into the furnace since it translates wire velocity into a volume flow rate. The relationship between these two is as follows

$$\text{volume flow rate}=(\text{wirefeed velocity})*\pi(R_{wire})^2$$

So the resulting K_V is:

$$K_V=\pi(.00045m)^2$$

The flow out of the crucible is treated as a disturbance as shown in the block diagram. The main measure of performance of the closed loop system is how well it can reject this disturbance and maintain a constant voltage/molten metal level. The net volume flow

rate into the crucible is the wirefeed volume flow rate minus the outflow from the crucible. The relationship between this net mass inflow rate and the molten metal height is given here (it should be noted that the slight slope of the crucible wall is unaccounted for here)

$$\frac{dV_{in}}{dt} = \pi R^2_{crucible} \cdot \frac{dh}{dt}$$

$$h = \frac{1}{\pi R^2_{crucible}} \int \frac{dV}{dt} dt$$

$$h(s) = \frac{1}{s\pi R^2_{crucible}}$$

The height then translates into an arc voltage, this relationship should be similar to the relationship between arc voltage and arc length for a TIG welding process. The possible problems with determining the height by sensing the arc voltage is that the arc voltage is also a function of arc current which fluctuates with the temperature control action. It is also a weak function of the temperature of the argon as well as the concentration of metal vapor in the arc. However the arc voltage is primarily a function of arc length and will be initially be assumed to be linearly related to arc length as the proportionality block K_r indicates. A suggested alternative was to measure the molten metal level by measuring R since both V and I are known. It turns out that R is even less reflective of height, being highly dependent on the arc current. This is apparent when the current is doubled from 100 A to 200 A, at 100 A the arc resistance is 0.16 ohms and at 200 A its 0.095 ohms. On the other hand, the voltage only changes from 16 V at 100 A to 19 V at 200 A. The value of K_r was found experimentally. The measured arc length of 4 mm resulted in an arc voltage of 13.8 Volts. Hence K_r is roughly 3.44 Volts/mm.

The differencing amplifier was constructed of a +-15 volt power supply, an LF741 operational amplifier, and some accompanying resistors. The dynamics of the amplifier can be neglected since its bandwidth is orders of magnitude higher than the rest of the system. A schematic of the amplifier is shown in Figure 27, its gain is 0.24.

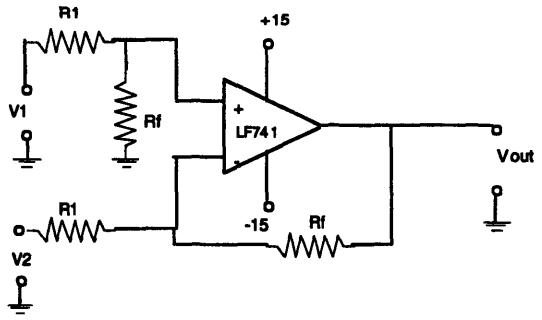

R_f=14.8KOhms

R_1=61.5KOhms

V1=Positive electrode voltage

V2=Negative Electrode Voltage

Vout=Voltage out to ADC

Figure 27: Differencing Amplifier for Arc Voltage Sensing

The block in Figure 26 which has the biggest effect on the performance of the system is the saturation block. As mentioned before, the maximum melting rate of the wire limits the maximum feed rate. To verify the damaging effect on the crucible, when feeding faster than the melting rate of the wire, a experiment was carried out where the wire was fed faster than the calculated melting rate. The temperature was maintained at 1800 C and the wirefeed saturation limit was fixed at 9.8 cm/sec, well above the 7.7 cm/sec melting rate. The arc voltage was initially at 20 when the level controller was activated, the reference voltage was set to 18 volts. The wire fed for a couple of minutes before the wire poked through the bottom of the crucible. This verified that the wirefeed rate should not exceed the melting rate of the wire. Because of this wire melting rate limitation, the wire feeder cannot replenish as quickly as the molten metal is ejected unless the ejection rate is very low (less than 19 mm^3/sec at 1650C). It should also be noted here that the lower saturation limit is 0 since no negative control action is possible, this is due to the fact that mass can only be added and not withdrawn with the wire feeder. Because of the nature of this saturation, a simple on/off controller is used; something like a PID controller wouldn't improve the performance because of the upper saturation limit which is now discussed.

C. Determination of Maximum Wire Feed Rate

The following symbols are used in this section:

T - Temperature of the feed wire (K)

T_{mm} - Temperature of the molten metal (K)

Θ - $T-T_{mm}$

E - Energy (J)

t - Time (seconds)

h' - Generalized convective heat transfer coefficient (11,627W/m^{2}K from experiment)

ρ - Density of feed wire (7800 kg/m^3)

c - Specific heat of feed wire (434 J/kgK)

r_o - radius of wire (.45mm)

A_s - Surface area of wire immersed in molten metal (m^2)

V - Volume of wire immersed in molten metal (m^3)

r - Radial coordinate of wire

x - Axial coordinate of wire

k - Thermal conductivity of mild steel (60W/mK)

α - $k/\rho c_p$ ($18x10^{-6}$W/m^2)

H - Height of Molten Metal (1cm)

The maximum wirefeed rate is dictated by the maximum rate at which the solid steel wire melts when fed into the molten metal bath. This wirefeed rate will be a function of the temperature of the molten metal, at high temperatures the melting rate will be faster which allows higher wirefeed rates without risking damage to the crucible. To get an estimate of the melting rate, some heat transfer analysis was carried out that predicts the melting rate at various temperatures. A schematic of the problem parameters is shown in Figure 28.

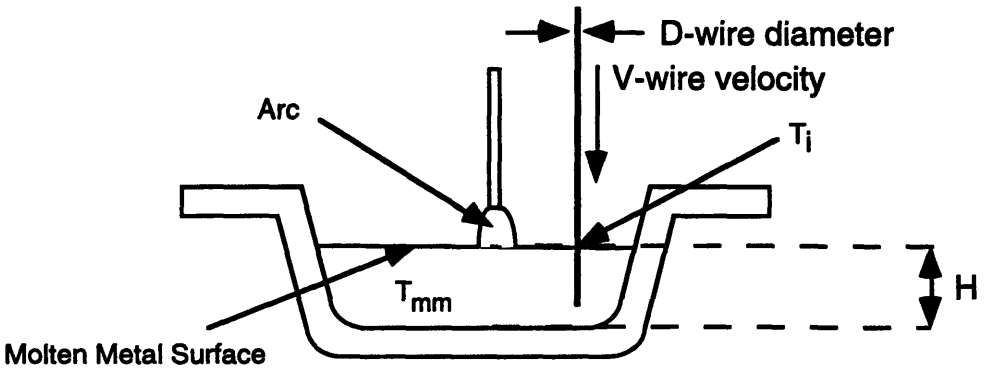

Figure 28: Parameters in Analyzing Wire Melting Rate

The Problem was approached by finding the time t that it takes to melt a wire segment of length H and then dividing H by t to get an approximation of the maximum wire feed rate. The diameter of the wire is D and it is at an initial temperature T_i before immersion in a molten metal at temperature T_{mm}. Two methods are used to determine the time t, the lumped capacitance method or, more accurately, solving the appropriate form of the heat equation which accounts for multidimensional effects. Both methods have convection as a boundary condition. The convective heat transfer coefficient, h', was determined experimentally at one temperature and assumed to remain constant for the range of analysis temperatures. It should also be noted that latent heat effects are accounted for in the convective heat transfer coefficient as will become apparent when explaining how the value for h' was determined. Each method gives similar results in predicting the wire melting rate as will be shown.

a. Lumped Capacitance Method

The time t can be calculated using an energy balance as follows:

$$h' A_s (T - T_{mm}) = \rho V c \frac{dT}{dt}$$

Here the change in internal energy of the wire segment is proportional to the heat flux across the wire due to convection. By letting $\Theta = T - T_{mm}$:

$$\frac{\rho V c}{h' A_s} \frac{d\theta}{dt} = \theta$$

Separating the variables Θ and t and integrating yields:

$$\frac{\rho V c}{h' A_s} \ln \frac{\theta_i}{\theta_f} = t$$

Θ_f is defined as the molten metal temperature minus the melting temperature of the steel, and Θ_i is the molten metal temperature minus the initial temperature of the wire segment. The only unknowns are h' and Θ_i. The value of Θ_i will be highly dependent on the instantaneous wirefeed rate, the faster the wirefeed, the less preheated the wire will be. To simplify the situation, T_i is assumed to be 500 C and then h' was found

experimentally based on this assumption. These values of h' and Θ_i will be used in subsequent calculations in determining the maximum wirefeed rate for various temperature ranges. In experimentally determining h' the temperature was held constant at 1650 C while I manually feed a 300mm length of wire as fast it melted (this was apparent from continually hitting the bottom of the crucible). The time to feed a segment of this length turned out to be 6 seconds. Hence the resulting maximum wirefeed rate is 50.8mm/sec at this temperature, and the value of h' is 11,627W/m^{2}K (assuming Ti is 500 C).

With the values of h' and Θ_i as given above it is possible to estimate the maximum wire feed rate at various temperatures by simply dividing H by the expression for t given above. Using this lumped capacitance analysis the maximum wire feed rate at 1800 C is 7.7 cm/sec, at 2000 C it is 10.36 cm/sec and at 2200 C it is 13 cm/sec.

b. Accounting for Spatial Effects

To reinforce the lumped capacitance results the same problem will be solved using a more rigorous method that accounts for transient conduction in the r and x directions . Figure 29 shows a segment of wire immersed in the molten metal, again we want to find the time t after the segment is submerged when point T(0,H) reaches the melting temperature of steel.

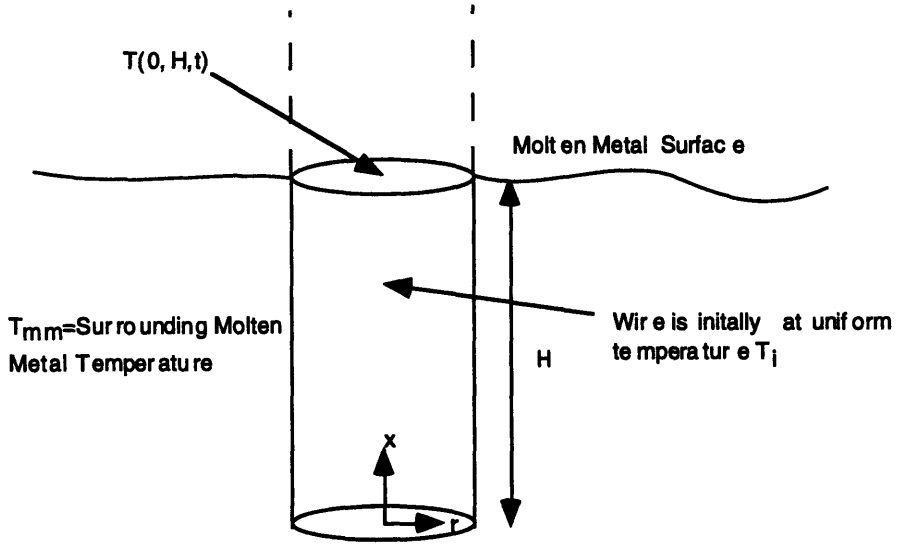

Figure 29: Schematic of Wire Segment Immersed in Molten Metal

The appropriate form of the heat equation that needs to be solved is of the form

$$\frac{1}{r}\frac{\partial}{\partial r}(r\frac{\partial T}{\partial r})+\frac{\partial^2 T}{\partial x^2}=\frac{1}{\alpha}\frac{\partial T}{\partial t}$$

A closed form solution of this partial differential equation can be obtained using the separation of variables technique. The result may be expressed in the following form [Incropera and Dewitt, 1990]:

$$\frac{T(r,x,t)-T_{mm}}{T_i-T_{mm}}=\left[\frac{T(x,t)-T_{mm}}{T_i-T_{mm}}\right]_{\substack{semi-\inf inite\\ solid}}\cdot\left[\frac{T(r,t)-T_{mm}}{T_i-T_{mm}}\right]_{\substack{\inf inite\\ cylinder}}$$

So the two-dimensional solution is expressed as a product of one-dimensional solutions that correspond to a semi-infinite solid wall and an infinite cylinder with the same radius as the wire.

The one dimensional semi-infinite solid solution is given by the following (erf denotes the Guassian Error Function)

$$\left[\frac{T(x,t)-T_{mm}}{T_i-T_{mm}}\right]_{\substack{semi-\inf inite\\ solid}}=1-\left[erf\left(\frac{x}{2\sqrt{\alpha t}}\right)-\left[e^{\left(\frac{hx}{k}+\frac{h^2\alpha t}{k^2}\right)}\right]\cdot\left[erf\left(\frac{x}{2\sqrt{\alpha t}}+\frac{h\sqrt{\alpha t}}{k}\right)\right]\right]$$

The approximate graphical representation of this function is given in [Incropera and Dewitt, 1990] and is shown at the end of Appendix D. The graphical solution only requires the following dimensionless coefficients:

$$\frac{h\sqrt{\alpha t}}{k}$$

and

$$\frac{x}{2\sqrt{\alpha t}}$$

The one dimensional infinite cylinder solution is given by the following:

$$\left[\frac{T(0,t)-T_{mm}}{T_i-T_{mm}}\right]_{\substack{\inf inite\\ cylinder}}=\sum_{n=1}^{\infty}C_n\exp\left(-\zeta^2{}_nFo\right)J_o\left(\zeta_n\frac{r}{r_o}\right)$$

where

$$C_n = \frac{2}{\zeta_n} \frac{J_1(\zeta_n)}{J^2{}_o(\zeta_n) + J^2{}_1(\zeta_n)}$$

Here J_1 and J_0 are Bessel functions of the first kind and the discrete values of ζ_n are the positive roots of the transcendental equation

$$Bi = \zeta_n \frac{J_1(\zeta_n)}{J_o(\zeta_n)}$$

A graphical representation of the infinite cylinder solution at r=0 is given in the heat transfer text [Incropera and Dewitt, 1990] and also provided at the end of Appendix D. This graphical solution requires the inverse Biot and Fourier Coefficients which are as follows

$$Bi^{-1} = \frac{k}{hr_o} = \frac{17 \frac{W}{mK}}{11{,}627 \frac{W}{m^2 K} .00045m}$$

$$Fo = \frac{at}{r_o^2} = \frac{4.2 \times 10^{-6} \frac{m^2}{\sec} \cdot t}{(.00045m)^2}$$

The value of t was solved for recursively and the results agree fairly well with the lumped capacitance method. At 2200 C the answers from each method differed the most, the lumped capacitance predicts a t of 0.078 seconds and the more rigorous method predicts a t of 0.099 seconds. Dividing H by these times yields maximum wirefeed velocities of 13cm/sec and 10cm/sec.

D. Control Scheme

Since the main factor limiting the performance of the level control system is the melting rate of the wire, the control system uses the analysis above and changes the wire feed saturation limits as a function of temperature. If this temperature feedback were not incorporated, the wire feed rate would be limited to the maximum wire feed rate at the lowest operating temperature. The wire feed rate as a function of temperature used in the C program pyropid.c, is given below:

$$wirefeedrate = \frac{T_{mm} - 1650}{550} \cdot 5 \frac{cm}{\sec} + 3 \frac{cm}{\sec}$$

The wire feed rate is slightly less than the maximum calculated melting rate to allow for some margin of deviation between the calculated maximum melting rate and the actual melting rate. This measure of safety is incorporated because when the feed wire punctures the crucible a dangerous situation results, molten metal flows uncontrollably out of the furnace. Another safeguard incorporated in the program pyropid.c is that the system will only feed wire if the furnace temperature is above 1650 C.

To analyze the performance of the molten metal level controller, simulations were carried out using Simulink. Analysis techniques such as root locus are not easily applied given the saturation nonlinearity that has such a big effect on the system. The wire feeder will only be able to maintain a constant level if the flow out is less than the mass flow in from the wire feeder. At 1650 C the outflow should be less than 19.6 mm^3/sec, for the wire feeder to maintain a constant level; and at 2200 C the outflow should be less than 40.2mm^3/sec. A block diagram of the discrete closed loop system is shown below.

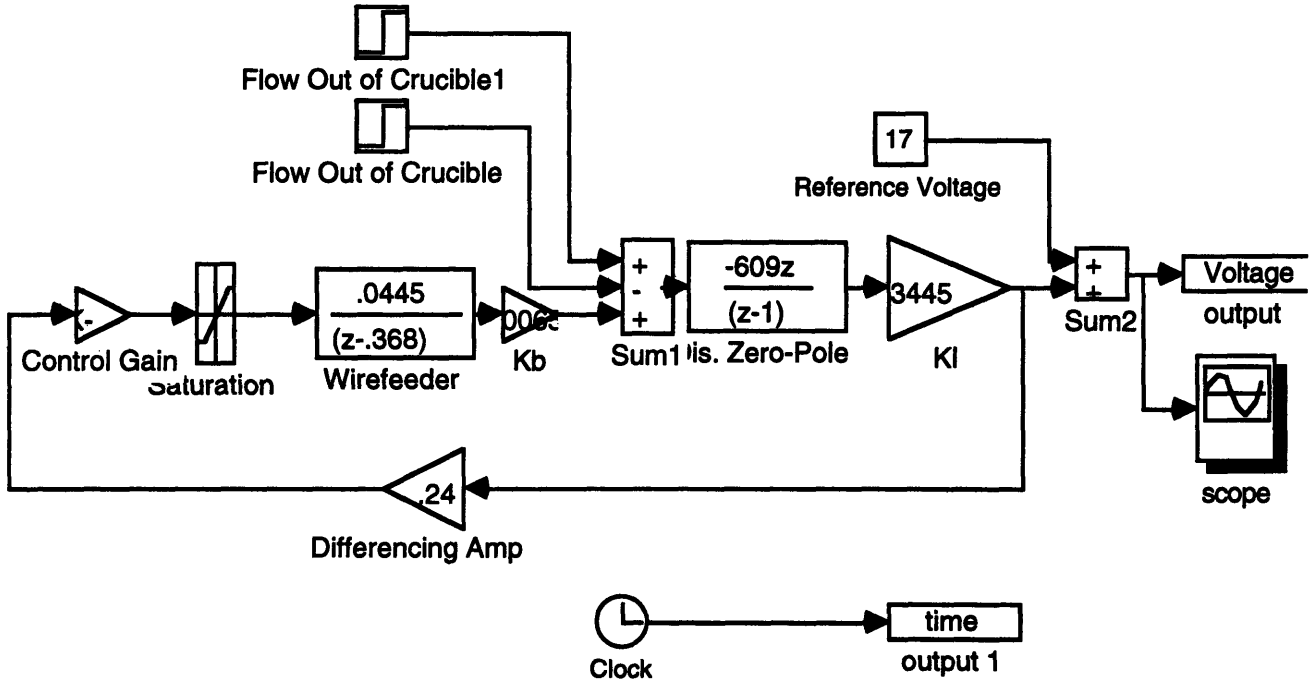

Figure 30: Simulation Block Diagram for Closed Loop Wirefeed Controller

The first simulation was carried out assuming that the sensed temperature is 2200 C, so if the controller is in the on state, the replenishing rate is 40.2 mm^3/sec. The system is responding to a molten metal ejection rate of 100 mm^3/sec. which starts at T=2 seconds and stops at T=5 seconds which is represented by the two step blocks labeled 'flow out of crucible.' The on/off control scheme is represented by a very high gain proportional

controller with saturation limits restricting the magnitude of the control action. The lower magnitude is 0 for the off state and the upper magnitude is the voltage corresponding to the feed rate at 2200 C.

The response is shown in Figure 31. When the flow starts exiting the crucible, a ramp in the arc voltage is observed as expected. After the outflow stops, the molten metal level gets back to the reference level in about 4 seconds.

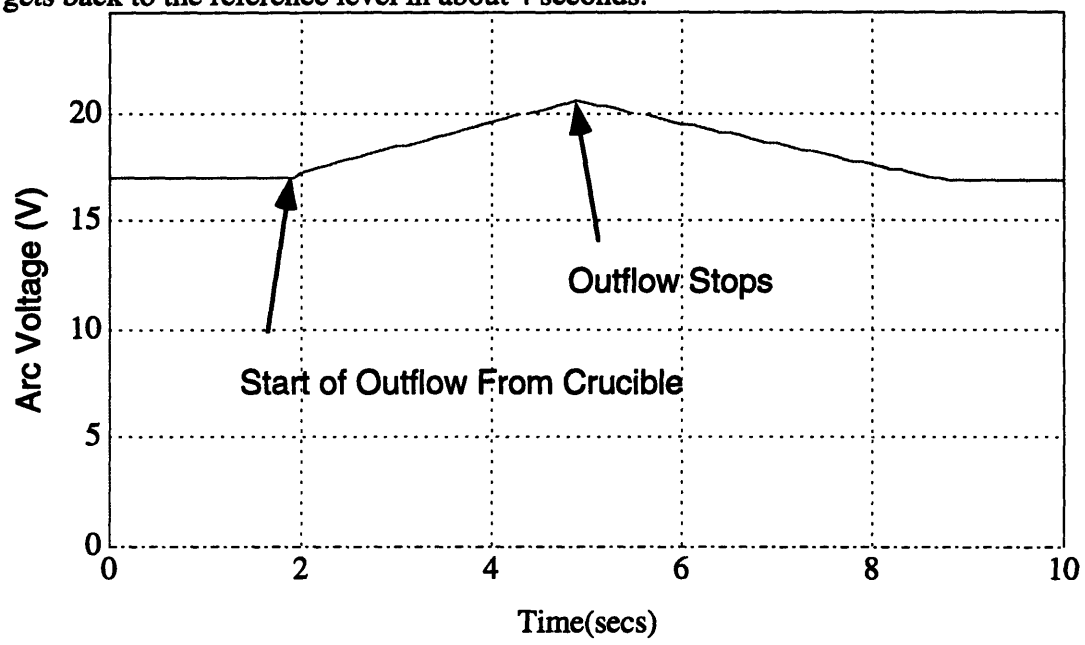

Figure 31: Simulated Closed Loop Molten Metal Level Controller Response (T=2200 C) Replenishing Rate of 40.2 mm^3/sec

Another simulation shows the response at 1650 C, the flow out of the crucible is the same as the above simulation. Notice that it takes roughly twice as long to recover at this lower temperature.

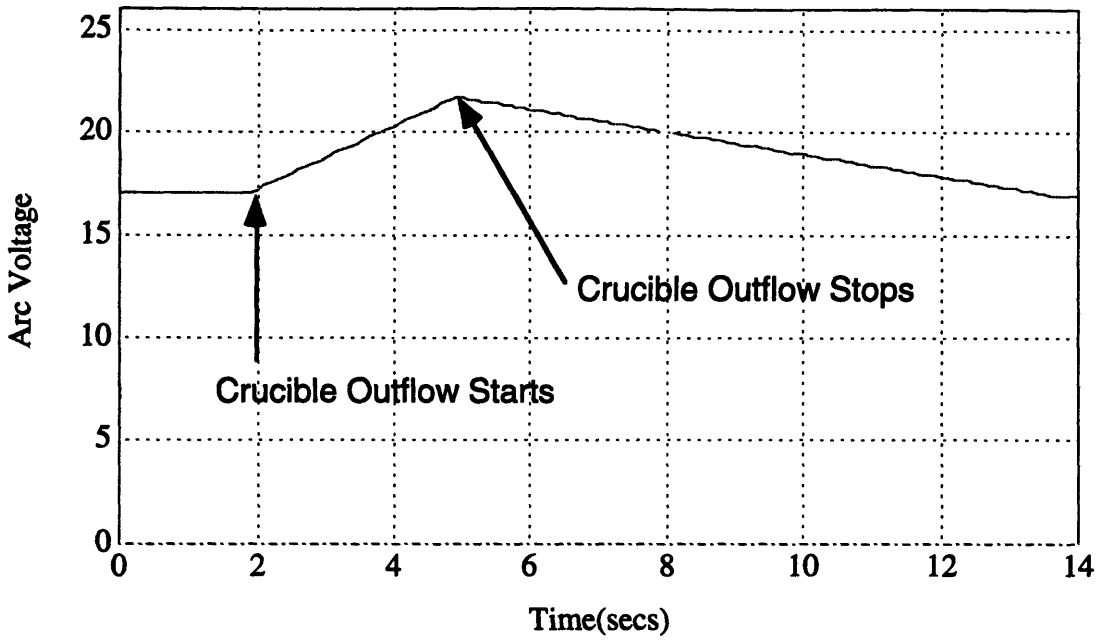

Figure 32: Simulated Closed Loop Molten Metal Level Controller Response (T=1650 C) Replenishing Rate of 19.6 mm^3/sec

From these closed loop responses it is obvious that the wirefeed saturation melting rate limits the performance of the system under continuous, high deposition rate circumstances. However, for intermittent welding where the time average of flow rate is low, the present system could work.

E. Actual Results

For the first closed loop molten metal level control run, no molten metal was expelled from the furnace. The reference voltage was arbitrarily set to some value that was less than the current voltage, so the wire feeder is just filling up the crucible. It was found that feeding wire into the molten metal chamber caused severe voltage fluctuations as shown in Figure 33.

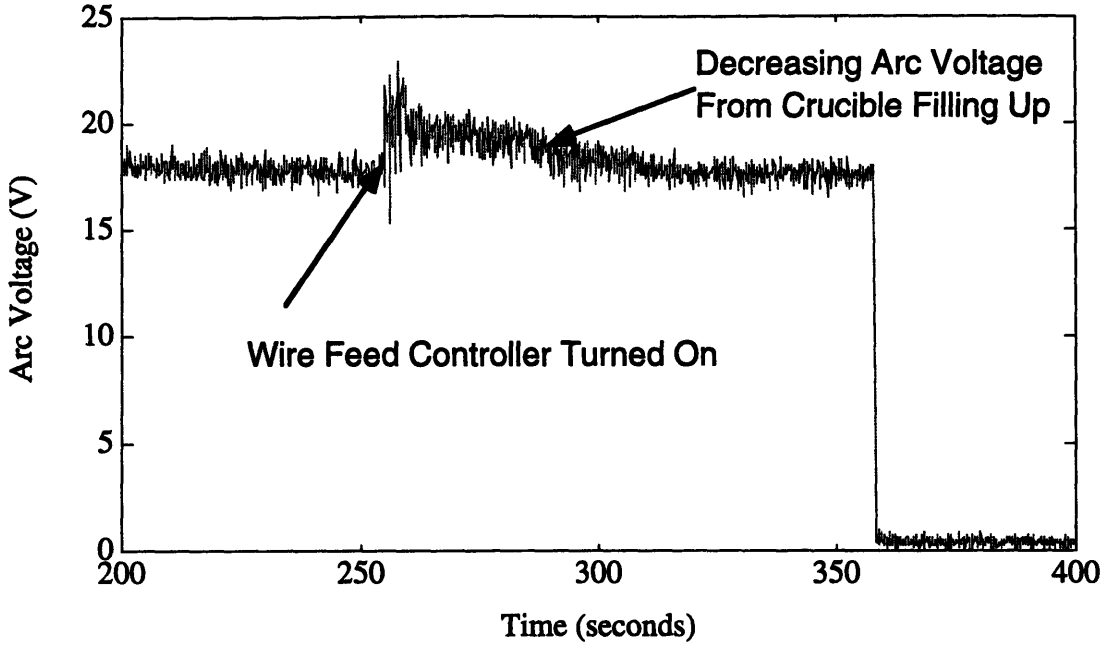

Figure 33: Initial Closed Loop Level Control Response
with a Replenishing Rate of 24.2 mm^3/sec
(from feed512.dat)

Notice that the arc voltage is noisy to begin with, but when the wire feed system is activated the noise level increases and the average arc voltage suddenly increases too. Why the arc voltage suddenly increases is still a mystery, it may be that the wire feeding is inducing some instability in the arc that causes the arc to become spatially non stationary which in effect increases the time averaged arc length. To eliminate the noise, a low pass RC filter was added to the output of the differencing amplifier. The cut-off frequency of the filter is 3 Hz which is 3 times the apparent characteristic frequency of the observed noise. This smoothed out the arc voltage signal dramatically as will be apparent in later responses.

For the data shown in Figure 34, the temperature reference was 1800 C and the wirefeed saturation limit was set to 3.8 cm/sec. Note that this experiment did not incorporate the variable wirefeed limits discussed previously. No metal was ejected, the goal was simply to fill the crucible from some low level corresponding to about 19.6 V to a level that corresponded to 18.6 V. The response is shown below, the controller is activated at roughly T=165 seconds. One can see the odd behavior of the immediate increase in the arc voltage.

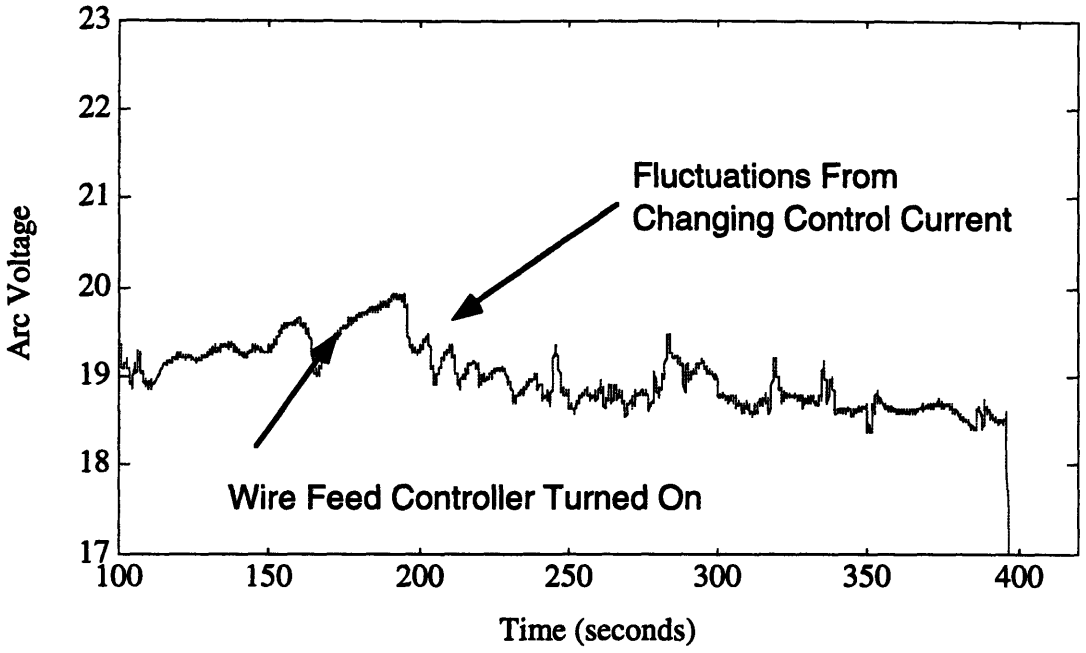

Figure 34: Closed Loop Level Control Response
with a Replenishing Rate of 24.2 mm^3/sec, No Ejection of Molten Metal,
Fluctuating Control Current
(from feed520.dat)

The arc voltage signal is far from the idealistic one in the simulation, but the voltage is decreased to a level below the set point of 18.6 V. The erratic voltage is due primarily to changes in the temperature control current which affects the arc voltage.

In a situation where the arc current is constant, the results of the level controller is more obvious. The following data more clearly shows how the arc voltage steadily decreases down to the desired set point of 15.5 volts, this is with a constant arc current of 190 amps and a constant wire feed rate of 3.8 cm/sec. Here the reduction in arc voltage from filling up the crucible is more obvious.

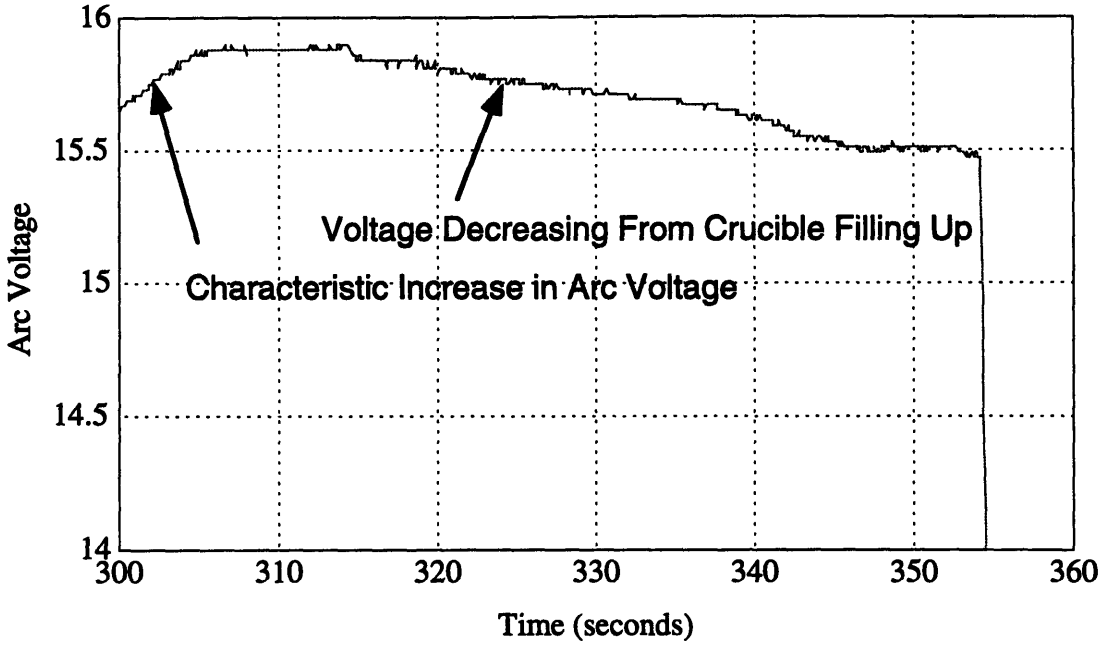

Figure 35: Closed Loop Level Control Response
with a Replenishing Rate of 24.2 mm^3/sec, No Ejection of Molten Metal,
Constant Current Conditions, Controller Turned On at t=300 seconds
(from feed525.dat)

Since the molten metal level is not one of the ultimate outputs being controlled, like temperature and flow of the molten metal, it will not be necessary for it to be as refined. The present system described has operated successfully for a number of experiments and should serve its purpose as long as large sustained flow rates out of the crucible are not desired. However further research must be done to improve the metal replenishing capabilities of the wirefeed system.

Chapter 4: Analyzing the Capabilities of Stream Welding

A. Prediction of Penetration with a Finite Difference Model

In developing this new stream welding process it is important to know its potential to produce desired weld characteristics, such as penetration, given a certain molten metal stream temperature and a certain initial temperature of the workpiece. Here a thermal model is developed using the finite difference method to predict the temperature distribution in a stream welded workpiece as a function of time. From this information it is possible to estimate the penetration of a stream weld. A similar model is also developed for Gas Tungsten Arc Welding (GTAW) which serves as a benchmark in validating the stream welding model. For both situations the weld is being made in the middle of a mild steel bar with a 2 cm x 0.5 cm cross section.

Some simplifications that apply to both models are that the properties of the mild steel are treated as constant, rather than being functions of temperature. Latent heat effects are also neglected. Another assumption for the stream welding model is that the bead and workpiece are treated as a continuum which means their properties are the same and also that there is no contact resistance between the two. The problem of contact resistance would arise in a stream welding situation if the outer layer of the steel stream oxidized before deposition onto the workpiece or if any gases were to get trapped between the deposited metal and the workpiece.

The following symbols are used in this chapter:

$T_{i,j}$ - Temperature of the node in the i^{th} column and the j^{th} row
t - Time (discretized time intervals of .001 seconds)
Δx - Node separation distance in the x direction (.5 mm)
Δy - Node separation distance in the y direction (.5 mm)
ρ - Density of mild steel (7800 kg/m^3)
c_p - Specific heat of mild steel (434 J/kgK)
k - Thermal conductivity of mild steel (60 W/mK)
q - Heat flux into a nodal element
q_{gen} - Nodal heat generation (for GTAW simulation only)
α - $k/\rho c_p$
h - Convective heat transfer coefficient (assumed to be 10 W/m^2K)

a. Generation of Finite Difference Equations

The appropriate form of the heat equation being solved here is

$$\frac{1}{\alpha}\cdot\frac{\partial T}{\partial t}=\frac{\partial^2 T}{\partial x^2}+\frac{\partial^2 T}{\partial y^2}$$

The finite difference form of this equation is obtained using central-difference approximations of the spatial derivatives as given in Figure 36

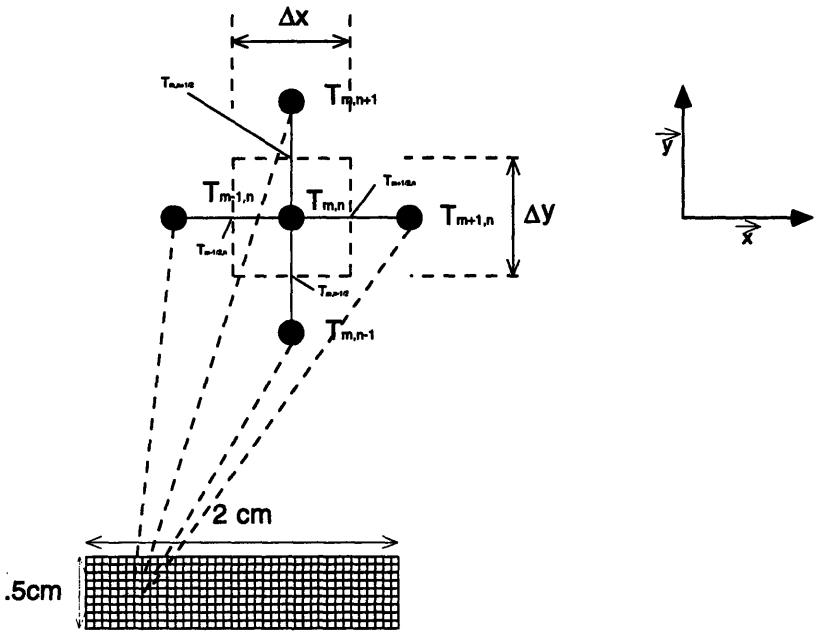

Figure 36: Parameters in Deriving Finite Difference Equation for Internal Nodes

$$\left.\frac{\partial^2 T}{\partial x^2}\right|_{m,n} \cong \frac{\left.\frac{\partial T}{\partial x}\right|_{m+1/2,n} - \left.\frac{\partial T}{\partial x}\right|_{m-}}{\Delta x}$$

$$\left.\frac{\partial T}{\partial x}\right|_{m+1/2,n} \cong \frac{T_{m+1,n}-T_{m,n}}{\Delta x}$$

$$\left.\frac{\partial T}{\partial x}\right|_{m-1/2,n} \cong \frac{T_{m,n}-T_{m-1,n}}{\Delta x}$$

So the approximated second derivative of temperature with respect to x is:

$$\left.\frac{\partial^2 T}{\partial x^2}\right|_{m,n} \cong \frac{T_{m+1,n} + T_{m-1,n} - 2T_{m,n}}{\Delta x^2}$$

The finite difference equation approximating the spatial derivative with respect to y is derived the same way.

$$\left.\frac{\partial^2 T}{\partial y^2}\right|_{m,n} \cong \frac{T_{m,n+1} + T_{m,n-1} - 2T_{m,n}}{\Delta y^2}$$

So the resulting equation for an interior node is (since $\Delta x = \Delta y$)

$$\frac{1}{\alpha}\frac{\partial T_{m,n}}{\partial t} = \left.\frac{\partial^2 T}{\partial x^2}\right|_{m,n} + \left.\frac{\partial^2 T}{\partial y^2}\right|_{m,n} \cong \frac{T_{m+1,n} + T_{m-1,n} + T_{m,n+1} + T_{m,n-1} - 4T_{m,n}}{\Delta x^2}$$

The periphery nodes must account for the convective heat transfer boundary condition and hence the form of the equations is different. The finite difference equations for a left edge node are derived below by applying conservation of energy.

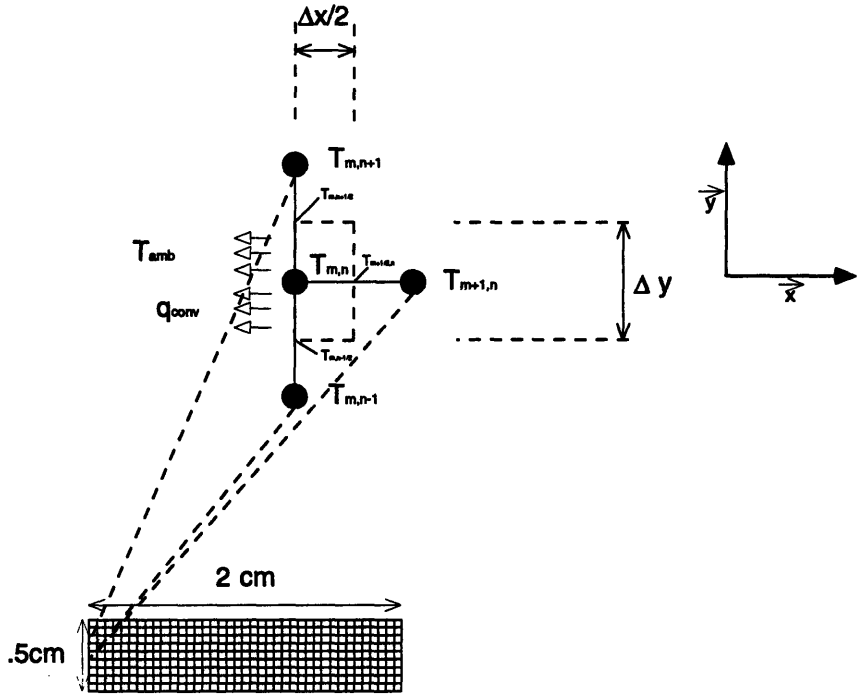

Figure 37: Parameters in Deriving Finite Difference Equation for Exterior Nodes

$$\rho c_p(\Delta x \cdot \Delta y \cdot 1)\frac{dT}{dt} = \sum q_{in}$$

$$\sum q_{in} = q_{(m,n+1)\to(m,n)} + q_{(m+1,n)\to(m,n)} + q_{(m,n-1)\to(m,n)} + q_{conv}$$

$$q_{(m,n+1)\to(m,n)} = k\left(\frac{\Delta x}{2}\cdot 1\right)\frac{T_{m,n+1} - T_{m,n}}{\Delta y}$$

$$q_{(m+1,n)\to(m,n)} = k(\Delta y \cdot 1)\frac{T_{m+1,n} - T_{m,n}}{\Delta x}$$

$$q_{(m,n-1)\to(m,n)} = k\left(\frac{\Delta x}{2}\cdot 1\right)\frac{T_{m,n-1} - T_{m,n}}{\Delta x}$$

$$q_{conv} = h(\Delta y \cdot 1)(T_{amb} - T_{m,n})$$

which result in an equation of the form (again $\Delta x = \Delta y$):

$$\frac{\partial T_{m,n}}{\partial t} \cong \frac{k}{2\rho c_p \Delta x^2}\left[T_{m,n+1} + T_{m,n-1} + 2T_{m+1,n}\right] - T_{m,n}\left[\frac{2k}{\rho c_p \Delta x^2} + \frac{h}{\rho c_p \Delta x}\right] + T_{amb}\left[\frac{h}{\rho c_p \Delta x}\right]$$

Combining all of the interior and exterior nodal equations gives a system of equations of the form

$$\frac{dT}{dt} = AT + Bu$$

T represents the temperature of all of the nodes. The conduction in the solid is characterized in the A matrix and the convective heat transfer is accounted for in both A and the input u. The number of equations is equal to the number of nodes which means A is 400 x 400 for the case of the bar cross section being 2 cm x 0.5 cm with a spatial discretization of 0.5 mm.

The A, B, and u matrices were set up by creating some Matlab metafiles, RATOMATO.M, and RATMAT6.M, for the stream welding simulations, and RATMAT2.M for the GTAW simulation. The following code excerpt shows the formulation of the A matrix interior nodes:

```
for i=1:m*n;                              %m=10 n=40
        a(i,i)=-4*k/(r*cp*dx^2);
                if (i-n)>=1,
                        a(i,i-n)=1*k/r*cp*dx^2);
                end
                if (i+n)<=m*n,
                        a(i,i+n)=1*k/r*cp*dx^2);
                end
                if (i-1)>=1,
                        a(i,i-1)=1*k/r*cp*dx^2);
                end
                if (i-1)<=m*n,
                        a(i,i+1)=1*k/r*cp*dx^2);
                else
                end
end
```

Most of the if-statements are to ensure that numbers are not placed outside the boundaries of the matrix. The rest of the code for the programs mentioned above is in Appendix B.

After formulating the matrices A, B, and u, the system of equations was solved to get the temperature in the bar as a function of time. Simulink was used to solve the system using the state space block diagram given below:

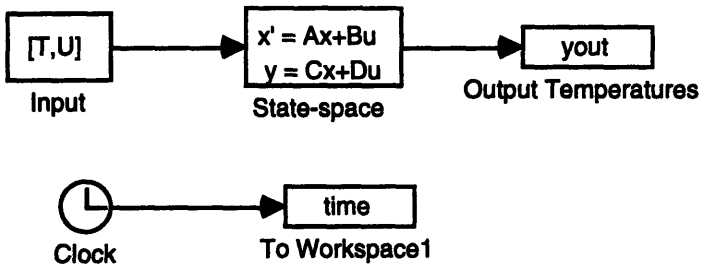

Figure 38: Simulink Block Diagram for Simulation

In solving this system of equations Simulink uses the explicit method in solving for temperature as a function of time. The simulated time duration was 1 second and the time discretization interval was 0.001 seconds, both of which proved adequate. Smaller time increments would have increased the already lengthy computation time while significantly longer time steps (an order of magnitude larger) would cause numerical instabilities in the simulation. The simulated duration was chosen to be 1 second since maximum penetration is typically achieved in 0.05 to 0.3 seconds.

b. GTAW Model

The GTAW model was developed to reinforce the validity of the thermal models being developed since simulation results can be readily compared to an actual GTA weld. This model was also developed to eventually compare resulting characteristics, such as penetration, with the stream welding process.

First, the actual GTAW process is described, and then the simplified finite-difference model is presented along with accompanying assumptions and conditions. The situation being modeled is a typical one, the torch is traversing at 1 cm/sec along a mild steel bar with cross section dimensions of 2 cm x 0.5 cm. The arc voltage is 15 V and the arc current is 100 A, which results in a heat input of 1500 W. The heat flux is distributed similarly to a Guassian Distribution. Given the geometry of the workpiece, the standard deviation of an arc with the above power input is roughly 1.5 mm [Masubuchi, 1980]. Figure 39 depicts the situation pictorially

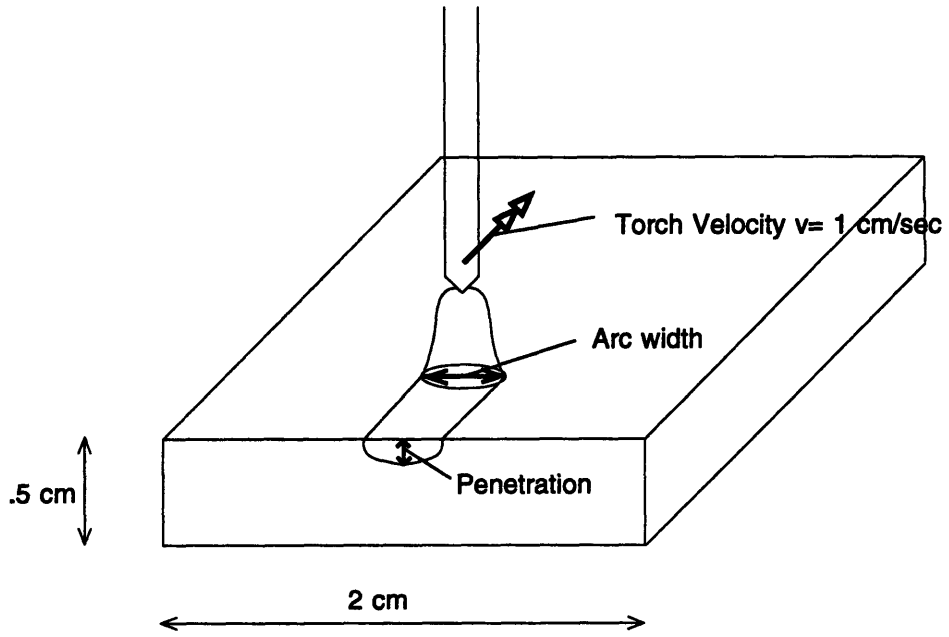

Figure 39: GTAW Process

A 2-Dimensional model was developed for the GTAW process described above to predict the temperature distribution in a stationary cross section as the torch passes by the cross section. The discretized cross section is given in Figure 40:

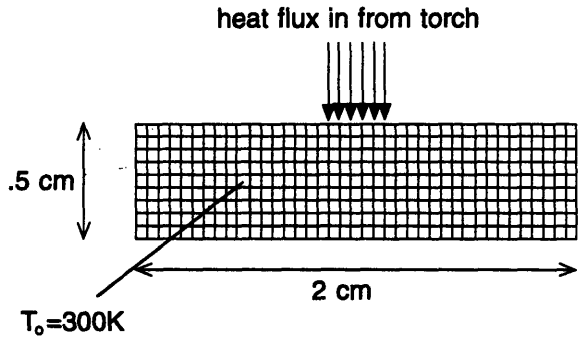

Figure 40: Cross Section used for GTAW Model

The heat flux from the torch is treated as heat generation in the top center nodes. Since the heat flux of the arc has a standard deviation of 1.5 mm, the heat flux is chosen to be distributed over the top six nodes, a 3 mm width. The magnitude of the heat flux into each node is based on the 1500 W input from above. Since the unit thickness of the cross section is 1 m as derived in the previous generation of equations section, the heat flux per node can be calculated as follows:

$A_1=(1.5mm)^2*\pi$ (area of heat influx in actual GTAW)

$A_2=3mm*1m$ (area of heat influx in simulation nodes have unity (1m) thickness)

Simulation Power Input= A_2/A_1*1500 Watts= 636,000 Watts

Power generated per node=636,000/6 nodes=106,000 Watts/node

In reality, the heat generated per node will be considerably less than 106,000 Watts since there will be losses in the form of radiative heat transfer away from the arc as well as conduction up the electrode. The typical arc efficiency, defined as the percentage of the arc energy that is supplied to the workpiece, for GTA welding mild steel is between 21-48% [Masubuchi, 1980]. Here an efficiency of 45% will be assumed, which means the generation will be 47,700 Watts/node.

The duration of the heat flux into the cross section is found from knowing the velocity of the torch and the width of the arc in the direction of the weld seam. Since the arc can be considered axisymmetric, the width of it in the direction of the weld seam is the same as that transverse to the weld seam which is 3 mm as described above. Figure 41 below shows that the duration of 0.3 seconds is found by simply by dividing 3 mm by the torch velocity.

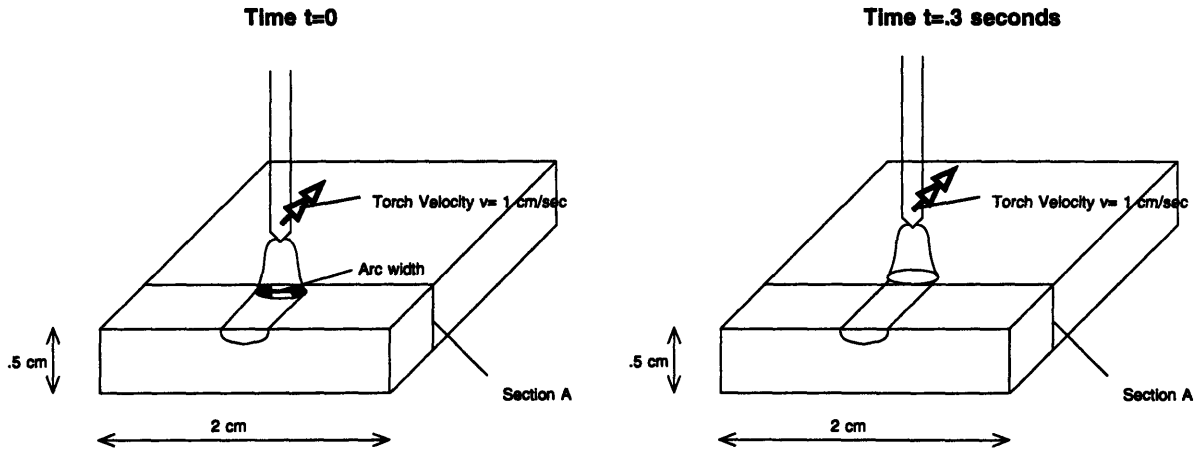

Figure 41: Determination of Heat Flux Duration

Before the heat flux is incident on the cross section, it is assumed to be at 300K, which is the initial condition on all of the nodes. In reality though, the initial temperature will be higher than this since heat is being transmitted ahead of the torch. There will also be some post heating, but both of these effects are neglected. Neglecting these effects will result in simulation results that predict less penetration than would actually occur. This

will be taken into account when analyzing results and comparing them with the stream welding process. The boundary conditions are natural convective cooling at all of the periphery nodes with a convective cooling coefficient of h=10 W/m^2K.

Overall the penetration predicted by the model was a little less than reality as expected. The figures on the following page show the progression of the temperature with time. The maximum penetration is achieved at t=.3 seconds and is approximated by the area above the temperature that corresponds to the melting temperature of steel (1803 K). The penetration appears to be about 1.2 mm from the contour plot of the temperature distribution at t = .3 seconds. A real GTA weld made in similar circumstances had a penetration of 2 mm, a cross section of this weld is shown in Figure 42.

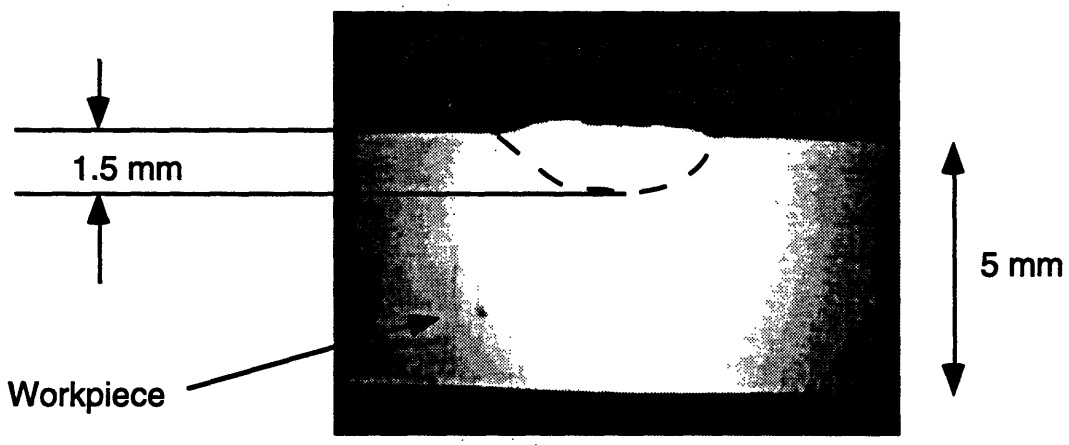

Figure 42: Cross Section of GTA weld at 100A and approximately 15 V

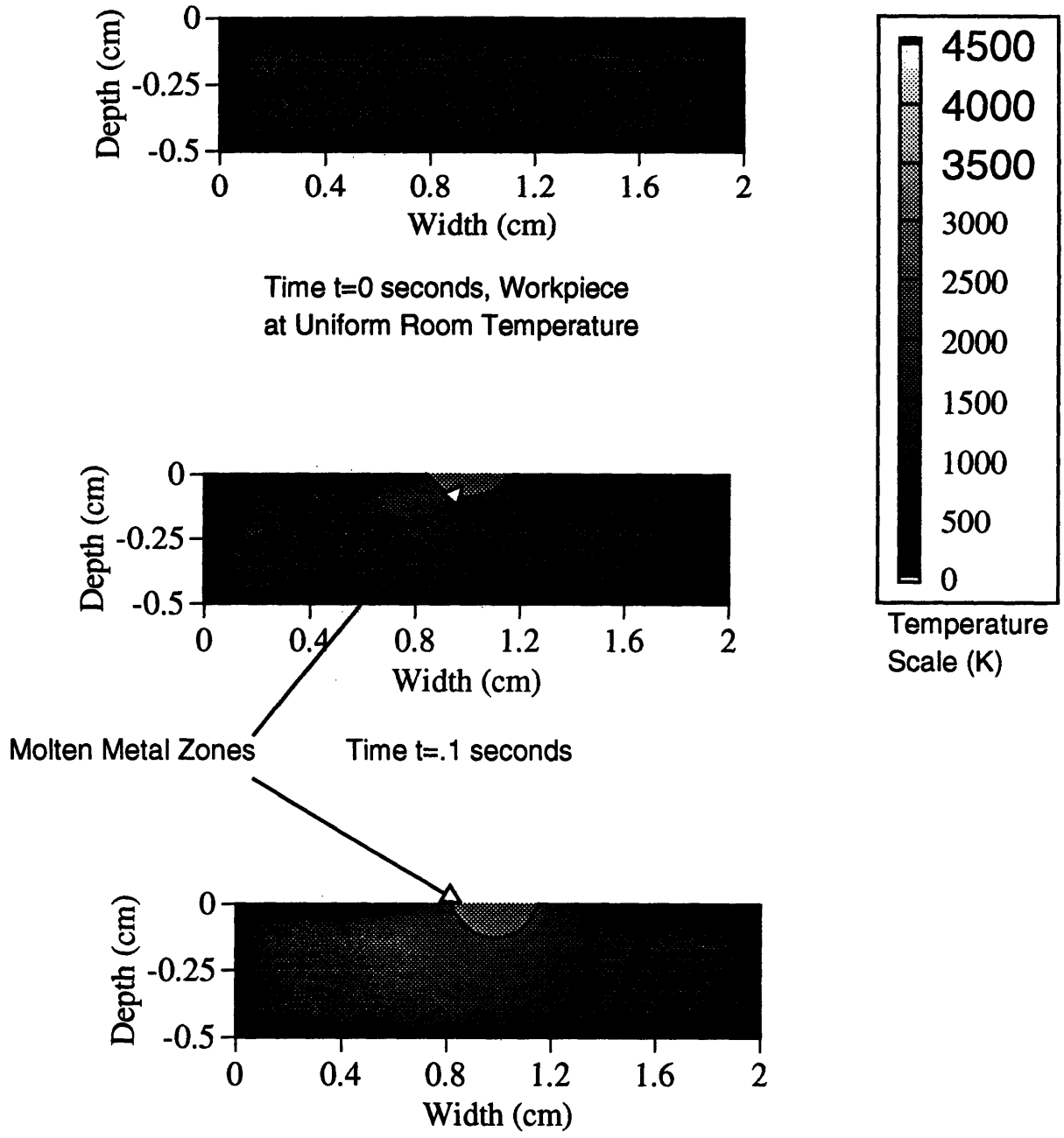

Figure 43: Simulated Temperature Distribution for Gas Tungsten Arc Welding (GTAW)

c. Stream Welding Model

Three different stream welding simulations are presented here to show the resulting temperature distributions as a function of time, the resulting penetration can then be compared to the results of the GTAW simulation. In case 1, the molten metal stream initially at 2900 K, is deposited directly on top of the workpiece that is initially at room temperature (300 K). In case 2, the molten metal is deposited on a workpiece preheated to 1000 K. In case 3, the molten metal is deposited into a groove in a workpiece which is at 300 K.

The main difference between modeling the Stream Welding and GTAW processes is the way that the heat is imposed on the workpiece to make a weld. For the GTAW, there is a well defined power input that is modeled as a specific heat generation in the 6 top center nodes. For the stream welding case, a well defined bead of molten metal at a well defined temperature is deposited on the workpiece.

A schematic of the model for case 1 is shown below

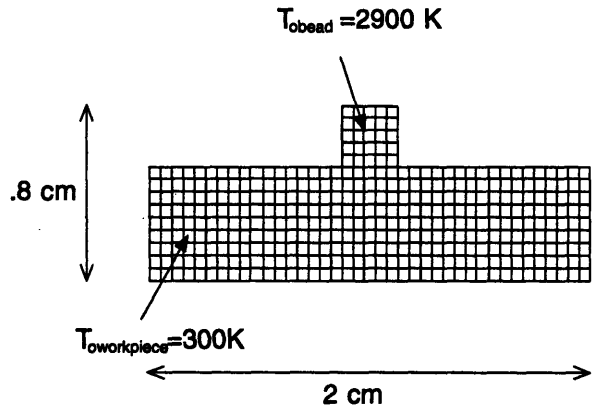

Figure 44: Cross Section used for Stream Welding Models (Case 1)

The modeled bead geometry is square with a 3 mm x 3 mm bead and is initially at a temperature of T_{obead}=2900 K. The initial conditions for the workpiece for case 1 are that it is at an initial temperature of 300K. The boundary conditions for all of the periphery nodes of the workpiece and bead are convective heat transfer with the same convective heat transfer coefficient as the GTAW simulation (h =10 W/m^2K), this boundary condition also applies to all of the following stream welding cases.

The case 2 simulation is nearly the same as case 1, the main difference is that the workpiece is preheated to 1000 K. This simulation was carried out to see if the penetration depth can be significantly improved through preheating the workpiece.

For case 3, the geometry of the workpiece and bead are shown in the Figure 45.

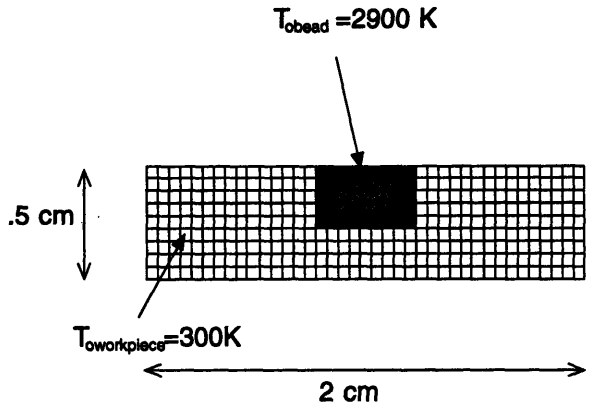

Figure 45: Cross Section used for Stream Welding Model (Case 3)

The workpiece initially has a groove that is being filled with molten metal at 2900 K. This situation more closely resembles a butt-weld situation.

The model predicted significantly less penetration will occur for stream welding than for GTA welding, again the penetration is predicted by locating how far the isotherm corresponding to the melting temperature of steel extends into the workpiece. The evolution of the temperature with time is shown for all three stream welding cases in Figures 47, 48 and 49. All three situations predict little if any penetration.

The heat is dissipated away from the deposited metal most quickly in case 3. This simulation predicted no penetration at all, which means this welding geometry should probably be avoided unless the workpiece is substantially preheated. A cross section where the molten metal stream is actually deposited in a groove is shown in Figure 46 below. Notice that the heat is extracted from the molten bead so quickly that it solidifies before filling the groove. The molten stream was initially at a temperature above 2000 C although the magnitude above 2000 C is unknown since the pyrometer cannot presently measure higher than this, this is the case with all of the actual cross sections of stream welds presented in this chapter.

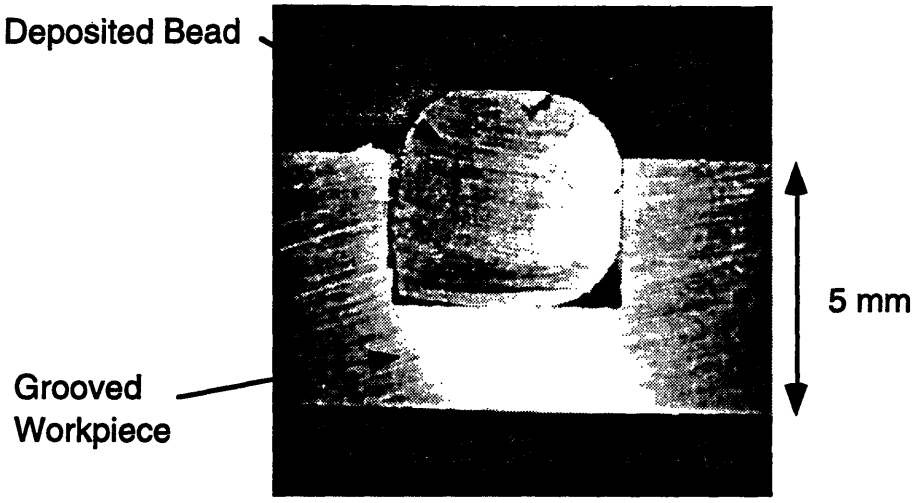

Figure 46: Stream Weld with Bead Deposited in Groove

For the first two simulation cases one can see that the top center nodes nearly reach the melting temperature of steel which mean that good adhesion may be achievable for both of these situations. Although the model predicts no penetration for cases 1 and 2 it turns out that penetration was achieved without a preheated workpiece as shown in Figure 50. This slight but significant discrepancy between the model and reality can be accounted for by the previously mentioned model simplifications. This discrepancy indicates that there would be better penetration if the workpiece is preheated.

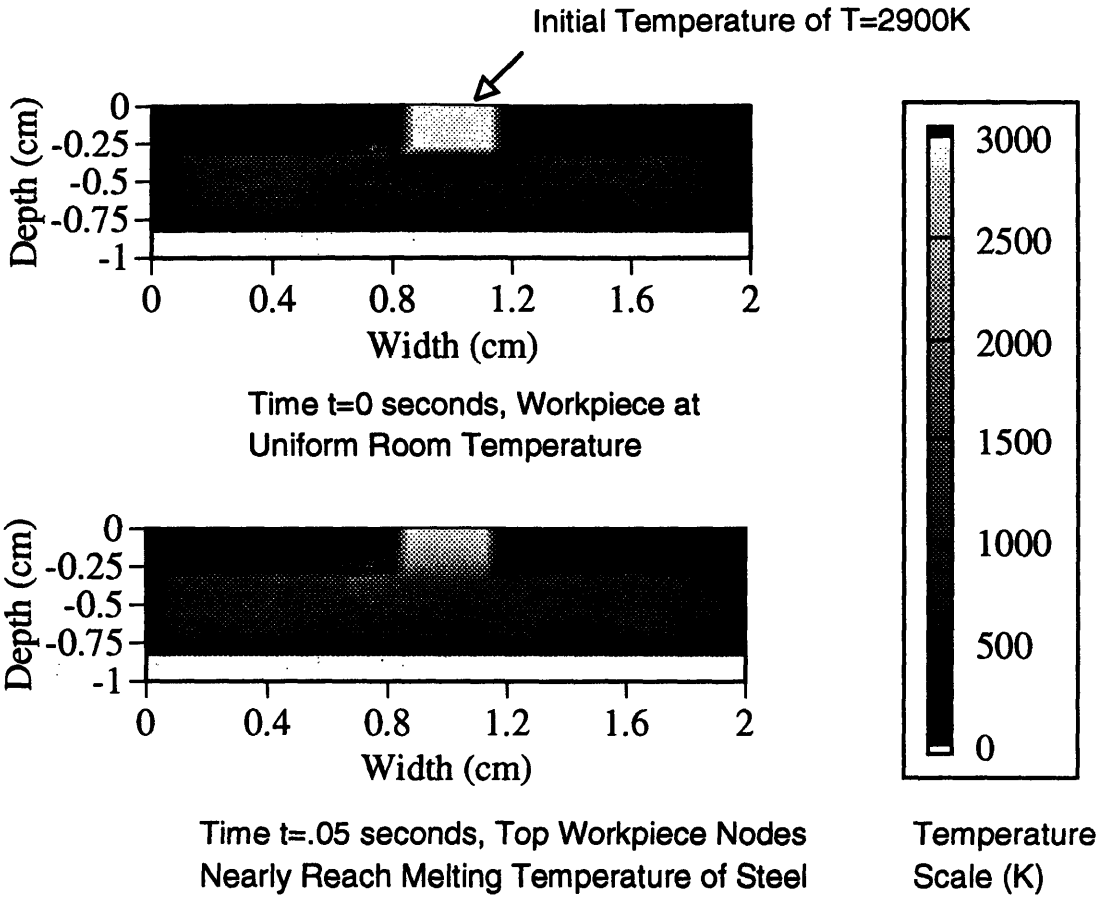

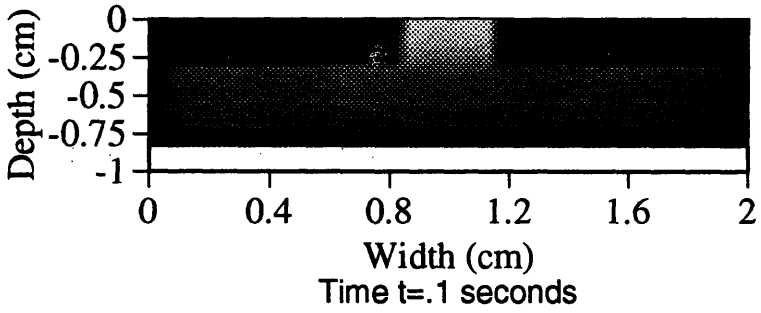

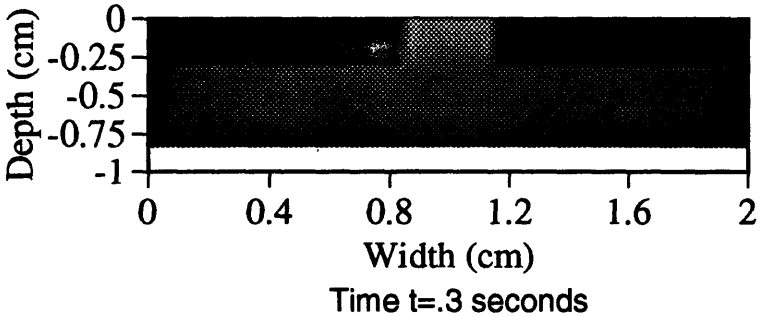

Figure 47: Simulated Temperature Distributions for Stream Weld on Non-Preheated Workpiece

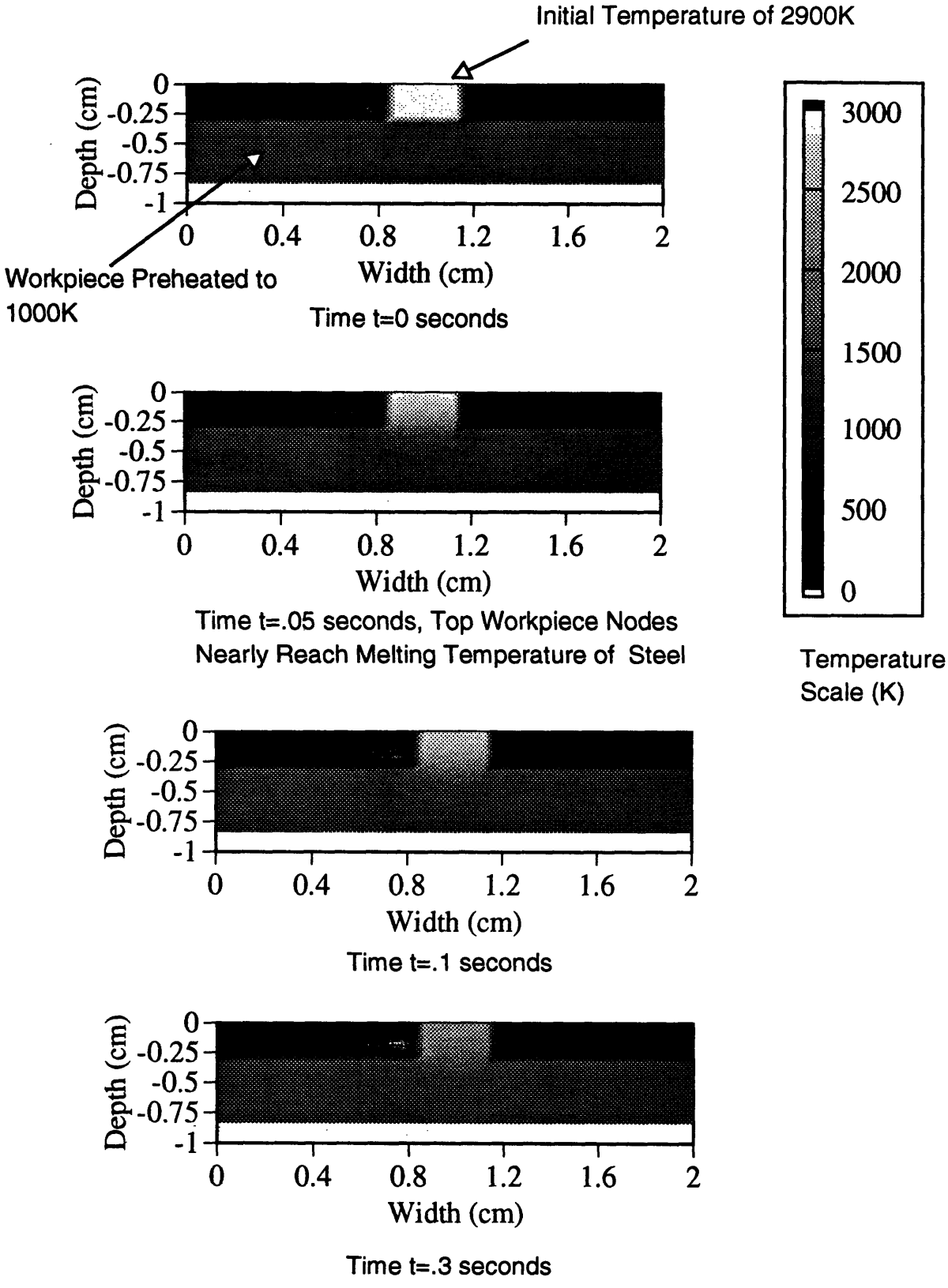

Figure 48: Simulated Temperature Distributions For Stream Weld on Preheated Workpiece

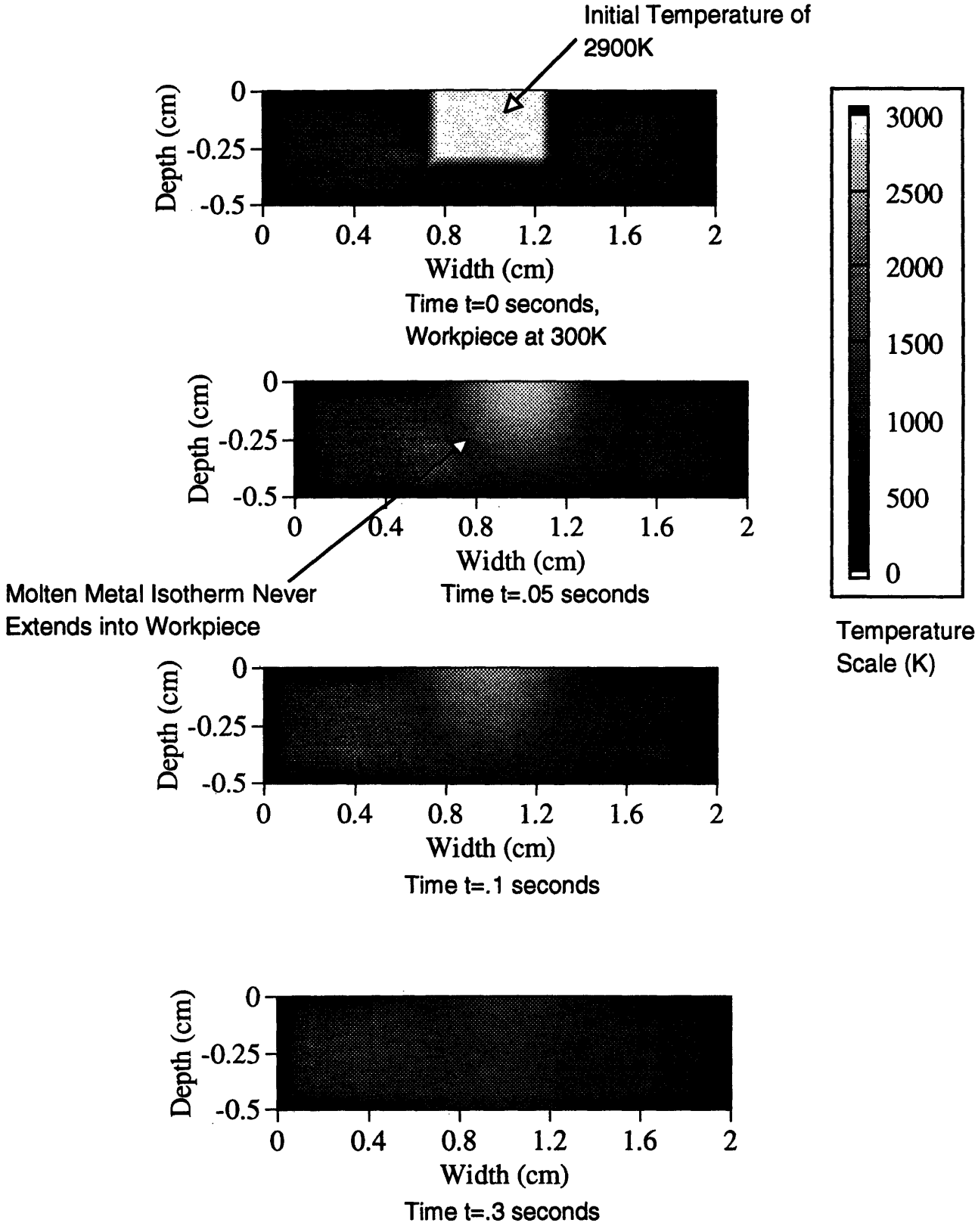

Figure 49: Simulated Temperature Distributions for Molten Metal Deposition in Grooved Work Piece

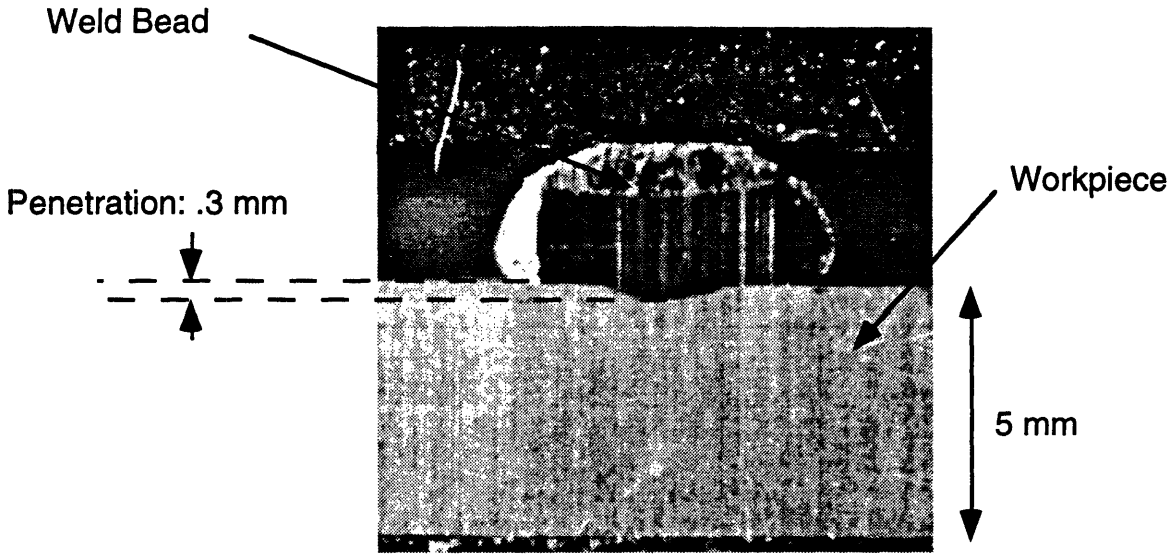

Figure 50: Stream Weld without Preheated Workpiece

It is important to note here that this deposited bead is approximately 25% tin by volume.

Because of all of the assumptions previously mentioned, this model does not predict the exact penetration. It does, however, give a good indication of the minimal penetration achievable with stream welding which was shown from the experimental results given above. Although stream welding is not capable of the penetration of more conventional welding processes, this does not eliminate the possibility of making good welds with this process. With most conventionally designed weld joints, penetration is important, however it may be possible to design weld joints where only minimal penetration is necessary to making a good weld.

B. Characterizing Beads Made Thus Far

Although a flow control system does not yet exist for the stream welder it is possible to manually control the flow with the valve regulating molten metal chamber pressure. Under these circumstances, a number of 'weld' beads were made to characterize them and get a better idea of how to approach the closed loop flow control system and identify any peculiarities that may need to be dealt with.

Figure 51, 52 and 53 show three beads made with a sensed temperature of 1900 C. For Figure 51 the cross section dimensions are .8mm x 5.08 cm, substantial distortion in the workpiece occurred in this case. The workpiece cross section dimensions for Figure

52 and 53 are .5cm x 5.08 cm. The workpieces are all 5.7 cm below the crucible exit orifice and traversing at a constant velocity of 10 mm/sec while the stream is being deposited. No significant penetration was achieved for any of the beads due to the relatively low stream temperature of 1900 C; the purpose here was not necessarily to make a good weld but to document the character of the beads made under known conditions which meant that the sensed temperature had to be less than 2000 C.

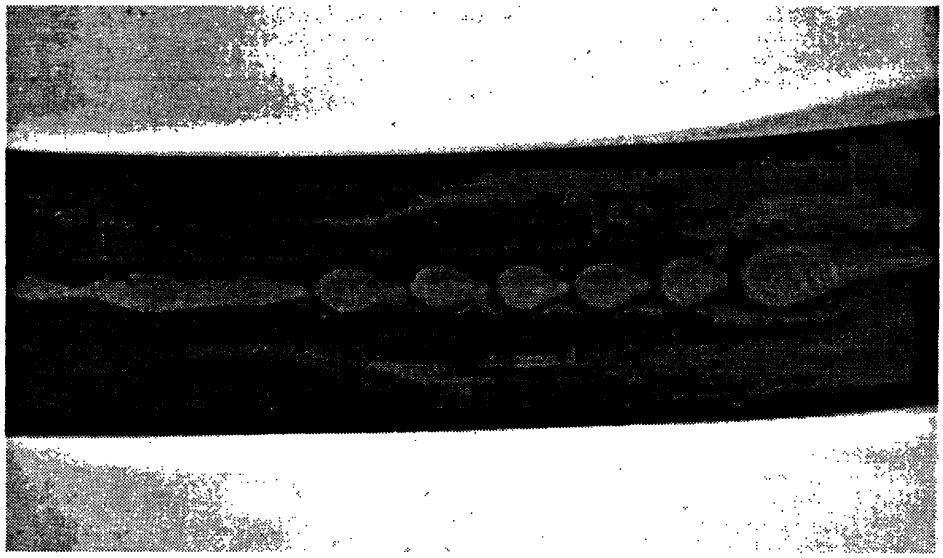

Figure 51: Bead Deposited on Workpiece of Cross Section Dimensions .8mm x 5.08 cm

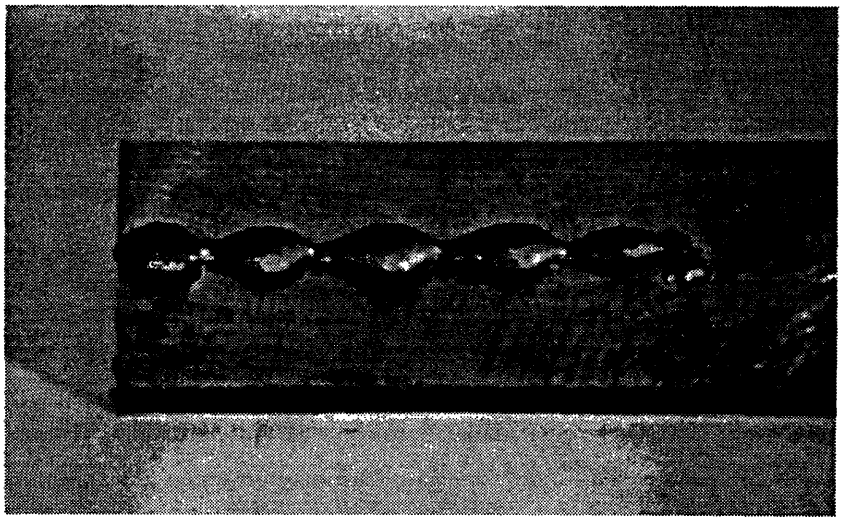

Figure 52: Bead Deposited on Workpiece of Cross Section Dimensions 5mm x 5.08 cm

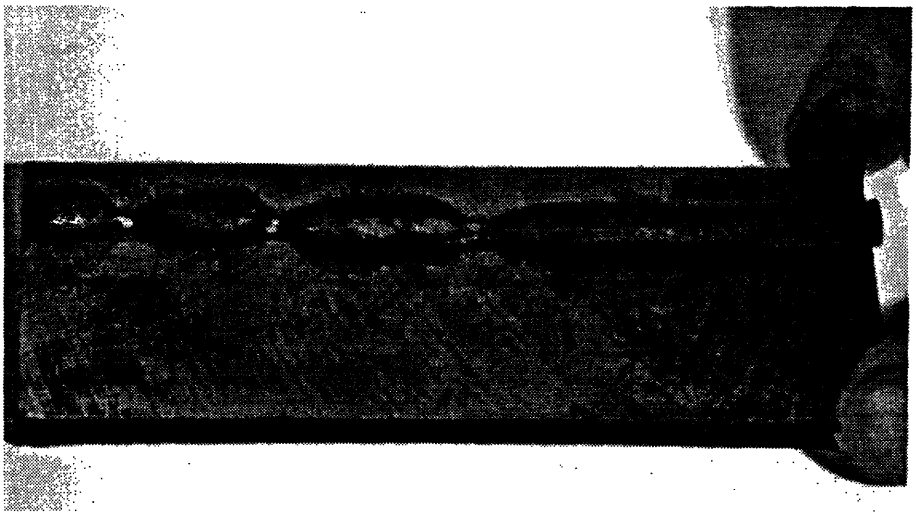

Figure 53: Bead Deposited on Workpiece of Cross Section Dimensions 5mm x 5.08 cm

All of the beads appear to have an undulating bead size. These undulations were probably not caused by variations in the molten metal flow rate since the pressure regulator was fixed at one setting and visually the stream appeared to have a constant flow rate. Considering these conditions, it is likely that these undulations are caused by surface tension flows due to temperature gradients on the surface of the molten steel. However with the bead in Figure 53 the undulations vanish halfway along the bead. The bead itself also widens as the undulations stop which indicate that the flow rate increases at this point. This increase in flow rate is a result of enlargement of the graphite exit orifice from wear imposed by the steel flow.

A number of other beads were deposited other than the ones shown in the previous figures and most of these were made under even less controlled circumstances. From all of the bead depositing experiments thus far it is apparent that two things must happen to have a successful flow controller. First a more wear resistant material must be found since graphite has proved inadequate. The graphite exit orifices are typically worn to the extent of being many times bigger than their original size after depositing beads less than 30 cm in length. After the problem with crucible material has been solved it will be necessary to do more refined experiments that include some way to sense the flow rate of the molten metal. Measuring the flow rate is not a trivial problem for a substance that is at these extremely high temperatures, but its essential if there is to be precision control of the flow rate.

Chapter 5: Addressing Problems with Present Prototype

A. Overview of Problems with Present Prototype

For stream welding to become a viable manufacturing process, there are a few problems with the present design that need to be overcome. The main problem is the diffusion of the graphite from the crucible into the molten steel. This has resulted in high carbon welds and is also the reason behind the erosion of the exit orifice. Erosion of the exit orifice is a severe problem because it has a negative effect on the stability of the stream and changes the pressure vs. flow relationship. The photograph in Figure 54 depicts this problem. One can see that not only is the exit orifice thoroughly worn, but substantial amounts of the crucible wall have eroded.

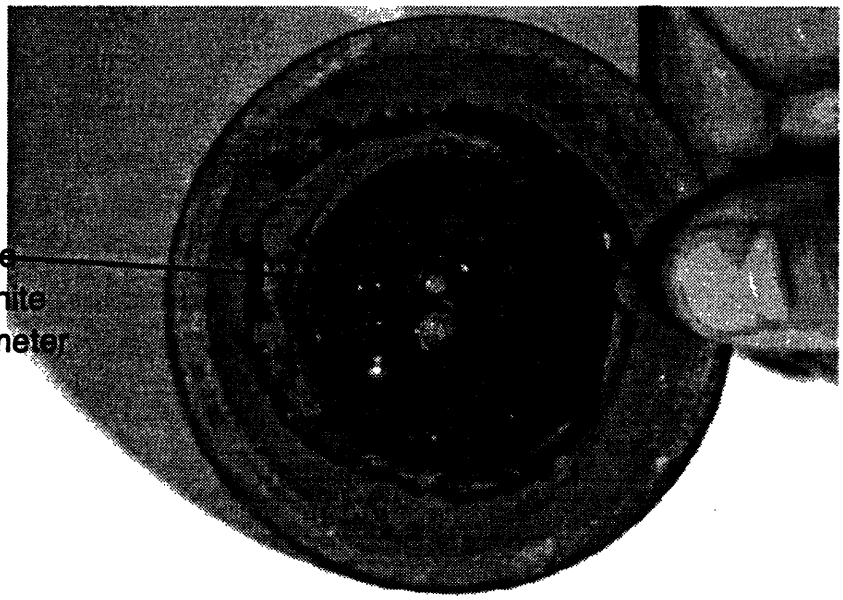

Figure 54: Graphite Crucible Damage from Diffusion into Steel

These conditions will have to be corrected since one of the objectives of this process is to precisely control the flow out of the crucible.

Another problem, that has been improved upon but needs further improvement, is not being able to replenish the molten metal as fast as it is ejected out of the furnace as discussed in chapter 3. Some other important, but less crucial, aspects of the welder could also be improved, such as making it more compact, increasing the thermal bandwidth, and making it easier to assemble and disassemble. In this section, two redesign options will be presented which strive to solve these problems from two

different approaches. The first approach keeps the crucible as the negative electrode, as with the present prototype, which means finding a material that has a high melting temperature and is electrically conducting like graphite, but is more wear resistant and does not react or diffuse into steel at elevated temperatures. The second approach introduces an additional tungsten electrode and does not use the crucible as the negative electrode. This gives the design flexibility in using a crucible material that does not have to be electrically conductive and may be less prone to diffusion into molten steel. AutoCAD drawings of each design are given in Appendix A.

B. Crucible Redesign

a. Available Materials

The first approach that keeps the crucible as the negative electrode means that the crucible material must be electrically conductive, have a high melting temperature (at least 2500 C), resistant to thermal shock, unreactive with steel at elevated temperatures and also wear resistant at these elevated temperatures. Very few materials meet all of these requirements. Some that may are given in Table 1 below. Relevant properties and typical uses are also given in this table. Properties such as thermal expansion, thermal conductivity, and hardness are included to get an idea of thermal shock resistance, machinability, and wear resistance.

Table 1: Properties and Uses of, Electrically Conducting, High Temperature Materials

Material	**Properties/Relevant Uses**
TiC	Electrode sheaths of thermocouples for measurement of temperature up to 2500 C, has high temperature strength Specific electrical resistance: 52.5 μohm/cm Thermal Expansion Coefficient: 7.74×10^{-6} 1/C Thermal Conductivity: .46 J/cm C sec Hardness (Rockwell C scale): 93 Melting Temperature: 3150 C

TiB_2	Resists the action of molten metals, been used for crucibles for precision melting. Resistant to scaling Specific electrical resistance: 14.4 μohm/cm Thermal Expansion Coefficient: $8.1x10^{-6}$ 1/C Thermal Conductivity: .264 J/cm C sec Hardness (Rockwell C scale): 86 Melting Temperature: 2980 C
ZrB_2	Electrode sheaths for high temperature thermocouples for measuring temperature of molten steel, cast iron, nonferrous and rare metals, and their alloys. Resistant to scaling Specific electrical resistance: 16.6 μohm/cm Thermal Expansion Coefficient: ? Thermal Conductivity: .264 J/cm C sec Hardness (Rockwell C scale): 84 Melting Temperature: 3040 +-100C
ZrC	Crucibles, boats, tubes. Resists the action of molten metals Specific electrical resistance: 50 μohm/cm Thermal Expansion Coefficient: $6.73x10^{-6}$ 1/C Thermal Conductivity: .4186 J/cm C sec Hardness (Rockwell C scale): 87 Melting Temperature: 3530 C
TiN	Coatings on titanium and graphite components, high electrical conductivity, resistant to action of molten metals Coefficient of Thermal Expansion: $9.35x10^{-6}$/C Specific electrical resistance: 25 μohm/cm Thermal Expansion Coefficient: $9.35x10^{-6}$ 1/C Thermal Conductivity: .293 J/cm C sec Hardness (Rockwell C scale): 75 Melting Temperature: 3205 C

SiC	High electrical resistance, thermal shock resistance, coatings of graphite. Specific electrical resistance: >.05x10^6 μohm/cm Thermal Expansion Coefficient: 5.68x10^{-6} 1/C Thermal Conductivity: .4186 J/cm C sec Hardness (Rockwell C scale): 70 Melting Temperature: 2827C
Sintered Tungsten (W)	High melting temperature, Rockwell hardness of 32 (c scale)-machinable, high electrical conductivity. May creep under its own weight at elevated temperatures. Specific electrical resistance: 5.5 μohm/cm Thermal Expansion Coefficient: 7.74x10^{-6} 1/C Thermal Conductivity: .174 J/cm C sec Hardness (Rockwell C scale): 32 Melting Temperature: 3422 C
Graphite (C)	High electrical conductivity, reacts with oxygen, low hardness-easily machined Specific electrical resistance: 200 μohm/cm Thermal Expansion Coefficient: .66x10^{-6}/C Thermal Conductivity: 8.2 J/cm C sec Hardness (Rockwell C scale): very low Temperature: 3870 C

Graphite was used for the first design not only because is supposedly meets the criteria mentioned above, but it is also inexpensive and relatively easy to machine. It was also highly recommended [Lee quoting Campbell, 1993]. Campbell states that graphite is an excellent material for containing both high and low carbon molten steels; however our application has shown problems as previously mentioned. The discrepancy may be attributed to the temperatures in this application exceeding 2000 C where it seems that steel and graphite have an affinity for one another.

It should be noted here that no data was found concerning the chemical reactivity of any of the above materials with steel above the temperature of 1620 C. This lack of available data means the only definite way to determine if the materials are suitable is to test them. From reactivity data and descriptions of typical uses, one can get a good idea of which materials will be more chemically inert to molten steel. Zircon diboride does

not react with steel at 1620 C [Samsonov, 1964], while titanium diboride and titanium carbide react slightly at this temperature [Samsonov, 1964]. Silicon carbide reacts slightly with steel above 1600 C [Samsonov, 1964]. Titanium nitride does not react with steel at 1620 C [Samsonov, 1964]. Tungsten reacts slightly with steel at high temperatures, but tungsten seems like a good candidate since it or a tungsten-rhenium alloy is typically used as the electrode material for GTA welding of steel. No data was found concerning reactivity of zircon carbide. This reactivity data is somewhat ambiguous although it is worded the same in Samsonov's book. Its difficult to know what is meant by 'slightly reactive.' From the above information, it looks like titanium nitride, zircon diboride or possibly tungsten are good candidates for replacing graphite as the crucible material.

An important limitation is availability and price of these desirable materials, graphite is the only low cost crucible material ($75 per crucible), the other materials are much more expensive and very expensive to machine as well. The unmachined tungsten stock for one crucible cost $125 alone, the machining costs will be even higher in this low volume production situation. The rest of the materials are impossible to machine in a conventional way due to their high hardness. The way these materials are typically formed is through a successive chemical vapor deposition process or Electro-Discharge Machining (EDM). To give an idea of the cost of EDMing, it cost $100 to machine the 0.012" exit orifice hole in a tungsten crucible. Taking the cost of the materials above into account, a good alternative is to machine a graphite crucible and coat it with one of the other materials listed above using chemical vapor deposition. Many carbide cutting tool inserts are coated with TiN and it is possible to coat Graphite with TiN, SiC and ZrB_2 [Bowman, 1968] [Samsonov, 1964].

A coated graphite crucible should prove to be much more economical than a crucible made purely of any one of the other materials above. There are a number of companies that do SiC coatings, one company was located that does TiN coatings, but none were found that do ZrB_2 coatings. To get two crucibles coated with TiN the cost is $250 and for SiC coatings the cost is roughly $400.

There are some possible problems associated with coating the crucibles and the main one is cracking due to the graphite having a different coefficient of thermal expansion than the coating material. The problem was discussed with a materials coating engineer from Dallas Ceramics who says cracking is not a problem as long as the graphite is coated at a temperature that is higher than any future operating temperature, but the coatings are usually applied well under 2000 C. The problem was also discussed with a technical representative from MTC Carbide Group, a company that can do TiN and SiC

coatings. He said the coatings done at his company have not been tested at temperatures above 1600 C, but there is a high chance cracking will occur above this temperature. He also said that it would be impossible to coat the small diameter (0.012") exit orifice.

Since its impossible to coat the interior of an exit orifice and also since the exit orifice will probably be subject to some erosion no matter what material is used, it is proposed here to have the exit orifice consist of an insert that is easy to remove and replace. This way, a worn exit orifice can be discarded and replaced with a new one. The redesigned crucible is shown in the AutoCAD figures in Appendix A1. The insert will made of the material that proves to be the most durable. It should be noted here that the insert does not have to be electrically conducting because the electricity can still flow through the molten metal to the conducting crucible. The fact that the insert does not have to be electrically conductive adds to the selection of possible materials of which it will be made. The properties of some high temperature yet electrically insulating materials are given on the following table.

Table 2: Properties and Uses of, Non-Electrically Conducting, High Temperature Materials

Material	**Properties/Typical Uses**
BN	Good Refractory material, used for refractory coatings of molds and crucibles, refractory pouring spouts. Coefficient of Thermal Expansion: 7.51×10^{-6}/C Thermal Conductivity: 0.251 J/cm C sec Melting Temperature: 3000 C
ZrO_2	Thermocouple Protection Tubes Coefficient of Thermal Expansion: $.66 \times 10^{-6}$/C Thermal Expansion Coefficient: 9.9×10^{-6} 1/C Thermal Conductivity: 8.3 J/cm C sec Melting Temperature: 2537 C

MgO	Thermocouple Protection Tubes Resistant to Molten Metals and Slags Coefficient of Thermal Expansion: $.66x10^{-6}/C$ Thermal Expansion Coefficient: $13.5x10^{-6}$ 1/C Thermal Conductivity: 8.3 J/cm C sec Melting Temperature: 2800 C

One problem with these materials listed on Table 2 is that none of them are as thermally shock resistant as the materials on Table 1, as can be inferred from looking at the ratio of coefficient of thermal expansion to thermal conductivity. Because of this lack of thermal shock resistance, the temperature of the furnace should be brought up more slowly after initially firing up the arc. At operating temperatures the temperature changes will not be that dramatic and risk of thermal shock failure is low. Zirconia test tubes were used to sheath the C type thermocouples for temperature measurement in early experiments. They worked well for the most part and never melted even at temperatures above 1800 C, but on one occasion one broke from thermal shock while heating the furnace at maximum power input from room temperature.

b. Testing of Different Crucible Materials

Some of the possible crucible material for redesign 1 were tested with the present prototype since it is also in the configuration of the crucible serving as the negative electrode. Four Different materials were tested, a 97% pure tungsten crucible, a TiN coated graphite crucible, a graphite crucible with a BN insert and also a finer grade of graphite (SIC6) than what is presently used. The tungsten crucible was tested for 1000 seconds at a sensed temperature of 1500 C. There was very little crucible damage, there was some slight diffusion of the Tungsten into the molten Steel, but overall the results from this experiment were encouraging. The next experiment with the tungsten was carried out at higher temperatures with a sensed temperature above 1800C. During this experiment the Tungsten crucible failed from melting. The melting temperature of this 97% pure tungsten with the remaining 3% being primarily iron is estimated to be over 3000 C. This means that the temperatures inside the molten metal chamber are much hotter in some locations than the sensed temperature indicates. The photographs below show the damage to the tungsten crucible

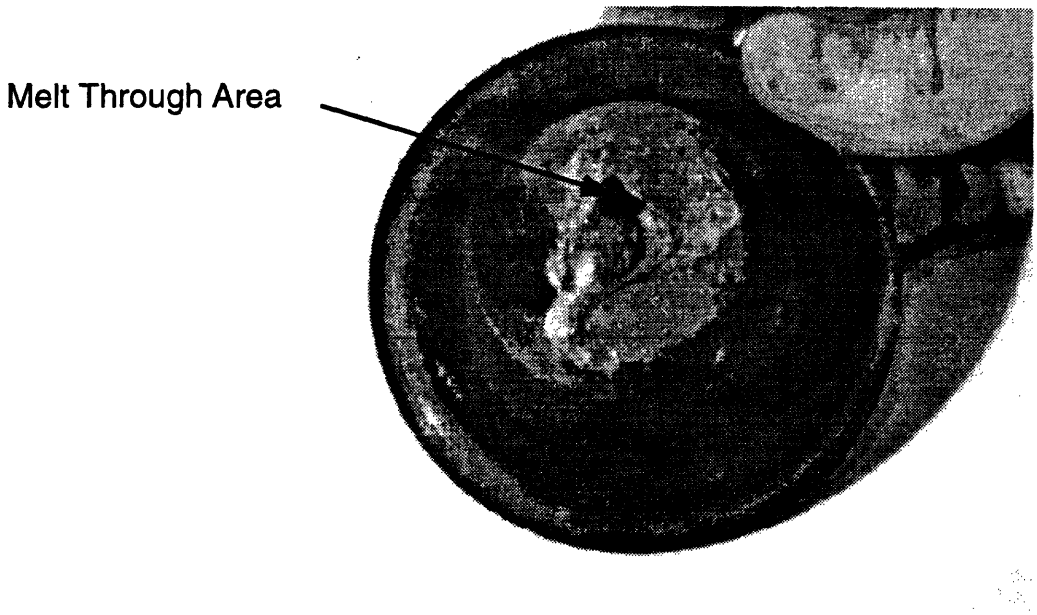

Figure 55: Results of Using Tungsten as Crucible Material

The titanium nitride coated graphite crucible also proved to be inadequate. The coating came off of the interior after running at a sensed temperature of 1800 C for a duration of 1000 seconds. On the exterior of the crucible, the TiN coating started to flake off.

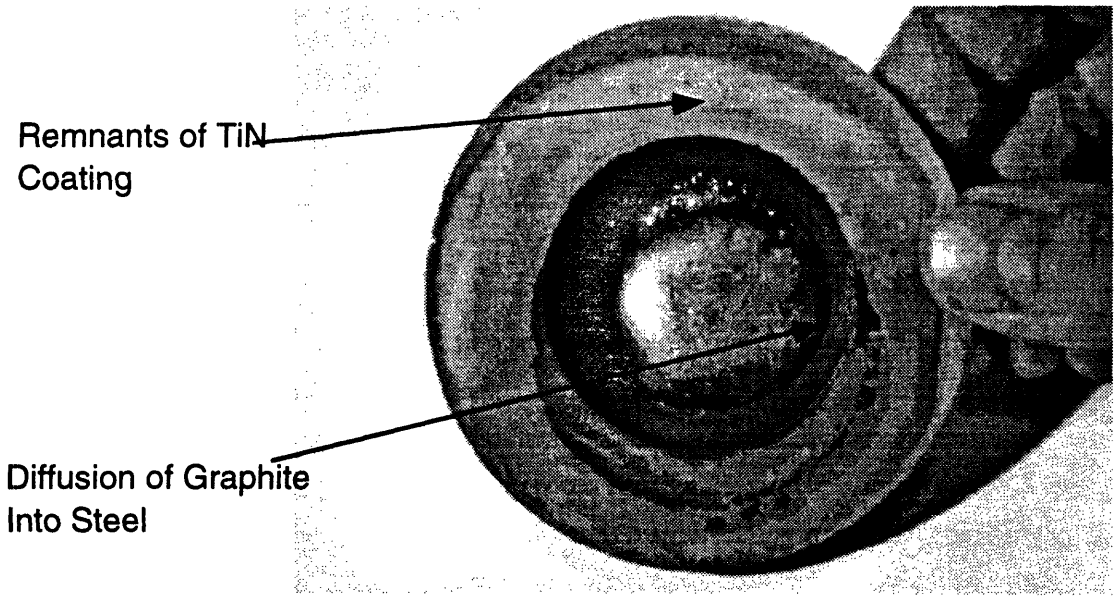

Figure 56: Results of TiN Coated Crucible

The higher grade, SIC6, of graphite did not improve much on the results from using the lower AGSR grade. The results in damage are no better than those shown at the beginning of this chapter.

The boron nitride insert stood up remarkably well to ejecting approximately 50 g of molten steel at a sensed temperature of 1800 C. The exit orifice enlarged slightly, but not nearly as much as with the graphite. The material was tested at the last minute and deserves more experimentation, but for now boron nitride appears to be the best material candidate for an insert material for this redesign 1 approach.

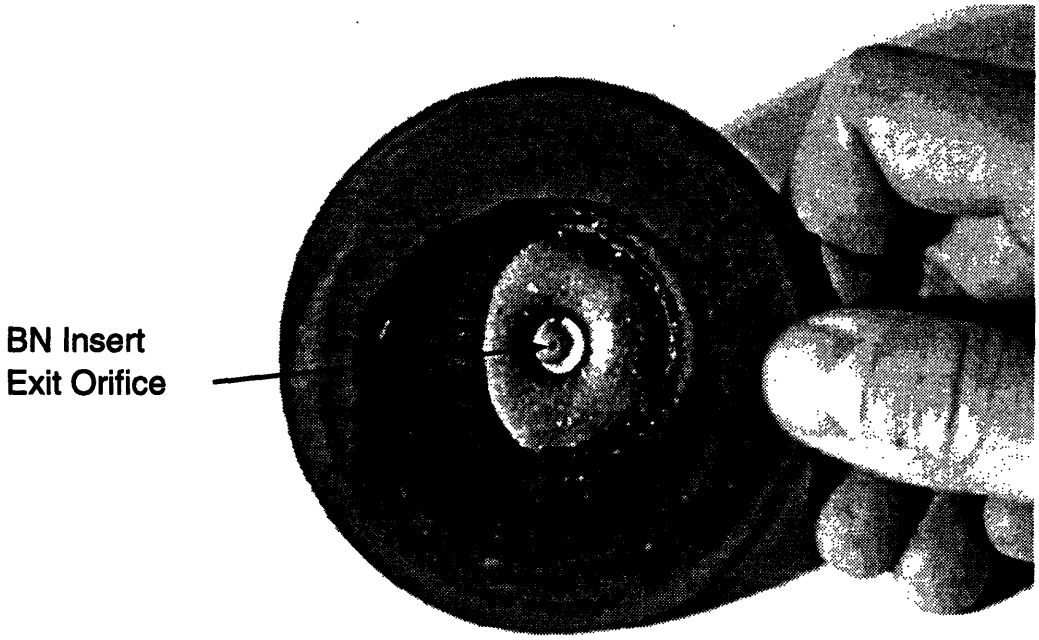

Figure 57: Results of BN Insert

The redesign 2 approach does not require that the crucible be electrically conductive since it won't serve as the negative electrode. There are two possible benefits in this approach. It would allow the use of an electrically insulating materials like boron nitride which may likely prove to be more durable than tungsten, graphite or a TiN coated graphite crucible in this furnace configuration. It may also reduce the damage to the crucible by eliminating direct crucible exposure to the arc so the crucible material would not have to be as durable. The geometry of the crucible remains the same as the previously discussed design with the most likely material being BN for both the insert and the surrounding crucible. However, the resulting furnace design will change since it

will have to cater to two tungsten electrodes rather than one. Both redesigns will be discussed in their entirety in the last section of this chapter

C. Molten Metal Replenishing Problem

In addition solving the problems of carbon diffusion into the molten metal and wear of the exit orifice it is necessary to replenish the molten metal as quickly as it is ejected out of the crucible. As discussed in the molten metal level control section, the maximum wirefeed rate is limited by the maximum melting rate of the wire being fed. If wire is fed faster than the melting rate, the feed wire pokes into the bottom of the crucible which eventually leads to intolerable crucible damage. The following picture shows the effect of feeding too fast into a graphite crucible.

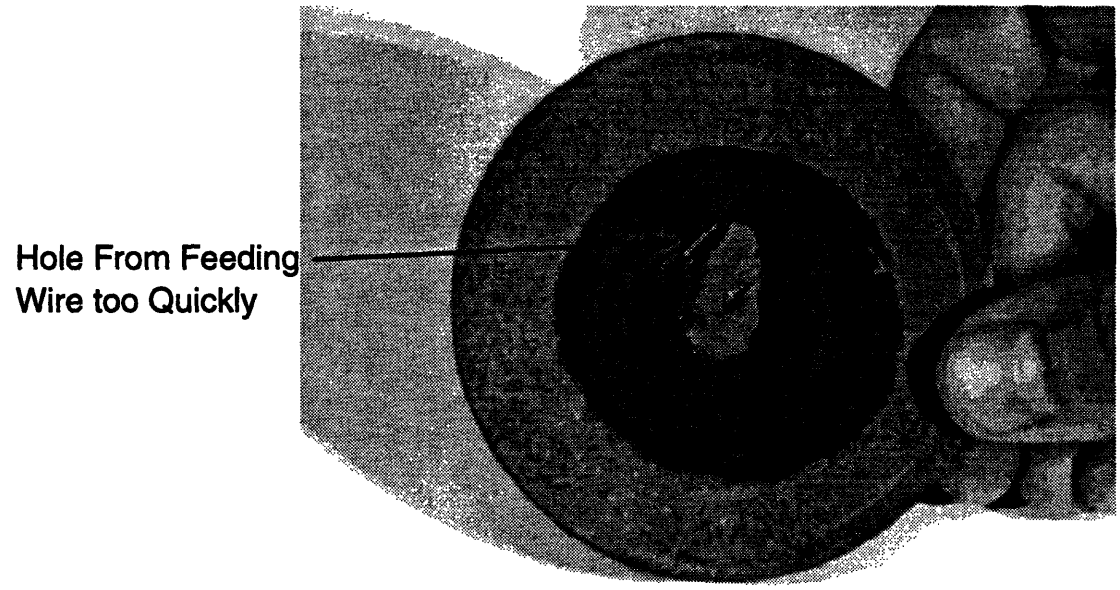

Figure 58: Effect of Wire Feed Velocity Exceeding Melting Rate of Wire

There are a number of options in solving this wirefeed rate limitation. One could deliver metal to the crucible in a powder or pellet form from a hopper. The mass flow rate probably could not be as tightly controlled with a hopper, but it could definitely deliver a higher mass flux without damaging the crucible. The main drawback to this method is building the hopper and the feeder and the bulk they would probably add to the entire system. Since one of the design objectives is compactness so the furnace will be easily maneuvered by a robot, the hopper idea will be ruled out for the time being. Another problem with large mass influxes to the crucible is the large disturbance the temperature controller will experience since the solid incoming metal will be at a much

lower temperature than the molten metal. However, this problem of thermal disturbances could be minimized with a more powerful DC power supply and possibly a feed forward temperature control feature. The rest of this subsection will be dedicated to describing potential improvements as well as improvements that have already been made to the present wire feed system.

A successful attempt was made to increase the wire melting rate into the crucible by feeding the wire into the arc rather than the molten metal. The reasoning behind this is that the arc is the most energy dense area in the molten metal chamber and hence the wire should melt quickest here. The diagram below shows the difference between the two wirefeed configurations.

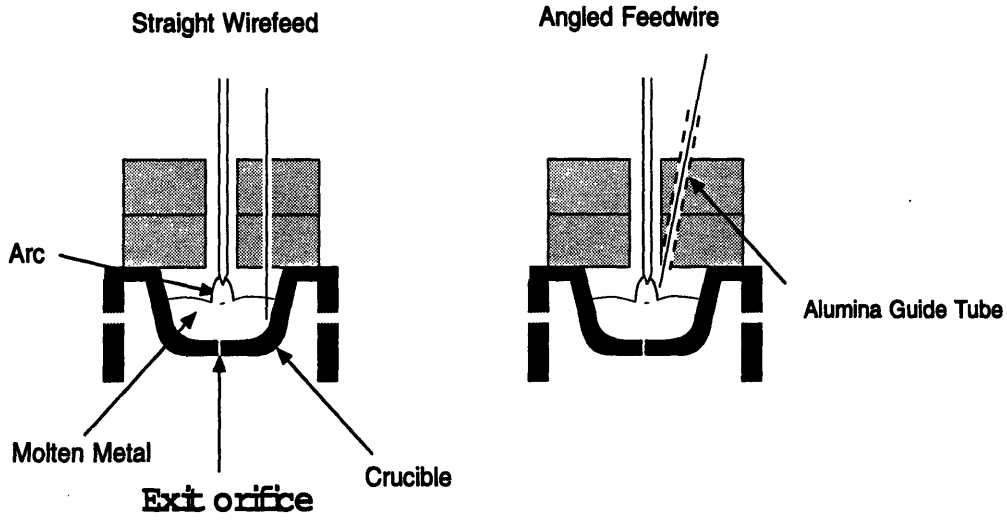

Figure 59a: Old Wire Feed Configuration and 59b: New Wire Feed Configuration

The melting rate was measured for each configuration at a fixed temperature of 1650 C using the temperature controller. A given length of wire was fed by hand as quickly as it melted while measuring the elapsed time. It was obvious than wire was fed at the melting rate from continually hitting the bottom of the crucible. The angled wirefeed melting rate turned out to be 6.4 cm/sec (.0416 cm^3/sec) versus the 5.0cm/sec (.0325 cm^3/sec) with the former straight wirefeed configuration. This is over a 20% improvement in the wire feed rate, but this mass inflow rate is still lower than the expected ejection rate of around .263 cm^3/sec.

a. Optimum Wire Diameter

Another way to improve the mass inflow rate is to determine the optimum wirefeed diameter. A larger diameter wire may have to be fed at a slower velocity, but the mass inflow may be higher since the volumetric mass flow in is equal to the wire velocity multiplied by the wire cross sectional area. This problem will be approached in the same manner as the problem of determining maximum melting rate at various temperatures in chapter 3, except here we're determining the melting rate with various diameters at a fixed temperature. Two analytical method will be used to approximate the volumetric melting rate as a function of diameter; both a lumped capacitance analysis and an analysis that accounts for spatial effects by solving the appropriate form of the heat equation are carried out.

The problem parameters and assumptions are the same as those in chapter 3. The value of H is the distance from the molten metal surface to the bottom of the crucible which is the maximum length of wire that can be submerged in the molten metal. The symbol r_o represents the wire radius. The volumetric melting rate is then approximated by dividing $\pi r_o^2 H$ by t. So the problem is one of finding the time t that it takes for the segment of wire to reach the melting temperature of steel for various wire diameters. Latent heat effects are accounted for in the convective heat transfer coefficient as described in chapter 3.

The diameter of the segment is limited to practical sizes, obviously a 3 cm diameter wire could not be used since it would not fit in the crucible and would be too rigid to feed from a spooling system presently used. Hence the analysis will be limited to diameters between 0.25 mm and 5 mm. Any smaller than 0.25 mm would probably not be rigid enough to feed with the present system and any larger than 5 mm would probably be too rigid. For the small diameter wire, the main mode of conduction is in the radial direction while with the larger diameter, axial and radial conduction may both be significant which is why distributed parameter analysis is also carried out.

To get an initial estimate of how diameter affects the net mass inflow, some simple lumped capacitance analysis results are shown in the following equation:

$$t = \frac{\rho V c}{h' A_s} \ln \frac{\Theta_i}{\Theta_f} = \frac{\rho \pi D^2 H c}{4h' H \pi D} \ln \frac{\Theta_i}{\Theta_f}$$

where t is the time to melt the wire segment, Θ_i is the initial temperature of the wire minus the molten metal pool temperature and Θ_f is the melting temperature of the wire

minus the molten pool temperature. The symbol conventions used are: ρ=density, V=volume of wire segment, D=diameter of wire, h'=experimentally determined convective heat transfer coefficient, and A_s=surface area of wire segment. Having found the value of t, the mass inflow rate as a function of diameter for a given molten metal temperature is as follows:

$$\text{Mass inflow rate}=\frac{H}{t}\cdot\frac{\pi D^2}{4}=H\left(\frac{h'}{\rho c\ln\frac{\Theta_i}{\Theta_f}}\right)\pi D=K_1 D$$

This indicates that volume inflow rate is directly proportional to the wirefeed diameter.

The verdict from this very simplistic lumped capacitance model is checked by doing analysis which accounts for spatial effects the same way as in chapter 3 a detailed analysis is given in Appendix D. The assumptions and parameters are the same and here the problem is analyzed for three different diameters, D=0.25 mm, D=1 mm, and D=5 mm. The 5mm diameter wire has a melting rate of $2\text{x}10^{-7}$ mm^3/sec, the 1mm diameter has a melting rate of $6.36\text{x}10^{-8}$ mm^3/sec, and the 0.25 mm diameter has a melting rate of $2.2\text{x}10^{-8}$ mm^3/sec. These results also show that relationship given by the lumped capacitance analysis is not altogether valid, but overall both results agree that a larger wire diameter should be used rather than the presently used 0.91 mm diameter wire. However, after performing this analysis, it was found that GMAW wire is not readily available in diameters larger than 1/16" (1.59mm) and this diameter is significantly more expensive. In conclusion, we will presently stick with the angled wirefeed and 0.91mm since the slightly larger, more expensive wire would yield only slightly better results. After problems with the crucible have been solved it will be necessary to come up with a system capable of replenishing as quickly as a typical GMA welder is capable of depositing (0.263cm^3/sec).

D. Two Final Designs Presented

Two stream welder designs are now presented that incorporate the revisions described in previous sections and also retain many aspects of the present prototype. The first design relies on the crucible to serve as the negative electrode, like the present prototype, the second design does not. Both designs are more compact than the present prototype primarily to reduce the weight and bulk of the overall assembly. By reducing the size and weight of the assembly it will be easier to maneuver the welder. This is important since

ultimately it is desired to position the furnace assembly with a robot. Some other aspects of the design that have been changed are: insulation materials and dimensions, mechanical fixtures and assembly of the furnace, the addition of a quartz window so that it will be possible to view within the molten metal chamber, and the copper cooling coils on the bottom plate are removed.

a. Redesign 1

Appendix A3 shows furnace redesign 1, where the crucible serves as the negative electrode. As described earlier, the crucible consists of TiN coated graphite along with a BN insert. As mentioned earlier the TiN coating reduces the diffusion of graphite into the molten steel pool and the BN insert is used as a more wear resistant exit orifice. The ground lead of the power supply is bolted to the base plate of the furnace which electrically shorts it with the crucible. As with the present prototype, the live electrode is a sharpened tungsten rhenium rod attached to a GTAW torch.

The fixture that secures the GTAW torch to the top plate is redesigned to improve ease of assembly and disassembly. The reason it is desirable to be able to quickly remove the torch, is to sharpen the tungsten electrode to enable arc starting before operating the furnace. The present prototype uses a ceramic fitting with an aluminum flange that is secured to the top plate by sandwiching the aluminum flange between the top plate and a retaining fitting. The retaining fitting is secured to the top plate with the Argon flow system swage-lok fittings. Needless to say, this is the most time consuming part of assembling and disassembling the furnace. The new way to secure the GTAW torch is with a custom Teflon fitting that remains threaded into the top plate (1/2" NPT threads). An additional cylindrical Teflon fitting is connected to the GTAW torch. The two Teflon fittings mate together as shown on the cross section figure which allow easy insertion and removal of the torch. The connection is sealed with an o-ring so argon does not leak out of the pressurization chamber. Using these Teflon fittings means the torch is still electrically isolated from the top plate and should significantly decrease time between successive experiments.

A zirconia tube is connected to the TIG torch adapter on the top plate, this tube directs the pressurizing argon flow coming from the TIG torch. Alumina was used with the first prototype, but it could not sustain the high temperatures, melting during high temperature experiments. One should also note that the electrode tube is shorter due to smaller overall dimensions of the furnace, this reduction in slenderness should make it easier to insert the torch/electrode assembly without breaking the zirconia tube.

The wirefeed guide tube used for the molten metal replenishing system, and the view tube, will also be made of zirconia and the surrounding insulation that holds them in place will be moldable alumina as used with the present prototype.

One of the most prominent differences between the present prototype and this new design is the quartz window that allows one to see inside the molten metal chamber. This allows observation of arc characteristics such as arc stability, location, and length. This will be important in determining the cause of failure of the crucible, if the arc is coming into direct contact with the crucible, it will be possible to see this (with a welding mask on to shield the dangerous radiation). The window will also allow the pyrometer to view the temperature within the molten metal chamber which will give a better idea of how much hotter it is within the crucible than on the surface of the crucible, where the temperature is presently sensed.

There are two possible problems with this quartz view window, it may get clouded up with condensed steel vapor or it may allow an excessive amount of heat to escape from the molten metal chamber. If either of these problems would prohibit using the quartz window, it would be a simple matter to modify the furnace by eliminating the window and filling in the view tube with moldable alumina insulation.

The present prototype has much more insulation than is necessary, most of the exterior of the furnace remains at room temperature while operating at crucible temperatures of approximately 2000 C. Two areas that do heat up substantially are the lower plate near the exit orifice and the top plate near the torch. These observations indicate that insulation can be more strategically placed with less emphasis on the radial thickness of the insulation and more emphasis directly above and below the crucible. Zirconia felt was added below the crucible and above the molded alumina insulation. The molded alumina insulation is also thicker than that used with the present prototype. The radial insulation thickness was decreased by 2" which in turn reduced the overall diameter of the furnace. A layer of alumina felt is situated around the periphery of the crucible as with the present prototype, felt was chosen to allow the shielding argon to flow through it while still insulating the molten metal.

The upper copper cooling coil that circulates tap water was retained while the bottom cooling coil was removed. Removing the lower cooling coil will result in a higher base plate temperatures but less heat transfer away from the furnace. If the base plate temperatures get too high, cooling coils can be added. Removing the lower cooling coils also improves the view angle of the pyrometer.

Stainless steel is still used for the furnace exterior. One change in the exterior is that 1/4" 20 stainless steel nuts and bolts are used rather than threaded rod to secure the upper

and lower plates. Having an airtight seal between the flanges and the upper and lower plates will prevent air from contaminating the argon atmosphere which may be the case with the air gaps that exist in the present design. Bolts rather than threaded rod should also reduce assembly time between experiments and improve the looks of the furnace. The upper lid is still electrically isolated from the upper flange with an insulating plastic gasket along with the presently used bolt inserts. These bolt inserts electrically isolate the bolts from the upper lid. Isolating the upper lid of the furnace from the rest of the furnace is an additional precaution against short circuit between the live electrode and the grounded base plate.

The rest of the design is the same as the present prototype using mullite ceramic to seal the pressurized molten metal chamber with swage-lok fittings connecting the argon flow system. The argon flow system will eventually be computer controlled with an electromechanical pressure regulator controlling the pressure in the molten metal chamber and an electrically actuated flow regulator to control the shielding flow.

b. Redesign 2

The second furnace design is very similar to the first in many respects, the overall external dimensions and insulation are the same, the main difference is that two tungsten-rhenium electrodes extend down from the top plate so the arc does not come into direct contact with the crucible. Two cross section schematics of this design are given in Appendix A4. There are two possible benefits in this design. It would allow the use of an electrically insulating materials like boron nitride which may prove to be more durable than other materials. It may also reduce the damage to the crucible by eliminating direct crucible exposure to the arc so the crucible material would not have to be as durable.

The tungsten-rhenium electrodes come down from upper lid of the furnace as shown in the Appendix. The live electrode and torch assembly are connected with the same fitting as in redesign 1. The ground electrode is connected to the top plate with a collet fitting that is similar to the one used to attach the live electrode to the torch. The ground electrode collet fitting is electrically shorted with the ground power supply lead that is bolted to the upper lid. It is very important that the live lead be electrically isolated from the top plate of the furnace, this is the reason for using the Teflon fitting which was also incorporated in the previous design. It is also vitally important to have good electrical contact between the ground electrode and the ground lead from the power supply that is secured to the top lid with a 1/4" 20 bolt. It is important to note that the neutral electrode is angled in towards the live electrode, this way we can achieve a large separation

distance between the electrodes on the upper lid while having the 5 mm arc length in the molten metal chamber.

A possible drawback to this design is that the arc that serves as the heat source is no longer in direct contact with the metal it is heating which could degrade the thermal performance of the furnace. Hopefully this will not pose a significant problem since the molten metal chamber is well insulated. Removing the arc from the molten metal will also make it impossible to sense the height of the molten metal level through the arc voltage since the arc length will be constant rather than proportional to the molten metal level. However there are other possibilities for measuring the molten metal level. One possibility is to sense the resistance between two leads that would be immersed in the molten steel when the level is sufficiently high. The leads would be shorted when the molten metal level is at or above its desired level, but when the level is below the desired level there would be an open circuit between the leads. This will only allow the use of an on/off controller, but that is what is presently used.

Both redesign 1 and redesign 2 address some of the problems of the present prototype and the one that should be used depends primarily on whether or not a suitable crucible material can be found. Observing that TiN coated graphite, tungsten, SIC6 and AGSR grades of graphite proved unsuccessful in the electrically conductive crucible configuration, suggests that the chances of using this design are getting slim. If BN proves to be the only material that will work in not diffusing into the molten steel, then redesign 2 should be pursued.

Chapter 6: Conclusion

A. Summary and Recommendations

Chapter 1 described some of the limitations of consumable electrode arc welding, one of the most widely used welding processes in industry today. The main problem is the lack of independent control over the heat and mass input to a weld seam. Another is the variations in modes of mass transfer when welding under different conditions. Both of these problems limit the precision and flexibility of consumable electrode welding processes.

Given these limitations in consumable electrode arc welding processes, it was proposed to have a new welding process called stream welding that allows precise, controllable, molten metal deposition that is independent of the molten metal temperature.

To successfully operate the stream welder, a closed loop temperature controller was developed. The temperature is sensed with a high temperature pyrometer and the PID controller, with an anti wind up feature, is implemented with a IBM compatible personal computer. The system controls the temperature of the molten metal being deposited onto the weld seam by controlling the temperature of the base of the crucible. Although the temperature control system successfully controls the temperature of the base of the crucible, which is probably close to the molten stream temperature, a more extensive analysis needs to be carried out to see how well the sensed temperature represents the stream temperature. This analysis may show that an estimator for the stream temperature, based on relevant furnace states, is necessary.

A closed loop wire feed system was also developed to replenish the molten metal supply as it is ejected out of the furnace. The control scheme for this wire feeder is essentially an on/off type with the feed magnitude being related to the molten metal temperature to maximize replenishing rates in different regimes of operation. There is, however, a problem with this replenishing system since it is impossible to replenish at desirable rates. The feed wire cannot be fed faster than it melts in the molten metal chamber, feeding faster than this results in severe crucible damage. Ultimately it is desired to have a full range of flow rates that range anywhere from no flow, to flow rates that are at least that of a typical GMA welder (0.263 cm^3/sec). So an improved molten metal replenishing system needs to be devised.

Before developing a flow control system, it is necessary to find a crucible exit orifice material that is more wear resistant than the presently used graphite. A number of

materials have been tested such as tungsten, two different grades of graphite, and titanium nitride coated graphite, all of these have proved inadequate. Boron nitride was also tested at the last minute and the results were encouraging, there was much less exit orifice wear than with the other materials. If further testing proves that boron nitride is a suitable exit orifice material, a flow controller can start being developed. One challenging problem in developing the flow rate controller will be how to sense the instantaneous molten metal flow rate.

There also needs to be an effort to better understand what is happening within the molten metal chamber during the stream welding process. To observe the arc during the welding process, a view window should be incorporated in the present prototype. Characteristics such as arc stability and location are important to the wire feed system and it may even be found that diffusion of the crucible material is being caused by the arc striking the crucible rather than the molten metal.

Another issue that needs to be probed into further is determining the capabilities of stream welding. Preliminary modeling and experimentation show the stream welding process is capable of very little penetration compared to conventional arc welding processes. However, the model should be more thoroughly developed with fewer simplifications to more fully explore the capabilities of stream welding and possibly survey resulting characteristics using different joint geometries. It may be possible to achieve good welds with little penetration.

If more penetration is found necessary then an alternate power source will be the most likely option to achieve better penetration. In this case, a heat source such as a CO_2 laser or a GTAW torch could serve as the heat source to ensure fusion between the filler metal and workpiece while the stream welder would be relied on for precision molten metal deposition.

Appendix A1: Crucible Redesign

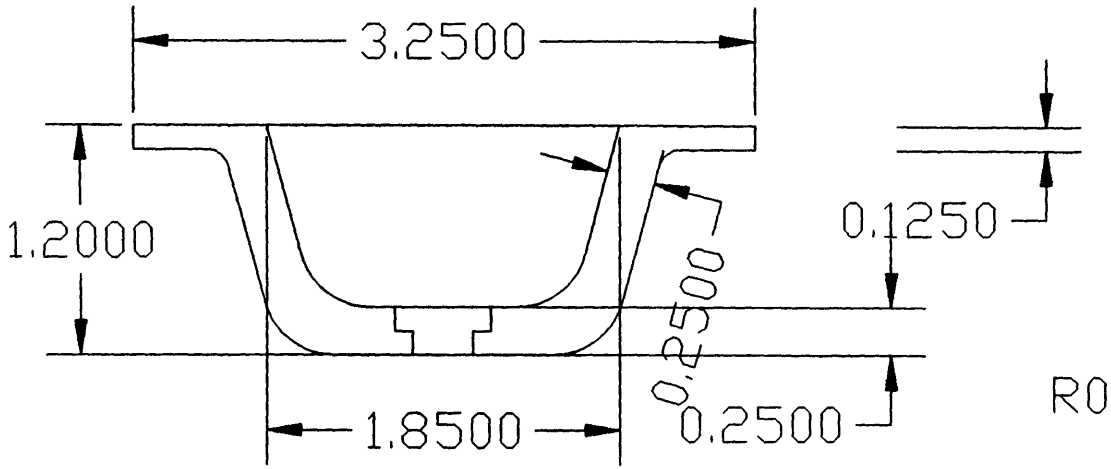

CRUCIBLE SECTION

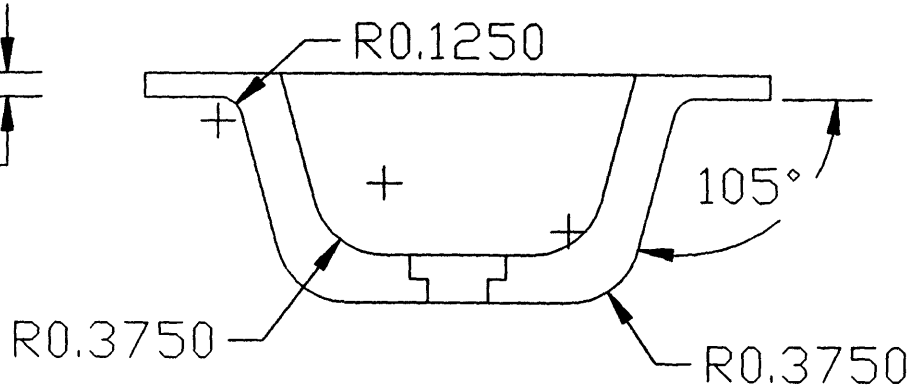

CRUCIBLE SECTION

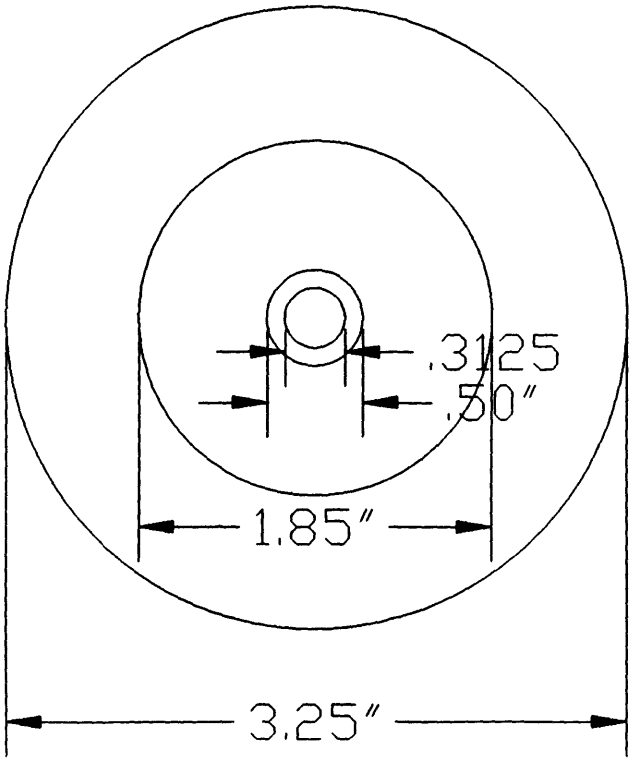

CRUCIBLE - TOP VIEW

GRAPHITE CRUCIBLE
TOLERANCES: +-.001" (IF POSSIBLE)
INSERT PRESS FITS IN CRUCIBLE
SCALE: FULL SCALE
CHRISTOPHER RATLIFF

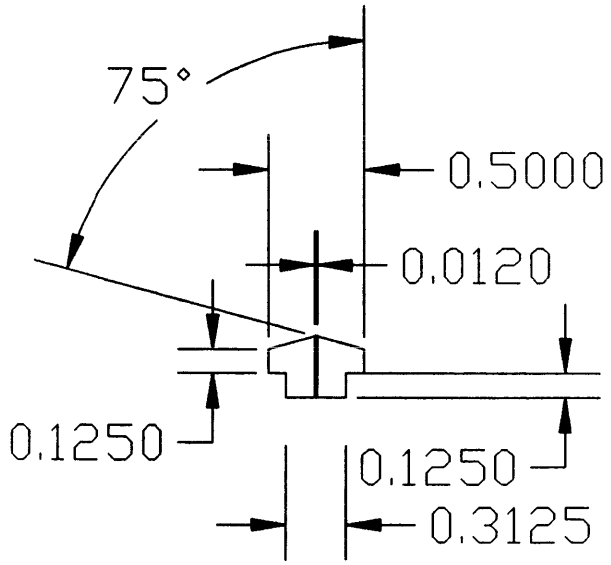

EXIT ORIFICE INSERT - SECTION

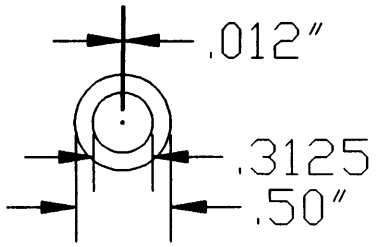

EXIT ORIFICE INSERT - TOP VIEW

BORON NITRIDE INSERT
TOLERANCES: +-.001" (IF POSSIBLE) INSERT PRESS FITS INTO CRUCIBLE
SCALE: FULL SCALE
CHRISTOPHER RATLIFF JUNE 6, 1994

Appendix A2: Present Prototype Design

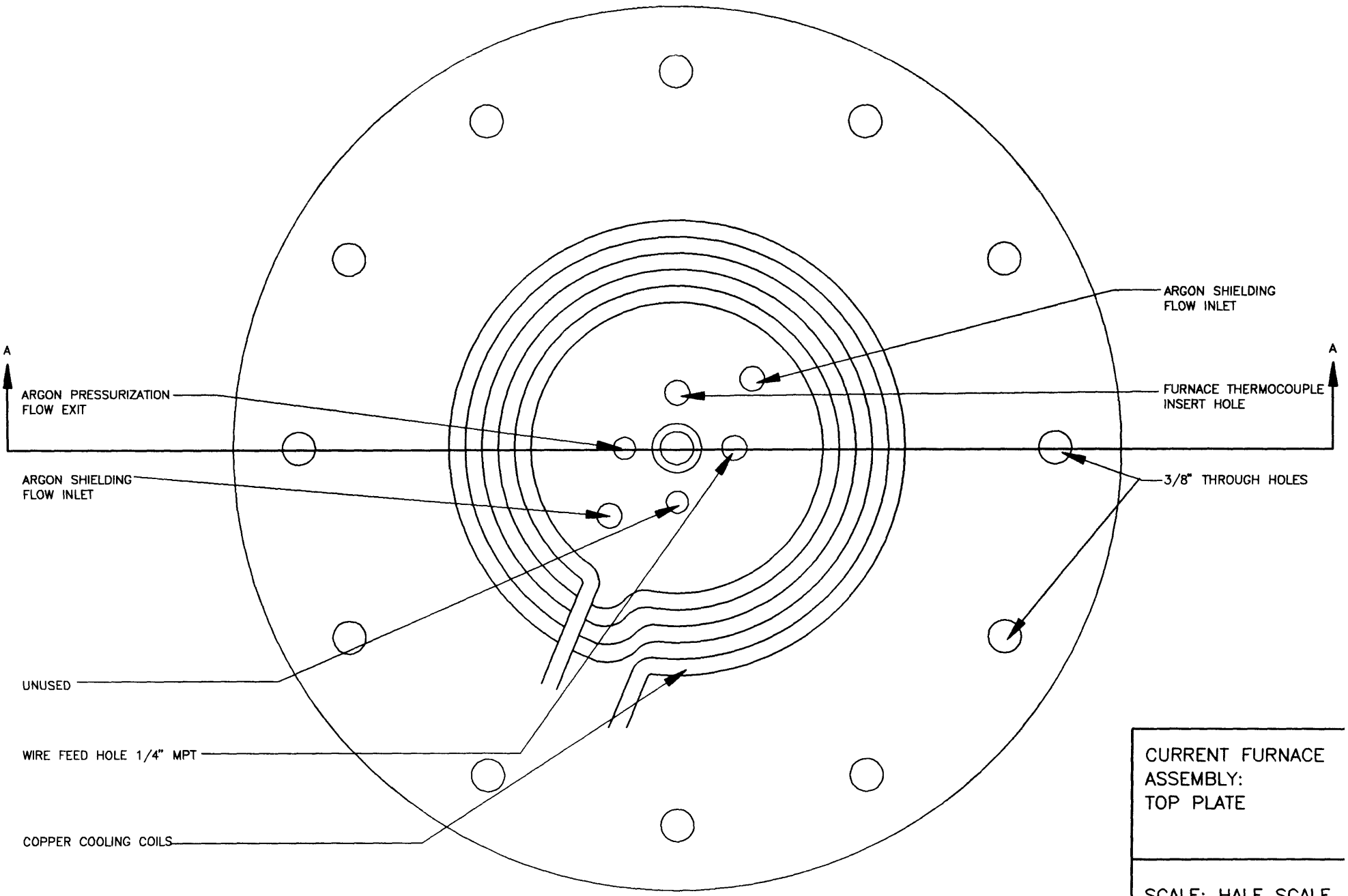

CURRENT FURNACE ASSEMBLY:
TOP PLATE

SCALE: HALF SCALE

CHRISTOPHER T. RATI
JUNE 10, 1994

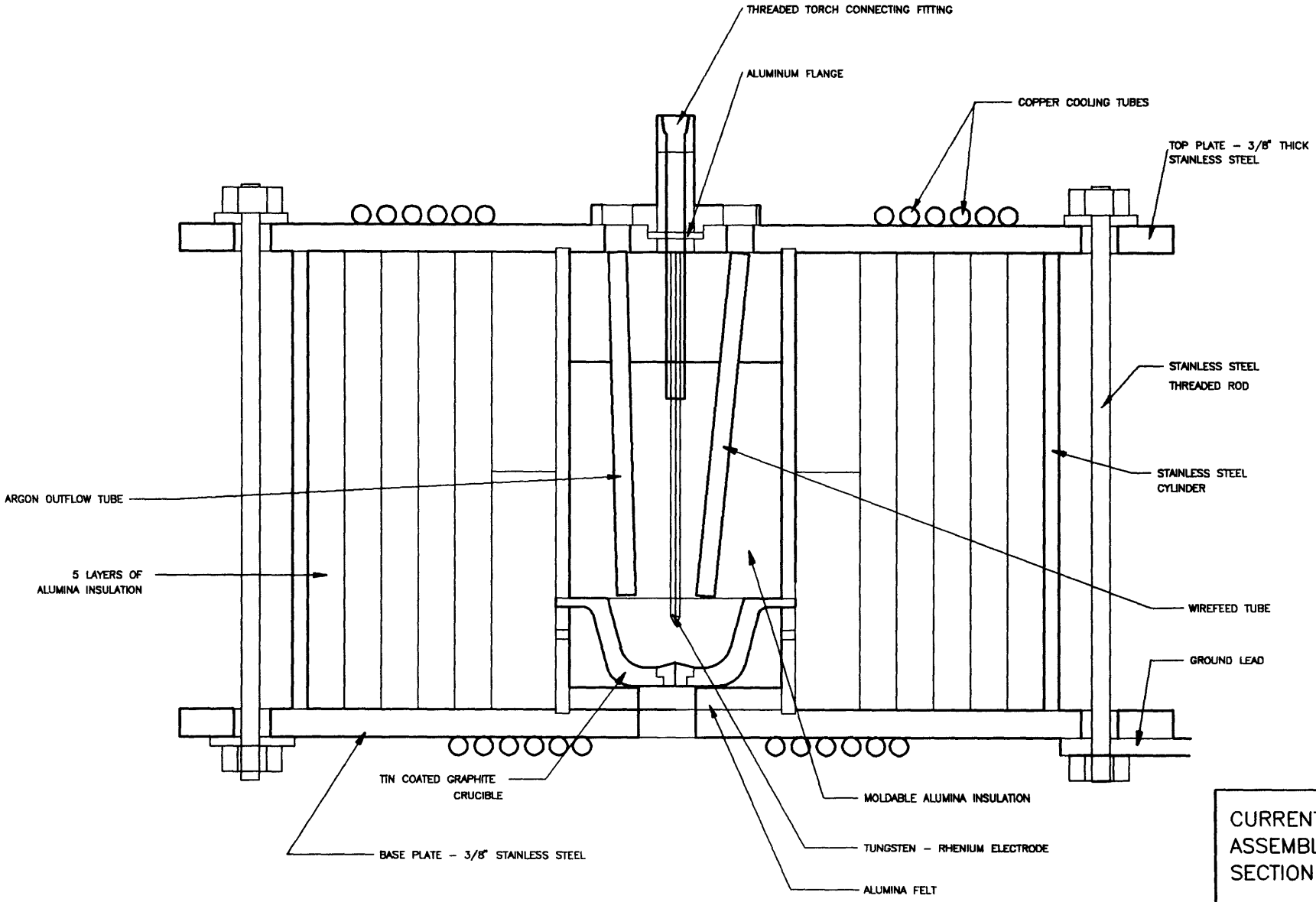

CURRENT FURNACE ASSEMBLY: SECTION A–A

SCALE: HALF SCALE

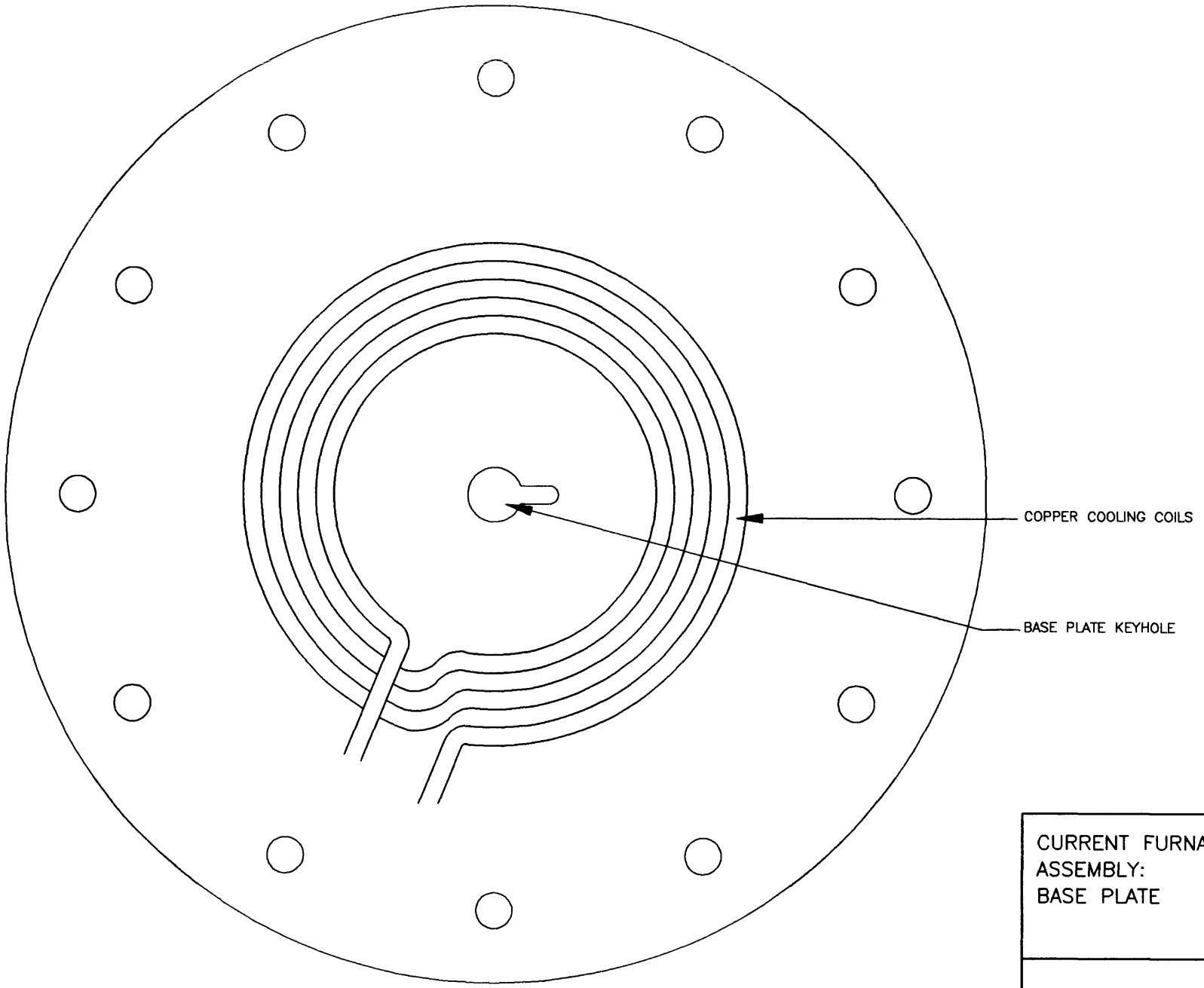

CURRENT FURNACE ASSEMBLY:
BASE PLATE

SCALE: HALF SCALE

CHRISTOPHER T. RAT
JUNE 10, 1994

Appendix A3: Redesign Number 1

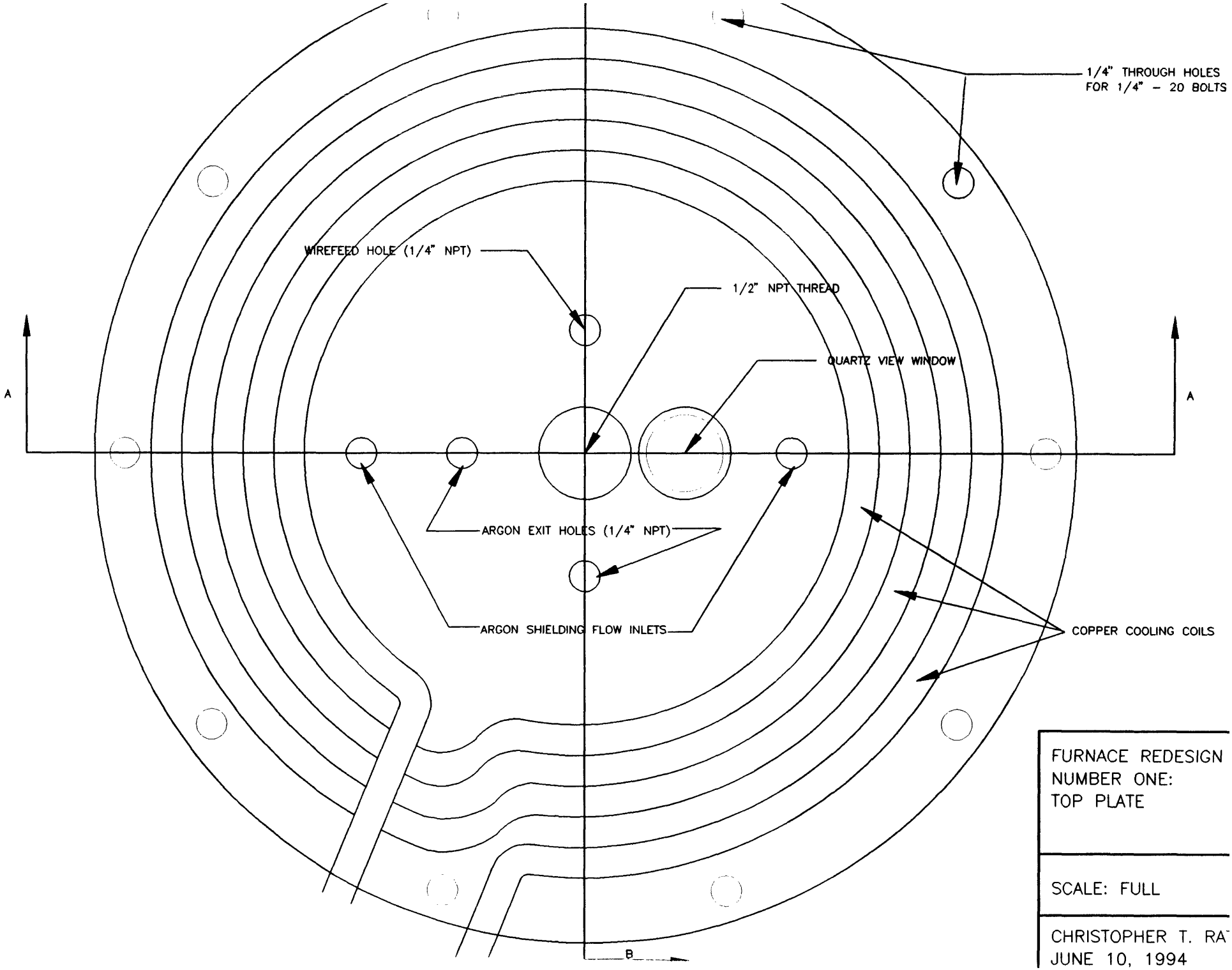

FURNACE REDESIGN
NUMBER ONE:
TOP PLATE

SCALE: FULL

CHRISTOPHER T. RA
JUNE 10, 1994

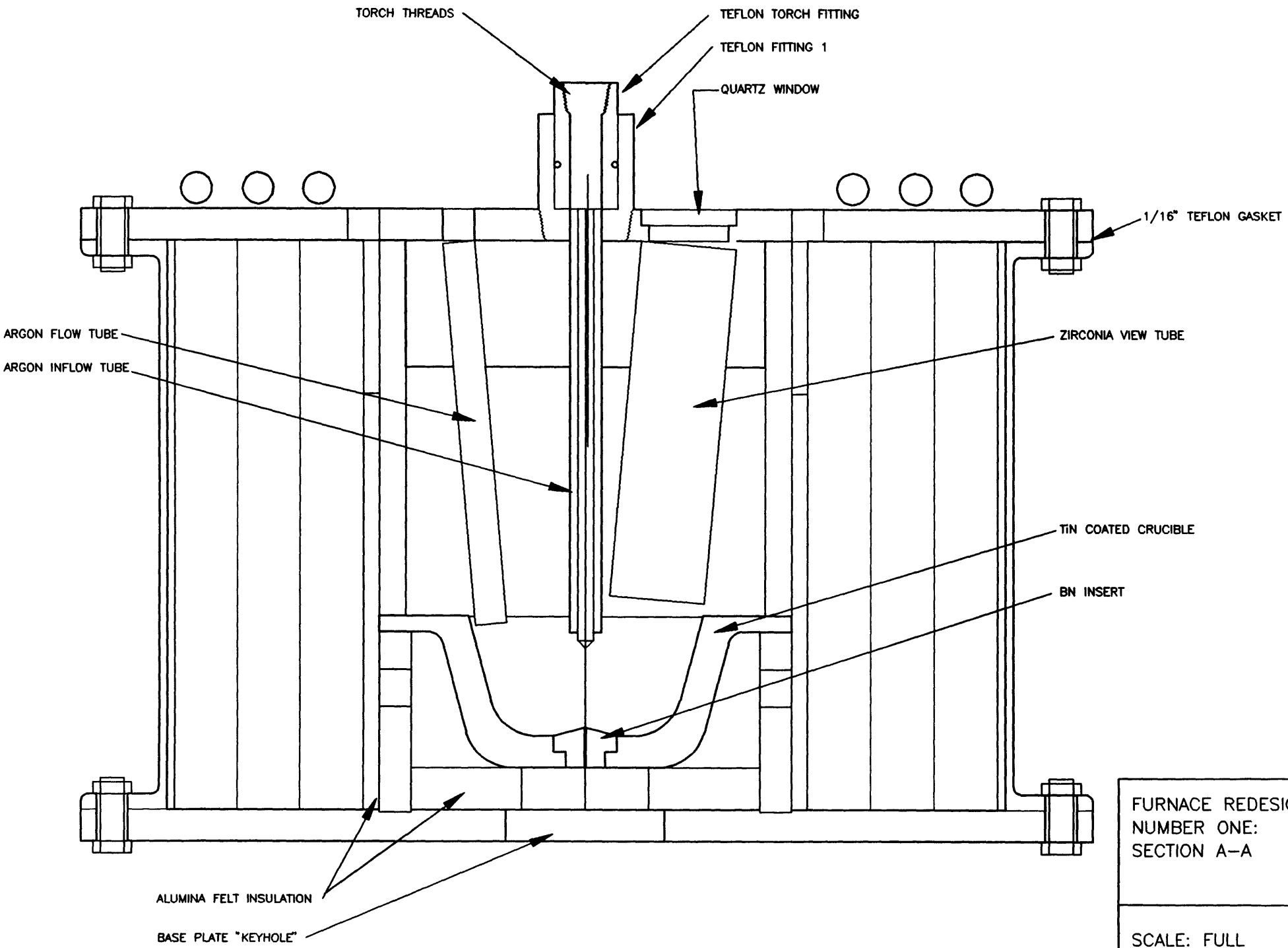

FURNACE REDESIGN
NUMBER ONE:
SECTION A–A

SCALE: FULL

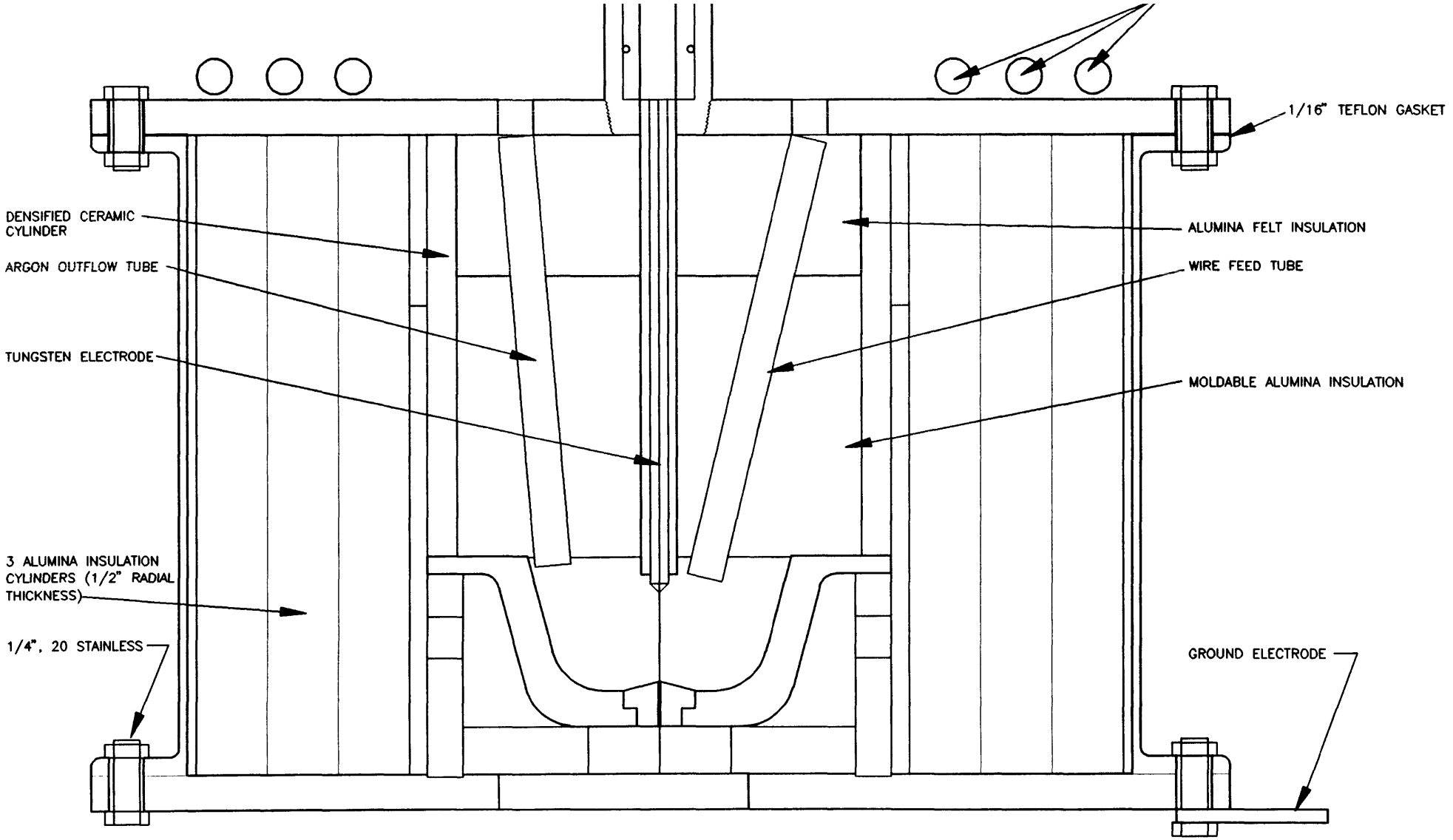

FURNACE REDESIGN
NUMBER ONE:
SECTION B–B

SCALE: FULL

CHRISTOPHER T. RA
JUNE 10, 1994

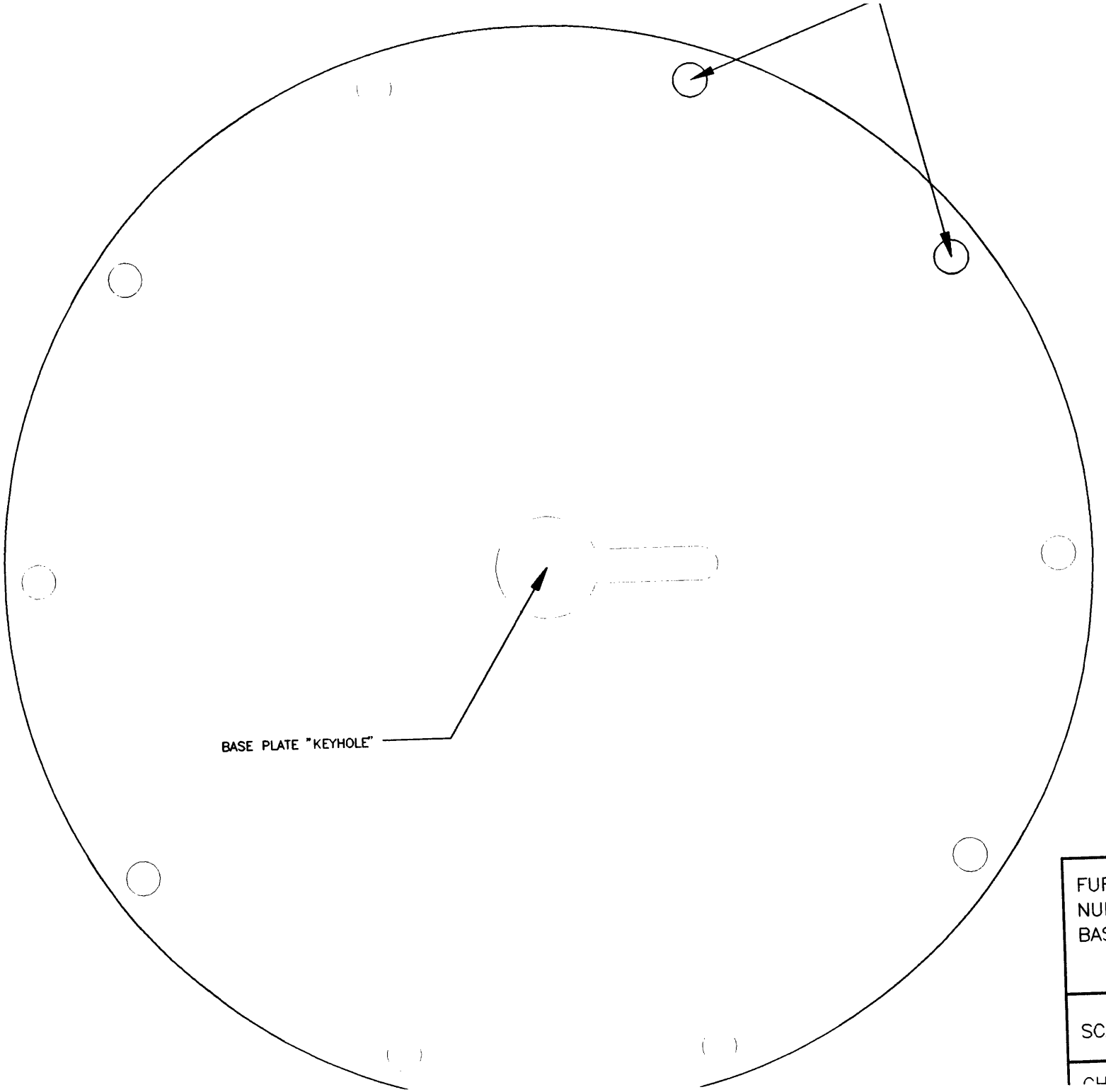

FURNACE REDESIGN
NUMBER ONE:
BASE PLATE

SCALE: FULL

CHRISTOPHER T. R

Appendix A3: Redesign Number 2

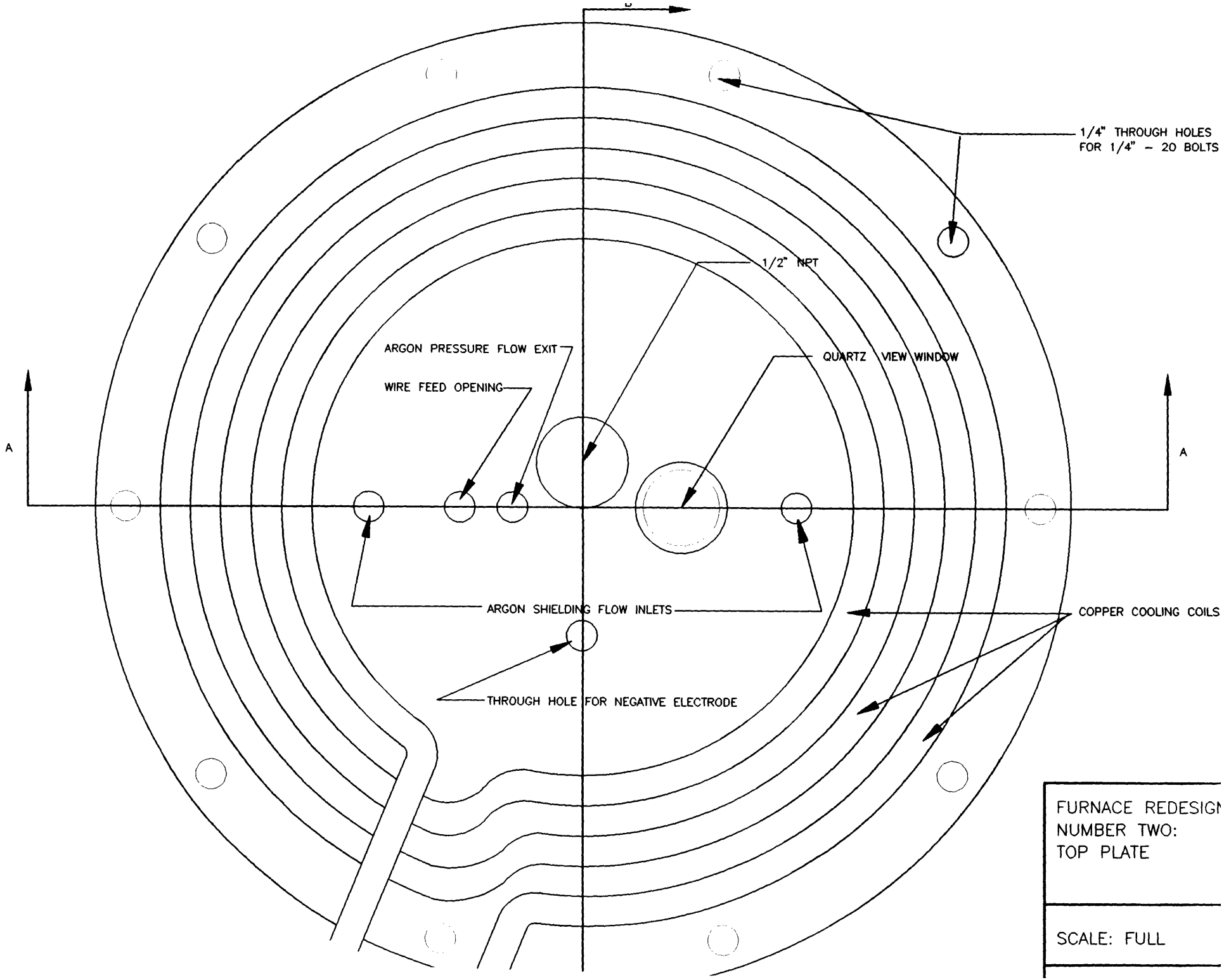

FURNACE REDESIGN
NUMBER TWO:
TOP PLATE

SCALE: FULL

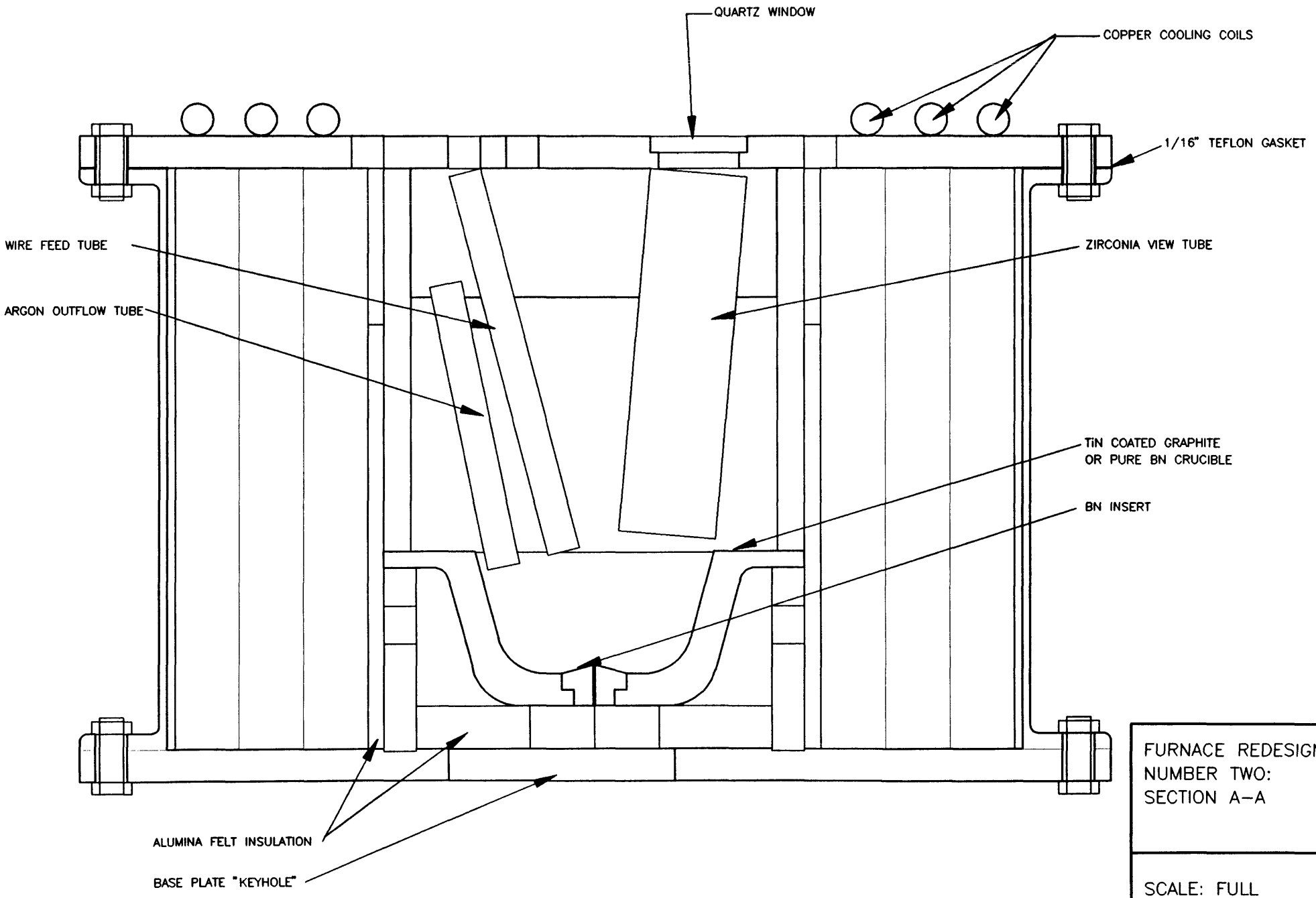

FURNACE REDESIGN
NUMBER TWO:
SECTION A–A

SCALE: FULL

CHRISTOPHER T. RAT
JUNE 10, 1994

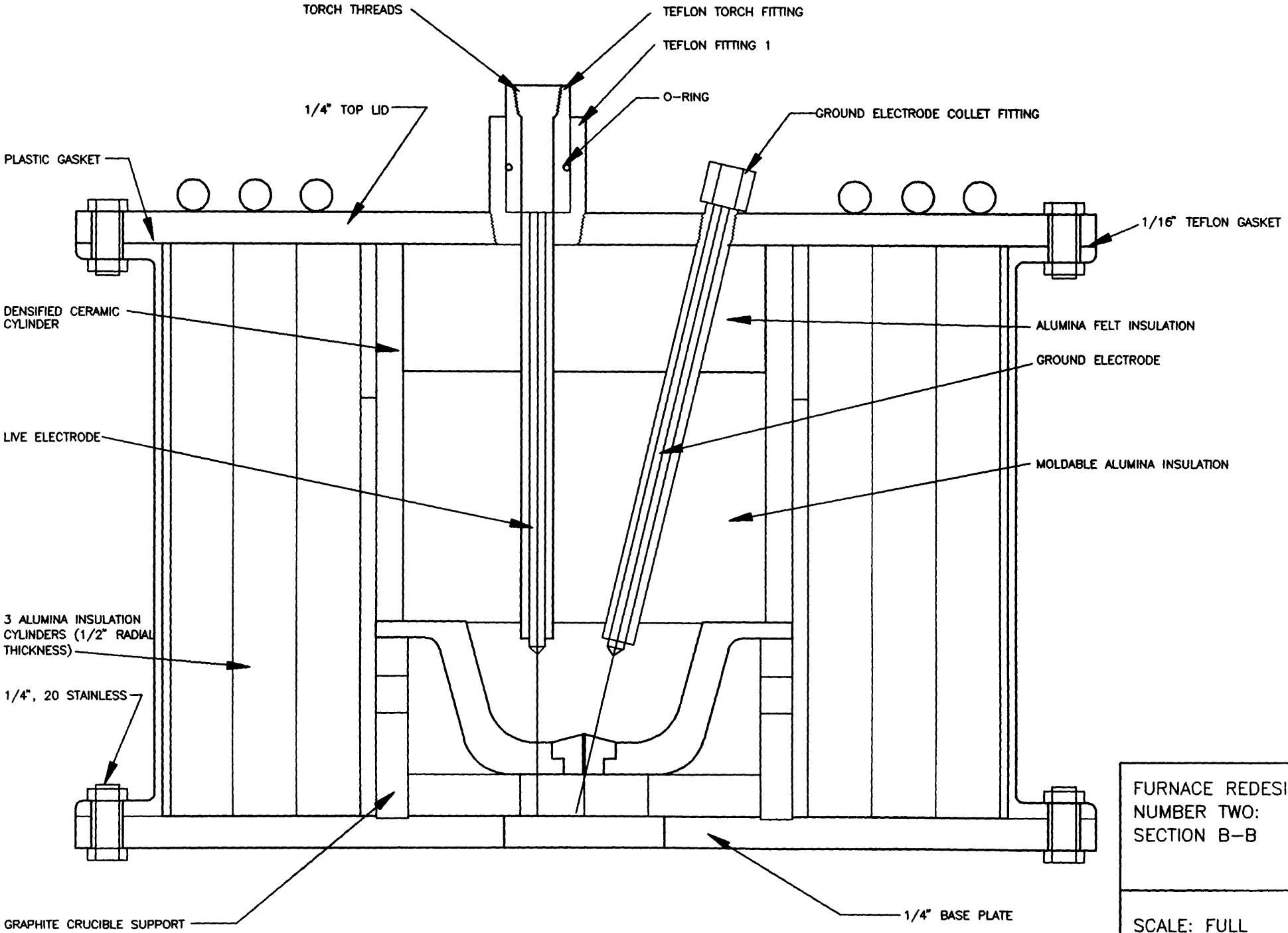

FURNACE REDESIGN NUMBER TWO: SECTION B-B

SCALE: FULL

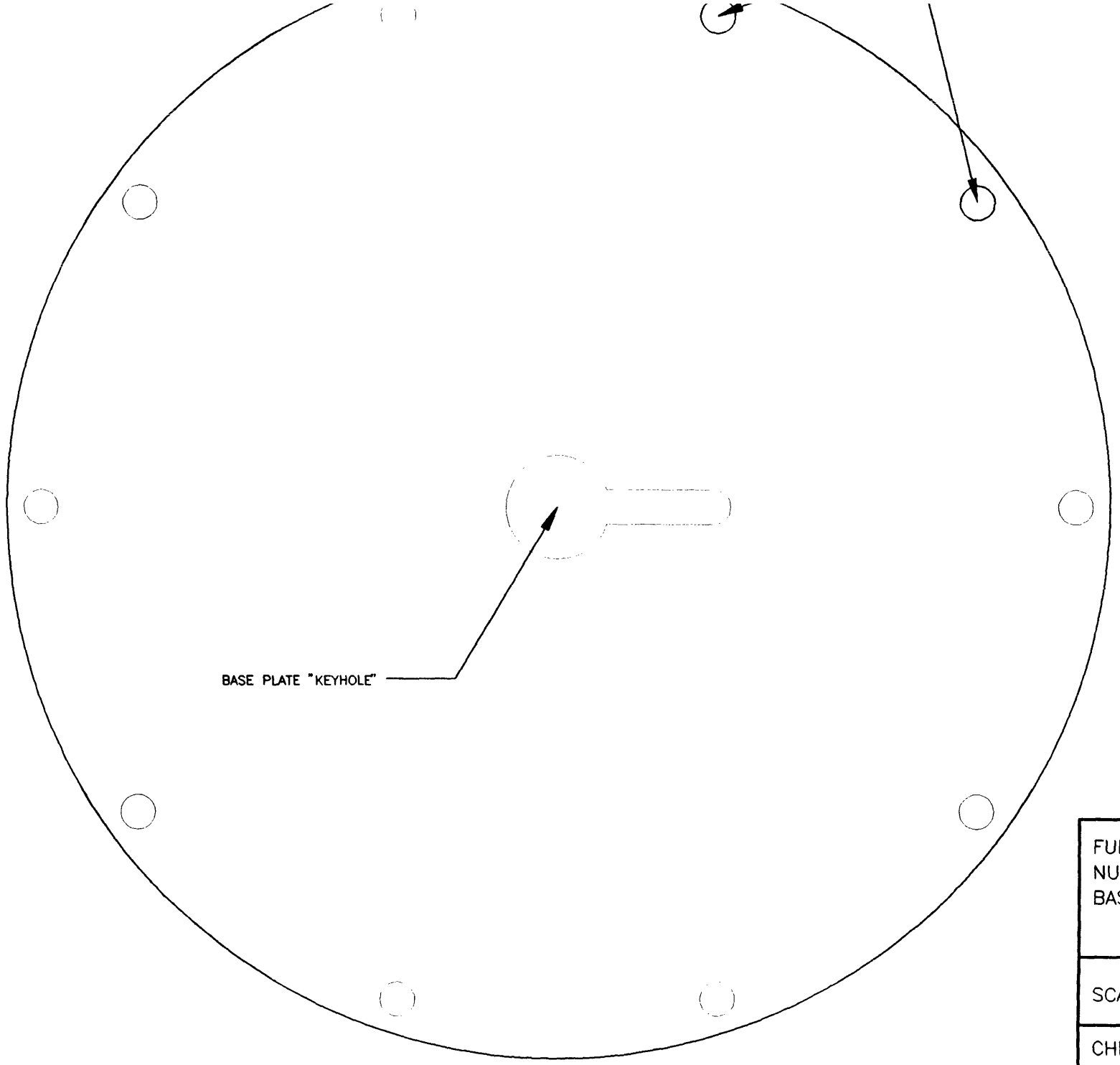

FURNACE REDESIGN
NUMBER TWO:
BASE PLATE

SCALE: FULL

CHRISTOPHER T. RAT
JUNE 10, 1994

Appendix B: Finite Difference Code
B1: Ratmat2.m

```
% GTAW Simulation; ratmat2
% 2 Dimensional Finite Difference Temperature Distribution
% Boundary Conditions: Convective heat transfer at all edge nodes
% Formulation of the parameter matrices A,B,C,D
% Christopher Ratliff 1-15-94
% debugged 1-18-94

function[a,b,c,d,input,u0]=ratmat(m,n)
r=7800;
q=47700;
cp = 434;
kc = 60;
to = 300;
ts = 300;
h= 10;
mn=m*n;
dx = .0005;
q1=n/2;
q2=n/2+1;
a=zeros(mn,mn);

% A matrix
% interior nodes
for i=1:mn;
                a(i,i) = -4*kc/(r*cp*dx^2);
                        if (i-n)>=1,
                                                a(i,i-n)=1*kc/(r*cp*dx^2) ;end
                        if (i+n)<= mn,
                                                a(i,i+n)=1*kc/(r*cp*dx^2);end
                        if (i-1)>=1,
                                                a(i,i-1)=1*kc/(r*cp*dx^2);end
                        if (i+1)<= mn,
                                                a(i,i+1)=1*kc/(r*cp*dx^2);
                        else
                        end
end


%
% LEFT EDGE
%
        for k=1:m
                                i=(k-1)*n +1;
                                        a(i,i)=-1*((h/(r*cp*dx))+2*kc/(r*cp*dx^2));
                                        if (i-n)>=1,
                                                        a(i,i-n)=.5*kc/(r*cp*dx^2);end
                                        if (i+n)<=mn,
                                                        a(i,i+n)=.5*kc/(r*cp*dx^2);end
                                        if (i+1)<=mn,
                                                        a(i,i+1)=kc/(r*cp*dx^2);end
%reset
                                        if (i-1)>0,
                                                a(i,i-1)=0;
```

```
                                                    else
                                                    end

%
% RIGHT EDGE
%

                                    i=(k-1)*n + n;
                                            a(i,i)=-1*((h/(r*cp*dx))+2*kc/(r*cp*dx^2));
                                            if(i-n)>=1,
                                                                    a(i,i-n)=.5*kc/(r*cp*dx^2);end
                                            if(i+1)<=mn,
                                                                a(i,i+n)=.5*kc/(r*cp*dx^2);end
                                            if(i-1)<=mn,
                                                                a(i,i-1)=1*kc/(r*cp*dx^2);end
%reset
                                            if (i+1)<(mn+1),
                                                    a(i,i+1)=0;
                                                    else
                                                    end
        end
%
%BOTTOM
%
        for k=1:n
                        i=(m-1)*n +k;
                        a(i,i) = -1*((h/(r*cp*dx))+2*kc/(r*cp*dx^2));
                        a(i,i-n)=1*kc/(r*cp*dx^2);
                        if (i-1)>=(mn-n+1),
                                        a(i,i-1)=.5*kc/(r*cp*dx^2);end
  if (i+1)<=(mn),
                                        a(i,i+1)=.5*kc/(r*cp*dx^2);end
%reset here
                        if (i+n)<(mn+1),
                                        a(i,i+n) =0;
                                        else
                                        end
end

%
%TOP
%
        for k=1:n
                        a(k,k) =-1*((h/(r*cp*dx))+2*kc/(r*cp*dx^2));

                        a(k,k+n)=1*kc/(r*cp*dx^2);
                        if k>1,
                                        a(k,k-1)=.5*kc/(r*cp*dx^2);end
                        if k<n,
                                        a(k,k+1)=.5*kc/(r*cp*dx^2);end
%reset
                        if (k-n)>0,
                                        a(k,k-n) =0;
                        else
                        end
        end
```

```
%CORNERS
%TOP LEFT

        a(1,1) = -1*((h/(r*cp*dx))+1*kc/(r*cp*dx^2));
 a(1,1+n)=.5*kc/(r*cp*dx^2);
 a(1,2)=.5*kc/(r*cp*dx^2);

%TOP RIGHT

a(n,n) = -1*((h/(r*cp*dx))+1*kc/(r*cp*dx^2));
 a(n,n+n)=.5*kc/(r*cp*dx^2);
 a(n,n-1)=.5*kc/(r*cp*dx^2);

%LOWER LEFT

a(mn-n+1,mn-n+1) = -1*((h/(r*cp*dx))+1*kc/(r*cp*dx^2));
 a(mn-n+1,mn-2*n+1)=.5*kc/(r*cp*dx^2);
 a(mn-n+1,mn-n+2)=.5*kc/(r*cp*dx^2);
%reset
 a(mn-n+1,mn-n)=0;

%LOWER RIGHT

a(mn,mn) = -1*((h/(r*cp*dx))+1*kc/(r*cp*dx^2));
 a(mn,mn-1)=.5*kc/(r*cp*dx^2);
 a(mn,mn-n)=.5*kc/(r*cp*dx^2);


%B,C,D


%b matrix
b=eye(mn,mn);
c=eye(mn,mn);
        %for i=1:mn;
        %c(1,1) = 1;
 %c(2,7)=1;
 %end;
d=zeros(mn,mn);
% For Simulink
%%%%
input=zeros(1000,mn+1);
  for i=1:1000;
    input(i,1)=i;
          for j=2:n+1;
                          input(i,j)=((h*ts)/(dx*r*cp));
   end;
                                  for j=1:(m-1);
                        input(i,j*n+1)=((h*ts)/(dx*r*cp));
                                  end;
                                  for j=1:(m-1);
                      input(i,j*n+2)=((h*ts)/(dx*r*cp));
   end;
                                  for k=((mn-n)+1):mn+1;
     input(i,k)=((h*ts)/(dx*r*cp));
          end;
                                  input(i,q1+1)=q/((dx^2)*r*cp);
                                  input(i,q1)=q/((dx^2)*r*cp);
```

```
                                        input(i,q1-1)=q/((dx^2)*r*cp);
                                        input(i,q2+1)=q/((dx^2)*r*cp);
                                        input(i,q2+2)=q/((dx^2)*r*cp);
                                        input(i,q2+3)=q/((dx^2)*r*cp);
  end;
%%%
for i=1:mn;
                u0(1,i)=300;
end;
end
```

B2: Ratomato.m

```
% Stream Welding Model 3 mm x 3 mm bead; ratomato.m
% 2 Dimensional Finite Difference Temperature Distribution
% Boundary Conditions: Convective heat transfer at all edge nodes
% Initial Conditions: Top center nodes at 2600c while rest of nodes at room % temp
% Formulation of the parameter matrices A,B,C,D
% Christopher Ratliff 1-31-94


function[a,b,c,d,input,u0]=ratomato(m,n)

e=6;
f=6;
ef=e*f;

r=7800;
cp = 434;
kc = 60;
t0 = 1000;
ts = 300;
h= 10;
mn=m*n;
mnef=ef+mn;
dx = .0005;
q1=n/2;
q2=n/2+1;
a=zeros(mnef,mnef);

%puddle matrix
%  interior nodes
for i=1:ef;
                    a(i,i) = -4*kc/(r*cp*dx^2);
                            if (i-f)>=1,
                                                    a(i,i-f)=1*kc/(r*cp*dx^2) ;end
                            if (i+f)<= ef,
                                                    a(i,i+f)=1*kc/(r*cp*dx^2);end
                            if (i-1)>=1,
                                                    a(i,i-1)=1*kc/(r*cp*dx^2);end
                            if (i+1)<= ef,
                                                    a(i,i+1)=1*kc/(r*cp*dx^2);
                            else
                            end
end
for i=ef+1:ef+mn;
                    a(i,i) = -4*kc/(r*cp*dx^2);
                            if (i-n)>=ef+1,
                                                    a(i,i-n)=1*kc/(r*cp*dx^2) ;end
                            if (i+n)<= ef+mn,
                                                    a(i,i+n)=1*kc/(r*cp*dx^2);end
                            if (i-1)>=1,
                                                    a(i,i-1)=1*kc/(r*cp*dx^2);end
                            if (i+1)<= ef+mn,
                                                    a(i,i+1)=1*kc/(r*cp*dx^2);
                            else
                            end
end
%
```

```
% LEFT EDGE
%
        for k=1:e
                                i=(k-1)*f +1;
                                        a(i,i)=-1*((h/(r*cp*dx))+2*kc/(r*cp*dx^2));
                                        if (i-f)>=1,
                                                        a(i,i-f)=.5*kc/(r*cp*dx^2);end
                                        if (i+f)<=ef,
                                                        a(i,i+f)=.5*kc/(r*cp*dx^2);end
                                        if (i+1)<=ef,
                                                        a(i,i+1)=kc/(r*cp*dx^2);end
%reset
                                        if (i-1)>0,
                                                a(i,i-1)=0;
                                                else
                                                end


%
% RIGHT EDGE
%

                                i=(k-1)*f + f;
                                        a(i,i)=-1*((h/(r*cp*dx))+2*kc/(r*cp*dx^2));
                                        if(i-f)>=1,
                                                                a(i,i-f)=.5*kc/(r*cp*dx^2);end
                                        if(i+1)<=ef,
                                                        a(i,i+f)=.5*kc/(r*cp*dx^2);end
                                        if(i-1)<=ef,
                                                        a(i,i-1)=1*kc/(r*cp*dx^2);end
%reset
                                        if (i+1)<(ef+1),
                                                a(i,i+1)=0;
                                                else
                                                end
        end
%
%TOP
%
        for k=1:f
                        a(k,k) =-1*((h/(r*cp*dx))+2*kc/(r*cp*dx^2));

                        a(k,k+f)=1*kc/(r*cp*dx^2);
                        if k>1,
                                        a(k,k-1)=.5*kc/(r*cp*dx^2);end
                        if k<f,
                                        a(k,k+1)=.5*kc/(r*cp*dx^2);end
%reset
                        if (k-f)>0,
                                        a(k,k-f) =0;
                        else
                        end
        end

%CORNERS
%TOP LEFT

        a(1,1) = -1*((h/(r*cp*dx))+1*kc/(r*cp*dx^2));
```

```
a(1,1+f)=.5*kc/(r*cp*dx^2);
a(1,2)=.5*kc/(r*cp*dx^2);

%TOP RIGHT
a(f,f) = -1*((h/(r*cp*dx))+1*kc/(r*cp*dx^2));
a(f,f+f)=.5*kc/(r*cp*dx^2);
a(f,f-1)=.5*kc/(r*cp*dx^2);

%bottom row of additional nodes
 for k=2:f-1
                              i=e*f-f+k;
                               a(i,i+n/2+f/2)=1*kc/(r*cp*dx^2);
 end
%corner nodes
%left
 i=e*f-f+1;
                    a(i,i)=-1*((h/(r*cp*dx))+2*kc/(r*cp*dx^2));
  a(i,i-f)=.5*kc/(r*cp*dx^2);end
  a(i,i+n/2+f/2)=.5*kc/(r*cp*dx^2);end
  a(i,i+1)=kc/(r*cp*dx^2);end
%right
 i=e*f;
                                                  a(i,i)=-1*((h/(r*cp*dx))+2*kc/(r*cp*dx^2));
                                                  a(i,i-f)=.5*kc/(r*cp*dx^2);end
                                                  a(i,i+n/2+f/2)=.5*kc/(r*cp*dx^2);end
                                                  a(i,i-1)=1*kc/(r*cp*dx^2);end

%Below additional nodes
        for k=1:f-2
                              i=(e)*f+n/2-f/2+1+k; %40+k
                                                   a(i,i) = -4*kc/(r*cp*dx^2);
                              if (i-f)>=1,
                                                        a(i,i-(n/2+f/2))=1*kc/(r*cp*dx^2) ;end
                              if (i+f)<= ef,
                                                        a(i,i+n)=1*kc/(r*cp*dx^2);end
                              if (i-1)>=1,
                                                        a(i,i-1)=1*kc/(r*cp*dx^2);end
                              if (i+1)<= ef,
                                                        a(i,i+1)=1*kc/(r*cp*dx^2);
                              else
                              end
        end
%LOWER LEFT
        i=e*f+n/2-f/2+1;
a(i,i) = -1*((h/(r*cp*dx))+3*kc/(r*cp*dx^2));
a(i,i-(n/2+f/2))=.5*kc/(r*cp*dx^2);
a(i,i-1)=.5*kc/(r*cp*dx^2);
a(i,i+1)=1*kc/(r*cp*dx^2);
a(i,i+n)=1*kc/(r*cp*dx^2);
%reset
a(mn-n+1,mn-n)=0;

%LOWER RIGHT

i=e*f+n/2-f/2+f
a(i,i) = -1*((h/(r*cp*dx))+3*kc/(r*cp*dx^2));
a(i,(i-(n/2+f/2+1)+1))=.5*kc/(r*cp*dx^2);
a(i,i+1)=.5*kc/(r*cp*dx^2);
```

```
a(i,i-1)=1*kc/(r*cp*dx^2);
a(i,i+n)=1*kc/(r*cp*dx^2);
a(i,i-n+1)=0;


%%%%%%%%%%%%%%%%%%%%%%%%%%%%%%%%%%%%%%%%%%%%%%%%%%%%%%%%%%%%%%%%
%%%%%%%%%%


%
% LEFT EDGE
%
        for k=1:m
                                i=(k-1)*n +1+ef;
                                        a(i,i)=-1*((h/(r*cp*dx))+2*kc/(r*cp*dx^2));
                                        if (i-(n+ef))>=1,
                                                        a(i,i-n)=.5*kc/(r*cp*dx^2);end
                                        if (i+n)<=mn+ef,
                                                        a(i,i+n)=.5*kc/(r*cp*dx^2);end
  a(i,i+1)=kc/(r*cp*dx^2);

%reset
                                                a(i,i-1)=0;


%
% RIGHT  EDGE
%

                                i=(k-1)*n + n+ef;
                                        a(i,i)=-1*((h/(r*cp*dx))+2*kc/(r*cp*dx^2));
                                        if(i-n)>=1,
                                                                a(i,i-n)=.5*kc/(r*cp*dx^2);end
                                        if(i+1)<=mn+ef,
                                                        a(i,i+n)=.5*kc/(r*cp*dx^2);end
                                        if(i-1)<=mn+ef,
                                                        a(i,i-1)=1*kc/(r*cp*dx^2);end
%reset
                                        if (i+1)<(mn+1+ef),
                                                a(i,i+1)=0;
                                                else
                                                end
        end
%
%BOTTOM
%
        for k=1:n
                        i=(m-1)*n +k+ef;
                        a(i,i) = -1*((h/(r*cp*dx))+2*kc/(r*cp*dx^2));
                        a(i,i-n)=1*kc/(r*cp*dx^2);
                        if (i-1)>=(mn-n+1+ef),
                                        a(i,i-1)=.5*kc/(r*cp*dx^2);end
 if (i+1)<=(mn+ef),
                                        a(i,i+1)=.5*kc/(r*cp*dx^2);end
```

```
%reset here
                        if (i+n)<(mn+1),
                                a(i,i+n) =0;
                                else
                                end
end

%
%TOP of first part
%
        for k=ef+1:(ef+1+n/2-f/2-1)
                        a(k,k) =-1*((h/(r*cp*dx))+2*kc/(r*cp*dx^2));

                        a(k,k+n)=1*kc/(r*cp*dx^2);

                        a(k,k-1)=.5*kc/(r*cp*dx^2);
        %       if k<=ef+n/2-f/2,
                                a(k,k+1)=.5*kc/(r*cp*dx^2);end
%reset
                        if (k-n)>0,
                                a(k,k-n);
                else
                end
        end
%
%TOP of second part
%
        for k=ef+1+n/2+f/2:ef+n
                        a(k,k) =-1*((h/(r*cp*dx))+2*kc/(r*cp*dx^2));

                        a(k,k+n)=1*kc/(r*cp*dx^2);
                        if k>1,
                                a(k,k-1)=.5*kc/(r*cp*dx^2);end
                        if k<n+ef,
                                a(k,k+1)=.5*kc/(r*cp*dx^2);end
%reset
                        if (k-n)>0,
                                a(k,k-n)=0;
                                a(k,k-n+1)=0;
                        else
                        end
        end
%CORNERS
%TOP LEFT

        a(ef+1,ef+1) = -1*((h/(r*cp*dx))+1*kc/(r*cp*dx^2));
 a(ef+1,ef+1+n)=.5*kc/(r*cp*dx^2);
 a(ef+1,ef+2)=.5*kc/(r*cp*dx^2);
 a(ef+1,ef+1-1)=0;


 %TOP RIGHT

a(ef+n,ef+n) = -1*((h/(r*cp*dx))+1*kc/(r*cp*dx^2));
 a(ef+n,ef+n+n)=.5*kc/(r*cp*dx^2);
 a(ef+n,ef+n-1)=.5*kc/(r*cp*dx^2);

 %LOWER LEFT
```

```
a(ef+mn-n+1,ef+mn-n+1) = -1*((h/(r*cp*dx))+1*kc/(r*cp*dx^2));
 a(ef+mn-n+1,ef+mn-2*n+1)=.5*kc/(r*cp*dx^2);
 a(ef+mn-n+1,ef+mn-n+2)=.5*kc/(r*cp*dx^2);
%reset
 a(ef+mn-n+1,ef+mn-n)=0;

%LOWER RIGHT

a(ef+mn,ef+mn) = -1*((h/(r*cp*dx))+1*kc/(r*cp*dx^2));
 a(ef+mn,ef+mn-1)=.5*kc/(r*cp*dx^2);
 a(ef+mn,ef+mn-n)=.5*kc/(r*cp*dx^2);
 a(361,360)=1*kc/(r*cp*dx^2);  %%%weirdo

%B,C,D


%b matrix
b=eye(mn+ef,mn+ef);
c=eye(mn+ef,mn+ef);
          %for i=1:mn;
          %c(1,1) = 1;
 %c(2,7)=1;
 %end;
d=zeros(mn+ef,mn+ef);
% For Simulink
%%%%
input=zeros(1000,mn+ef+1);
  for i=1:1000;
    input(i,1)=i;
   for j=2:f+1;
%top1
           input(i,j)=((h*ts)/(dx*r*cp));
    end;
          for j=1:e;
%upperrightside1
                    input(i,j*f+1)=((h*ts)/(dx*r*cp));
          end;
          for j=1:(e-1);
%upperleftside1
                    input(i,j*f+2)=((h*ts)/(dx*r*cp));
    end;
    for j=ef+2:(ef+2+n/2-f/2);
%top2left
                    input(i,j)=((h*ts)/(dx*r*cp));
    end;
    for j=(ef+2+n/2+f/2):(ef+1+n);
%top2right
          input(i,j)=((h*ts)/(dx*r*cp));
    end;
          for j=1:(m-1);
%rightside2
            input(i,ef+2+j*n)=((h*ts)/(dx*r*cp));
          end;
          for j=1:(m);
%leftside2
            input(i,ef+1+(j)*n)=((h*ts)/(dx*r*cp));
          end;
```

```
%bottom
        for k=ef+((mn-n)+2):ef+mn+1;
        input(i,k)=((h*ts)/(dx*r*cp));
        end;

  end;
%%%initial conditions
for i=1:ef;
                u0(1,i)=2900;
end;
for i=ef+1:ef+mn;
                u0(1,i)=t0;
end;
end
```

B3: Ratmat6.m

```
% Stream Welder Simulation bead deposited in groove; ratmat6
% 2 Dimensional Finite Difference Temperature Distribution
% Boundary Conditions: Convective heat transfer at all edge nodes
% Formulation of the parameter matrices A,B,C,D,inputs, and i.c.'s
% Heat Input at the 6 top center nodes
% Christopher Ratliff 1-15-94
% debugged 2-01-94

function[a,b,c,d,input,u0]=ratmat(m,n)
r=7800;
q=83300;
cp = 434;
kc = 60;
to = 300;
ts = 300;
h= 10;
mn=m*n;
dx = .0005;
q1=n/2+1;
q2=n/2+2;
a=zeros(mn,mn);

%  A matrix
%  interior nodes
for i=1:mn;
                a(i,i) = -4*kc/(r*cp*dx^2);
                        if (i-n)>=1,
                                                a(i,i-n)=1*kc/(r*cp*dx^2) ;end
                        if (i+n)<= mn,
                                                a(i,i+n)=1*kc/(r*cp*dx^2);end
                        if (i-1)>=1,
                                                a(i,i-1)=1*kc/(r*cp*dx^2);end
                        if (i+1)<= mn,
                                                a(i,i+1)=1*kc/(r*cp*dx^2);
                        else
                        end
end


%
% LEFT EDGE
%
        for k=1:m
                        i=(k-1)*n +1;
                                a(i,i)=-1*((h/(r*cp*dx))+2*kc/(r*cp*dx^2));
                                if (i-n)>=1,
                                        a(i,i-n)=.5*kc/(r*cp*dx^2);end
                                if (i+n)<=mn,
                                        a(i,i+n)=.5*kc/(r*cp*dx^2);end
                                if (i+1)<=mn,
                                        a(i,i+1)=kc/(r*cp*dx^2);end
%reset
                                if (i-1)>0,
                                        a(i,i-1)=0;
                                        else
                                end
```

```
%
% RIGHT EDGE
%
                        i=(k-1)*n + n;
                        a(i,i)=-1*((h/(r*cp*dx))+2*kc/(r*cp*dx^2));
                                if(i-n)>=1,
                                        a(i,i-n)=.5*kc/(r*cp*dx^2);end
                                if(i+1)<=mn,
                                        a(i,i+n)=.5*kc/(r*cp*dx^2);end
                                if(i-1)<=mn,
                                        a(i,i-1)=1*kc/(r*cp*dx^2);end
%reset
                                if (i+1)<(mn+1),
                                        a(i,i+1)=0;
                                else
                                end
        end
%
%BOTTOM
%
        for k=1:n
                        i=(m-1)*n +k;
                        a(i,i) = -1*((h/(r*cp*dx))+2*kc/(r*cp*dx^2));
                        a(i,i-n)=1*kc/(r*cp*dx^2);
                        if (i-1)>=(mn-n+1),
                                a(i,i-1)=.5*kc/(r*cp*dx^2);end
                        if (i+1)<=(mn),
                                a(i,i+1)=.5*kc/(r*cp*dx^2);end
%reset here
                        if (i+n)<(mn+1),
                                a(i,i+n) =0;
                        else
                        end
end

%
%TOP
%
        for k=1:n
                a(k,k) =-1*((h/(r*cp*dx))+2*kc/(r*cp*dx^2));

                a(k,k+n)=1*kc/(r*cp*dx^2);
                if k>1,
                        a(k,k-1)=.5*kc/(r*cp*dx^2);end
                if k<n,
                        a(k,k+1)=.5*kc/(r*cp*dx^2);end
%reset
                if (k-n)>0,
                        a(k,k-n) =0;
                else
                end
        end

%CORNERS
%TOP LEFT
```

```
        a(1,1) = -1*((h/(r*cp*dx))+1*kc/(r*cp*dx^2));
        a(1,1+n)=.5*kc/(r*cp*dx^2);
        a(1,2)=.5*kc/(r*cp*dx^2);

%TOP RIGHT

        a(n,n) = -1*((h/(r*cp*dx))+1*kc/(r*cp*dx^2));
        a(n,n+n)=.5*kc/(r*cp*dx^2);
        a(n,n-1)=.5*kc/(r*cp*dx^2);

%LOWER LEFT

        a(mn-n+1,mn-n+1) = -1*((h/(r*cp*dx))+1*kc/(r*cp*dx^2));
        a(mn-n+1,mn-2*n+1)=.5*kc/(r*cp*dx^2);
        a(mn-n+1,mn-n+2)=.5*kc/(r*cp*dx^2);
%reset
        a(mn-n+1,mn-n)=0;

%LOWER RIGHT

        a(mn,mn) = -1*((h/(r*cp*dx))+1*kc/(r*cp*dx^2));
        a(mn,mn-1)=.5*kc/(r*cp*dx^2);
        a(mn,mn-n)=.5*kc/(r*cp*dx^2);


%B,C,D


%b matrix
        b=eye(mn,mn);
        c=eye(mn,mn);
        %for i=1:mn;
        %c(1,1) = 1;
 %c(2,7)=1;
 %end;
        d=zeros(mn,mn);
% For Simulink
%%%%
        input=zeros(1000,mn+1);
        for i=1:1000;
                input(i,1)=i;
                for j=2:n+1;
                        input(i,j)=((h*ts)/(dx*r*cp));
   end;
                        for j=1:(m-1);
                           input(i,j*n+1)=((h*ts)/(dx*r*cp));
                        end;
                        for j=1:(m-1);
                                input(i,j*n+2)=((h*ts)/(dx*r*cp));
                        end;
                        for k=((mn-n)+1):mn+1;
                input(i,k)=((h*ts)/(dx*r*cp));
                        end;
%                                       input(i,q1)=q/((dx^2)*r*cp);
%                                       input(i,q2)=q/((dx^2)*r*cp);
%                                       input(i,q1-1)=q/((dx^2)*r*cp);
%                                       input(i,q2+1)=q/((dx^2)*r*cp);
```

```
%                                                   input(i,q1-2)=q/((dx^2)*r*cp);
%                                                   input(i,q2+2)=q/((dx^2)*r*cp);
  end;
%%%
for i=1:mn;
                    u0(1,i)=300;
end;
for i=0:5;
 for j=1:10;
    u0(1,(n/2-(10/2)+j)+i*n)=2900;20-5+j+i*40
 end;
end;
end
```

Appendix C: Control Software
C1: Pyropid.c

```
/*
   ************************************************************************
   *      Program    : pyropid.c
   *  Description : Controls both the temperature and the quantity
   *                   of the molten metal within the Arc Furnace.
   *                   The temperature Controller is a PID type with
   *                   an anti-windup feature. The wirefeed controller
   *                   is an on/off type with wirefeed rate being
   *                   determined by the sensed temperature. As a
   *                   safeguard, wire will not feed at temperatures
   *                   below 1650[C].
   *      Revision   : 1.16
   *      Date       : 5/18/94                C. RATLIFF
   ************************************************************************
*/

#include <stdio.h>
#include <conio.h>
#include <stdlib.h>
#include <dos.h>
#include <time.h>
#include <bios.h>
#include <math.h>
#include <graph.h>
#include "pclerrs.h"          /*DT2801-error codes fo board */
#include "pcldefs.h"          /*DT2801-PCLAB function definitions      */

#define FNAME "teste.dat"
#define WIREFEED_CAL 29.2      /*DT2801-count/(cm/sec) */
#define ichan 0               /*DT2801-A/D channel 0 and also D/A channel 0 */
#define gain 1                /*DT2801-mplification of incoming signal */
#define arcvoltchan 0
#define nPyroChannel 2        /*Pyrometer is hooked up to channel 2*/

main()
{
    clock_t ti, tf;
    float t_elap, igral, e, em1, t, kp, count;
    float tt, ki, u, uc, arc,kd,deriv;
    int ch, done;
    FILE *tmpread_filename;

    float fSum=0.0, fPyroVolt=0.0;  /*Pyrometer variables*/

    unsigned short sAnalogDataVal, sAver; /*ibid*/
    short nI;             /*ibid*/

    extern pcl711(int, unsigned int *);
    unsigned int param[60]; /*pcl711 parameter array for    */
    unsigned int dataA[40]; /*pcl711Conversion data buffer  */
        unsigned int far * datA;
    int upchan;           /*pcl711Upper channel to read on pcls789 */
    float chan[5];
    int param2[16];       /* specify parameters of thermocouples */
```

```
    float comp[16];       /* Cold junction compensation in volts */
    double a[4][10];      /* coefficients for volt to temp C    */
    double b[4][10];      /* coefficients for C to volts        */
    int GAIN;            /* Amplifier Gain of 789 board        */
    float fPyroTemp;
    unsigned int i, vi;
    unsigned int j,k,z;
    float DataBuf, sum, cjc, TCV, TCC;
    unsigned short
          analog_data_value;      /*DT2801 binary number
                                        0 to 4096=-10 to +10 volts*/
    unsigned short
          dac_data[2];    /*digital output signals to be converted by
                            the DT 2801-A board to an analog signal
                            which dictates the wirefeed rate and arc
                            current*/
    float voltage, wirefeed, desired_voltage, sumdt, v_out, v2_out;
                            /*elapsed time, input voltage sensed by
                            board, wirefeed in cm/sec, desired arc
                            voltage,accruer for average voltage,
                            D/A output voltage1, D/A output voltage
                            2*/
    float desired_temp, arc_current, difference, K,loops,gain2,bias;
    int tint, voltsi, aver;     /*DT2801-integer to be used for loops*/
    int error;              /*recieves possible DT2801 error    */
    void initialize_dt(void);
    igral=0;              /*initialize PI variables*/
        e=0;
        em1=0;
        t=.1;
        kp=1300;
        tt=.2;
        ki=1;
        deriv=0;
        kd=500;
        u=0;
        uc=0;
        done=0;
        ch=0;
        loops=10;   /*number of averaged arc voltages*/
        gain2=.233 ;   /*differencing amp gain*/

/* initialize the DT 2801-A board*/

    initialize();

    setup_adc(0,0,3,gain); /*sets DT 2801-A for software trigger with
                             internal clock, channels 0 to 3, gain of 1*/

    enable_for_output(1);  /*enable port 1 for digital output*/

    output_digital_value(1,0xff,0x00);
                           /*initializes 8 bits of digital output port1*/
    tint=0;

    printf("Enter desired arc voltage: ");
    scanf("%f", &desired_voltage);
    printf("Enter bias voltage: ");
```

```
    scanf("%f", &bias);
    printf("Enter desired Temperature: ");
    scanf("%f", &desired_temp);
    tmpread_filename = fopen(FNAME, "w");
    ti = clock();

  while (!done){
   while(kbhit()==0)
    {
//    count=count+1;


/* Pyrometer reading */
          fSum = 0.0;
          for (nI=0; nI<10; nI++) {
             adc_value(nPyroChannel,gain,&sAnalogDataVal);
             fSum += (float)sAnalogDataVal;
          }
          sAver = (unsigned short)(fSum/10.0);
          analog_to_volts(sAver,gain,&fPyroVolt);
          fPyroTemp = 500.0+150.*fPyroVolt;

/* Implement PID Control Law*/
          arc=20;  /*arc voltage*/
          e=desired_temp-fPyroTemp;
          if(e<100 && e>-100){
             igral=(t*(e+em1))/2+igral;
          }
          else if (e>=100){
              igral=igral+100*t;
          }
          else if (e<=-100){
              igral=igral-(100*t);
          }
          deriv=(e-em1)/t;
          uc=((kp*e+ki*igral+kd*deriv)*1/arc);  /***kpkikd***/
          u=(uc/200)*2048+2048;
          em1=e;       /*store previous error value for integration*/


         if(u<2200){              /*to avoid risk of extinguishing arc*/
           arc_current=20;
           dac_data[1]=(arc_current/200)*2048+2048;
           dac_value(1, &dac_data[1]); /*set arc_current at min of 20 AMPS
                                        (0-10 volts corresponds to 0-199 AMPS*/
           v2_out=(arc_current/200)*10;
          }


          if(u>3900){          /*to prevent dac roll over*/

                arc_current=190; /*max arc_current*/
                dac_data[1]=(arc_current/200)*2048+2048;
                dac_value(1, &dac_data[1]);
                v2_out=(arc_current/200)*10;

          }
```

```
        if(u<=3900 && u>=2200){
                arc_current=uc;
                dac_data[1]=u;
                dac_value(1,&dac_data[1]);
                v2_out=(arc_current/200)*10;
        }

        tf = clock();
        t_elap = (tf-ti);
                                /*the following returns a number
                                  informing analog voltage*/
          sumdt=0;
          for (vi=0; vi<loops ; vi++) {
                adc_value(arcvoltchan, gain, &analog_data_value);
                sumdt += analog_data_value;
                aver = (sumdt/loops+aver)/2;
          }
                analog_to_volts(aver, gain, &voltage);
//        voltage=voltage+bias;       /*n

                if((voltage/gain2)>(desired_voltage) && (fPyroTemp>=1650)){     /*if arc voltage
(which is proportional to
                                        arc length) is too high the feedrate is
                                        set for accordingly */
                  wirefeed=((fPyroTemp-1650)/550)*5+3;      /*100*((voltage/gain2)-
desired_voltage);*/
                                                /*wirefeed rate in cm/sec*/
                                                /*ceiling is 10cm/sec*/
                  dac_data[0]=(wirefeed*WIREFEED_CAL)+2048;
                                        /*determines count (2048 to 4096
                                          =0 to 10 volts=0 to 70 cm/sec*/

//                if (dac_data[0]>2281){
//                      dac_value(0, 2281);
//                    /*invokes D/A with above data using
//                      channel 0*/
//                      v_out=1.14;       /*was .94*/
//                      wirefeed=8    /*was 6.6*/
//          }
                  if (dac_data[0]<=2281){
                        dac_value(0, &dac_data[0]);
                                        /*invokes D/A with above data using
                                          channel 0*/
                        v_out=(((wirefeed*WIREFEED_CAL))/2048)*10;

                  }

                }
                else{
                  wirefeed=0;       /*wirefeed in cm/sec*/

                  dac_data[0]=(wirefeed*WIREFEED_CAL)+1000;
                                        /*determines count (2048 to 4096
                                          =0 to 10 volts=0 to 70 cm/sec*/
                  dac_value(0, &dac_data[0]);
                                        /*invokes D/A with above data using
                                          chanel 0*/
                  v_out=-5;
```

```
                }

                if((voltage/gain2)<=(desired_voltage)){
                        /*if voltage is at or below
                                the desired value molten metal level
                                is high enough      */
                  wirefeed=0;       /*wirefeed in cm/sec*/

                  dac_data[0]=(wirefeed*WIREFEED_CAL)+1000;
                                /*determines count (2048 to 4096
                                 =0 to 10 volts=0 to 70 cm/sec*/
                  dac_value(0, &dac_data[0]);
                                /*invokes D/A with above data using
                                 chanel 0*/
                  v_out=-5;
                }
                tint++;



          _clearscreen( _GCLEARSCREEN );
          printf("The Cold Junction Compensation Temperature (C) = %1.5f \n",cjc);
          printf("Temperature(C): %d is %6.2f\n\n",i,TCC);
          printf("Time(milliseconds):%6.0f \n\n",t_elap);
          printf("Arc Voltage:%2.4f\n",voltage/(gain2));
          printf("D/A voltage(to wirefeeder):%5.2f\n",v_out);
          printf("Wirefeed(cm/sec):%3.2f\n\n",wirefeed);
          printf("D/A voltage(to TIG welder):%5.2f\n",v2_out);
          printf("Arc Currents(Amps):%2.4f\n",arc_current);
          printf("Pyrometer output (C): %f\n",fPyroTemp);
//      printf("T= %6.2f \n",(t_elap/count));

          printf("\n");
          printf("press q to stop program, space to change desired Temp, v for arc voltage\n");



          fprintf(tmpread_filename,"%7.0f %5.2f %2.4f %f\n",t_elap,TCC,voltage/(.24),fPyroTemp);


    }    /*kbhit zero*/
/*Check Keyboard. If q, quit; if space, allow user to change desired
          temperature*/
    if (( ch=getch())=='q'){
          done=1;
    }
    else if (ch==' '){
          printf("Enter desired Temperature: ");
          scanf("%f", &desired_temp);
    }
    else if (ch=='v'){
          printf("Enter new arc voltage: ");
          scanf("%f", &desired_voltage);
    }
  } /** done? **/
     fclose(tmpread_filename);
     dac_data[1]=(unsigned short)(0);
     dac_value(1, &dac_data[1]);
```

```
        terminate();
}       /*end of main*/
```

Appendix C2: Testp.c

```
/*********************************************************************
   * Program    : testp.c                                    *
   * Description : Controls both the temperature and the quantity     *
   *            of the molten metal within the     *
   *            Arc Furnace; both are P controllers.
   *            Uses Thermocouple for   *
   *            the temperature acquistion.                  *
   * Revision   : 1.10                                  *
   * Date       : 12/20/93          C. RATLIFF                *
*********************************************************************/

#include <stdio.h>
#include <conio.h>
#include <stdlib.h>
#include <dos.h>
#include <time.h>
#include <bios.h>
#include <math.h>
#include <graph.h>
#include "pclerrs.h"          /*DT2801-error codes fo board */
#include "pcldefs.h"          /*DT2801-PCLAB function definitions      */

#define FNAME "teste.dat"
#define WIREFEED_CAL 29.2      /*DT2801-count/(cm/sec) */
#define ichan 0               /*DT2801-A/D channel 0 and also D/A channel 0 */
#define gain 1                /*DT2801-mplification of incoming signal */



main()
{
    clock_t ti, tf;
    float t_elap;
    FILE *tmpread_filename;


    extern pcl711(int, unsigned int *);
    unsigned int param[60]; /*pcl711 parameter array for    */
    unsigned int dataA[40]; /*pcl711Conversion data buffer  */
    unsigned int far * datA;
    int upchan=14;                    /*pcl711Upper channel to read on pcls789 */
    float chan[5];
    int param2[16];         /* specify parameters of thermocouples */
    float comp[16];         /* Cold junction compensation in volts */
    double a[4][10];        /* coefficients for volt to temp C     */
    double b[4][10];        /* coefficients for C to volts         */
    int GAIN;              /* Amplifier Gain of 789 board         */
    unsigned int i, vi;
    unsigned int j,k,z;
    float DataBuf, sum, cjc, TCV, TCC;
    unsigned short
            analog_data_value;        /*DT2801 binary number
                                              0 to 4096=-10 to +10 volts*/
    unsigned short
            dac_data[2];    /*digital output signals to be converted by
```

```
                        the DT 2801-A board to an analog signal
                        which dictates the wirefeed rate and arc
                        current*/
float voltage, wirefeed, desired_voltage, sumdt, v_out, v2_out;
                        /*elapsed time, input voltage sensed by
                        board, wirefeed in cm/sec, desired arc
                        voltage,accruer for average voltage,
                        D/A output voltage1, D/A output voltage
                        2*/
float desired_temp, arc_current, difference, K;
int tint, voltsi, aver;     /*DT2801-integer to be used for loops*/
int error;              /*recieves possible DT2801 error    */
void initialize_dt(void);



datA = dataA;           /* refer to pcl-711s for better
                                explanation of parameters below*/
param[0]  = 0;          /* Board number                  */
param[1]  = 0x220;      /* Base I/O address              */
param[4]  = 2;
param[5]  = 50;         /* Pacer rate = 2M /(50 * 400) = 100 Hz  */
param[6]  = 400;
param[7]  = 0;          /* Trigger mode, 0 : pacer trigger       */
param[8]  = 0;
param[10] = FP_OFF(datA); /* Offset of A/D data buffer A         */
param[11] = FP_SEG(datA); /* Segment of A/D data buffer A        */
param[12] = 0;          /* Data buffer B address, if not used,   */
param[13] = 0;          /* must set to 0.                */
param[14] = 20;         /* A/D conversion number               */
param[15] = 7;          /* A/D conversion start channel(for cjc updated for thermocouples       */
param[16] = 7;          /* A/D conversion stop channel (for cjc updated later in program as above */
param[17] = 0;          /* Overall gain code, 0 : +/- 5V         */
param[35] = 0;          /* Data buffer B address, if not used    */
param[36] = 0;          /* must be set to 0              */
param[37] = 1;          /* Digital ouput number              */
param[38] = 0;          /* Digital output port               */

a[1][0] = 1.46455905941072;  /* Parameters for C thermocouple  */
a[1][1] = 7.041868719945035e4; /* Given Volts convert to C */
a[1][2] = -2.40916104288838e6;
a[1][3] = 0.01342602300356e10;
a[1][4] = -0.33701977314938e10;
a[1][5] = 3.62131846489482e10;
a[1][6] = 0;
a[1][7] = 0;
a[1][8] = 0;
a[2][0] = -0.048868252;       /* Parameters for J thermocouple */
a[2][1] = 19873.14503;
a[2][2] = -218614.5353;
a[2][3] = 11569199.78;
a[2][4] = -264917531.4;
a[2][5] = 2018441314;
a[2][6] = 0;
a[2][7] = 0;
a[2][8] = 0;
a[3][0] = 0.226584602;         /* Parameters for K thermocouple */
a[3][1] = 24152.109;
```

```
    a[3][2] = 67233.4248;
    a[3][3] = 2210340.682;
    a[3][4] = -860963914.9;
    a[3][5] = 4.83506e10;
    a[3][6] = -1.18452e12;
    a[3][7] = 1.3869e13;
    a[3][8] = -6.33708e13;
    b[1][0] = -3.987221183160523e-7;      /* Parameters to convert C to volts */
    b[1][1] = 1.338768984709738e-5;   /* C type */
    b[1][2] = 1.225259318481225e-8;
    b[1][3] = -1.033848938419896e-11;
    b[2][0] = 0.02497930107e-4;           /* J Type */
    b[2][1] = 0.503162731417e-4;
    b[2][2] = 0.00028151039166e-4;
    b[2][3] = -0.00000050835061e-4;
    b[3][0] = -0.09432523270954e-4;       /* K Type */
    b[3][1] = 0.41413853095365e-4;
    b[3][2] = -0.00005177487284e-4;
    b[3][3] = 0.00000004731644e-4;
/* initialize the pcl-711b board*/
    pcl711(3, param);       /* Func 3 : Hardware initialization */
    if (param[45] != 0) {
            printf("1. DRIVER INITIALIZATION FAILED ! %1.7f",b[3][3]);
            printf("This is param[45] %2d %2d",param[45],param[0]);
            exit(1);
            }

    pcl711(4,param);        /* A/D initialization */
    if (param[45] != 0) {
             printf(" A/D INITIALIZATION FAILED !");
             exit(1);
             }

/* initialize the DT 2801-A board*/

    initialize();

    setup_adc(0,0,3,gain); /*sets DT 2801-A for software trigger with
                                internal clock, channels 0 to 3, gain of 1*/

    enable_for_output(1);  /*enable port 1 for digital output*/

    output_digital_value(1,0xff,0x00);
                            /*initializes 8 bits of digital output port1*/
    tint=0;

    printf("Enter desired arc voltage: ");
    scanf("%f", &desired_voltage);
    printf("Enter desired Temperature: ");
    scanf("%f", &desired_temp);
    printf("\nEnter # of thermocouples used : ");
    scanf ("%d", &upchan);
    printf("\nEnter GAIN of 789 Board: ");
    scanf("%d", &GAIN);
    for (i = 1; i<=upchan; i++) {
        printf("\nEnter thermocouple type for channel %2d\n",i-1);
        printf("Valid entries are 1 (C) , 2 (J), and 3 (K) : ");
        scanf ("%d", &param2[i]);
```

```
}

pcl711(9, param);       /* Func 9 : Pacer trigger A/D conversion
                                        with interrupt data transfer */
if (param[45] != 0) {
        printf("\nA/D PACER TRIGGER WITH INTERRUPT DATA TRANSFER FAILED !");
        exit(1);
        }
do {
        pcl711(10, param);          /* Func 10 : Check interrupt status */
} while( param[46] != 0 );      /* 0 : not active, 1 : active     */

sum = 0;              /* initialize sum */
for (i=0; i<param[14] ; i++) {
      DataBuf = dataA[i] & 0xFFF;
      DataBuf = ( (5 - (-5)) * DataBuf / 4096) + (-5);
      sum += DataBuf;
        /*
          (5 - (-5)) : A/D input range (-5V  to  5V)
          4096       : Full scale 12 bit A/D data
          DataBuf    : A/D input data
          (-5)       : A/D input range "-5" V
        */
}
cjc = sum /param[14];  /* Average CJC readings */
cjc = cjc/(0.0244);    /* Convert from mV to Centigrade */
printf("The Cold Junction Compensation Temp (C) = %1.5f \n",cjc);

for (i = 1; i<= 1; i++)  /* convert C to volts for 1 CJC */
      {
      z = param2[i];
      comp[i] = b[z][0] + cjc*(b[z][1] + cjc*(b[z][2] + cjc*b[z][3]));
      }


                                    /*  Digital output initialization */
pcl711(28,param);
if (param[45] !=0) {
        printf("Digital Output Initialization failed! ");
        exit(1);
}

param[15] = 0;          /* A/D conversion start channel for thermocouples */
param[16] = 0;          /* A/D conversion stop channel for thermocouples  */
tmpread_filename = fopen(FNAME, "w");
ti = clock();

while (kbhit() == 0)
 {


      unsigned int dataB[15]; /* Array of channels on 789 board */
      unsigned int far * datB;
      datB = dataB;
      param[33] = FP_OFF(datB);     /* Offset of digital output data buffer B */
      param[34] = FP_SEG(datB);     /* Segment of digital output data buff   */
      for (i = 0; i <= upchan; i++)  /* Array of 789 board channels      */
       dataB[i] = i;
```

```
for (i = 1; i <=upchan ; i++)   /* Reads only first upchan of 789 board */
{

      pcl711(29,param);          /* Set 711 to read proper chan on 789 */
      if (param[45] != 0)  {
          printf("Digital Output has failed! ");
          exit(1);
      }

     /* pcl711(30,param);  */       /* Check digital out value of 711 */
     /* if (param[45] != 0)  {
         printf("Digital check has failed! ");
         exit(1);
       }            */
     /* printf("This is the digital value out %2d\n",param[46]); */

      *datB += 1;
      param[33] = FP_OFF(datB);   /* Offset of digital output data buffer B */
      param[34] = FP_SEG(datB);   /* Segment of digital output data buff  */

      pcl711(9, param);          /* Func 9 : Pacer trigger A/D conversion */
      if (param[45] != 0) {      /*        with interrupt data transfer */
          printf("\nA/D PACER TRIGGER WITH INTERRUPT DATA TRANSFER FAILED !");
          exit(1);
      }
      do {
          pcl711(10, param);          /* Func 10 : Check interrupt status */
      }while((param[46] & 1) != 0);     /* 0 : not active, 1 : active     */

       sum = 0;
       for (j=0; j<param[14] ; j++) {
         DataBuf = dataA[j] & 0xFFF;
         DataBuf =( (5 - (-5)) * DataBuf / 4096) + (-5);
         sum += DataBuf;

       }
       TCV = sum/param[14];   /* Thermocouple volts */
       chan[i] = TCV/GAIN + comp[i];
       TCV = chan[i];


      z = param2[i];
      TCC = a[z][0] + TCV*(a[z][1] + TCV*(a[z][2] + TCV*(a[z][3] + TCV*(a[z][4]
          + TCV*(a[z][5] + TCV*(a[z][6] + TCV*(a[z][7] + TCV*a[z][8])))))));
      if(TCC>=desired_temp){
        arc_current=20;
        dac_data[1]=2254;

        dac_value(1, &dac_data[1]); /*set arc_current at min of 20 AMPS
                                      (0-10 volts corresponds to 0-199 AMPS*/
        v2_out=1;
      }
      if(TCC<desired_temp){
        difference=desired_temp-TCC;
        if(difference>100){
              arc_current=190; /*max arc_current*/
              dac_data[1]=3900;
```

```
        dac_value(1, &dac_data[1]);
        v2_out=9.04;
  }
  if(difference<=100){

        K=1.7;      /*proportional control constant*/
        arc_current=K*difference+20;
        dac_data[1]=((arc_current/199)*2047+2047 );
        dac_value(1, &dac_data[1]);
        v2_out=(arc_current/199)*10;
  }
}
 tf = clock();
 t_elap = (tf-ti);
                        /*the following returns a number
                          informing analog voltage*/
  sumdt=0;
  for (vi=0; vi<20 ; vi++) {
        adc_value(ichan, gain, &analog_data_value);
        sumdt += analog_data_value;
        aver = sumdt/20;
  }
        analog_to_volts(aver, gain, &voltage);



        if((voltage/.24)>(desired_voltage)){    /*if arc voltage (which is proportional to
                                                  arc length) is too high the feedrate is
                                                  set for accordingly */
          wirefeed=5*((voltage/.24)-desired_voltage);        /*was 100*/
                                                  /*wirefeed rate in cm/sec*/

          dac_data[0]=(wirefeed*WIREFEED_CAL)+2048;
                                  /*determines count (2048 to 4096
                                   0 to 10 volts=0 to 70 cm/sec*/
          if (dac_data[0]>4095){
                dac_value(0, 2160);
                                  /*invokes D/A with above data using
                                    channel 0*/
                v_out=.5;      /*was 10*/
                wirefeed=3.5;   /*was 70*/
          }
          if (dac_data[0]<4096){
                dac_value(0, &dac_data[0]);
                                  /*invokes D/A with above data using
                                    channel 0*/
                v_out=(((wirefeed*WIREFEED_CAL))/2048)*10;

          }
        }
        if((voltage/.24)<=(desired_voltage)){
                                  /*if voltage is at or below
                                    the desired value molten metal level
                                    is high enough      */
          wirefeed=0;       /*wirefeed in cm/sec*/
```

```
                dac_data[0]=(wirefeed*WIREFEED_CAL)+2048;
                                    /*determines count (2048 to 4096
                                      =0 to 10 volts=0 to 70 cm/sec*/
                dac_value(0, &dac_data[0]);
                                    /*invokes D/A with above data using
                                      chanel 0*/
                v_out=(((dac_data[0]-2048))/2048)*10;
              }
              tint++;

        _clearscreen( _GCLEARSCREEN );
        printf("The Cold Junction Compensation Temperature (C) = %1.5f \n",cjc);
        printf("Temperature(C): %d is %6.2f\n\n",i,TCC);
        printf("Time(milliseconds):%6.0f \n\n",t_elap);
        printf("Arc Voltage:%2.4f\n",voltage/(.24));
        printf("D/A voltage(to wirefeeder):%5.2f\n",v_out);
        printf("Wirefeed(cm/sec):%3.2f\n\n",wirefeed);
        printf("D/A voltage(to TIG welder):%5.2f\n",v2_out);
        printf("Arc Currents(Amps):%2.4f",arc_current);


    dac_data[0]=(unsigned short)(0);
    dac_value(0, &dac_data[0]);

          terminate();
}     /*end of main*/
```

Appendix D: Wire Melting Rate Calculations

Problem: Find the time t that it takes for a steel wire segment of diameter D and submerged length H to melt when immersed in a molten metal bath at temperature T_{mm}=2200C.

Schematic:

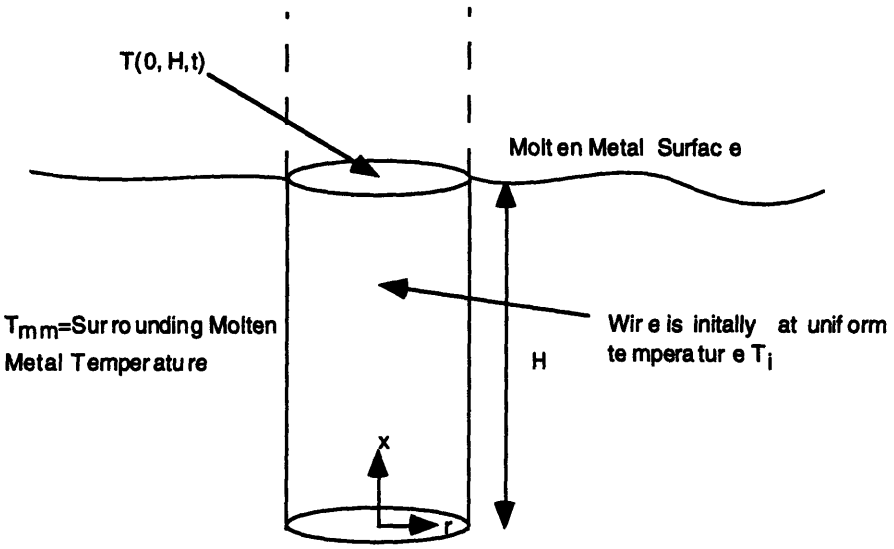

Assumptions:

1. Convective Boundary Condition with conduction in r and x
2. Constant properties for steel wire
3. Experimentally Determined Convection coefficient does not change with wire diameter
4. Initial Temperature of the wire segment is 773K and uniform throughout
5. Experimentally determined Convection coefficient sufficiently accounts for latent heat effects

Symbols/ Property values:

T - Temperature of the feed wire (K)

T_{mm} - Temperature of the molten metal (2573K)

Θ - $T-T_{mm}$

t - Time (seconds)

h - Generalized convective heat transfer coefficient (11,600 W/m^2K from experiment)

ρ - Density of feed wire(7800 kg/m^3)

c_p - Specific heat of feed wire(434 J/kgK)

r_i - Wire Radius (r_1=2.5 mm r_2=.5 mm r_3=.125 mm)

r - Radial coordinate of wire

x - Axial coordinate of wire

k - Thermal conductivity of mild steel (60 W/mK)

α - $k/\rho c_p$ ($18x10^{-6} W/m^2$)

H - Height of Molten Metal/ length of wire segment immersed in molten metal

Analysis:

The appropriate form of the heat equation that needs to be solved is of the form

$$\frac{1}{r}\frac{\partial}{\partial r}\left(r\frac{\partial T}{\partial r}\right)+\frac{\partial^2 T}{\partial x^2}=\frac{1}{a}\frac{\partial T}{\partial t}$$

A closed form solution of this partial differential equation can be obtained using the separation of variables technique. The result may be expressed in the following form [Incropera and Dewitt, 1990]:

$$\frac{T(r,x,t)-T_{mm}}{T_i-T_{mm}}=\left[\frac{T(x,t)-T_{mm}}{T_i-T_{mm}}\right]_{\substack{semi-\inf inite\\ solid}}\cdot\left[\frac{T(r,t)-T_{mm}}{T_i-T_{mm}}\right]_{\substack{\inf inite\\ cylinder}}$$

So the two-dimensional solution is expressed as a product of one-dimensional solutions that correspond to a semi-infinite solid wall and an infinite cylinder with the same radius as the wire.

$$T_i = 773K$$
$$T_{mm} = 2573K$$
$$T(0,.01,t) = 1833K$$

$$\frac{1833K(0,.01,t)-2573K}{773K-2573K}=\left[\frac{T(.01,t)-2573K}{773K-2573K}\right]_{\substack{semi-\inf inite\\ solid}}\cdot\left[\frac{T(0,t)-2573K}{773K-2573K}\right]_{\substack{\inf inite\\ cylinder}}$$

so the problem becomes one of finding the time t where the product of the semi-infinite solid and infinite cylinder solutions is .4111.

The one dimensional semi-infinite solid solution is given by the following equation (erf denotes the Guassian Error Function) or by referring to the table in [11] also given at the end of this appendix

$$\left[\frac{T(x,t)-T_{mm}}{T_i-T_{mm}}\right]_{\substack{semi-\inf inite\\ solid}} = 1-\left[erf\left(\frac{x}{2\sqrt{at}}\right)-\left[e^{\left(\frac{hx}{k}+\frac{h^2\alpha t}{k^2}\right)}\right]\cdot\left[erf\left(\frac{x}{2\sqrt{\alpha t}}+\frac{h\sqrt{\alpha t}}{k}\right)\right]\right]$$

The infinite cylinder solution can be found from graphs in a heat transfer text [Incropera and Dewitt, 1990] also given at the end of this appendix. These graphical solutions require the inverse Biot and Fourier Coefficients which are as follows

$$Bi^{-1} = \frac{k}{hr_o} = \frac{17W/mK}{11{,}600W/m^2K\cdot r_o}$$

$$Fo = \frac{at}{r_o^2} = \frac{5\times10^{-6}\frac{m^2}{\sec}\cdot t}{r_o^2}$$

Solution for Diameter D=5mm:

The value of t is solved for recursively, the first estimate for t is 0.6 second, this value is picked based on some lumped parameter analysis to more quickly arrive at the desired answer.

$$\frac{x}{2\sqrt{\alpha t}} = \frac{.01m}{2\sqrt{18\times10^{-6}m^2/\sec\cdot.6\sec}} = 1.52$$

$$\frac{h\sqrt{\alpha t}}{k} = \frac{11{,}600W/m^2K\sqrt{18\times10^{-6}m^2/\sec\cdot.6\sec}}{60W/mK} = .63$$

hence

$$\left[\frac{T(x,t)-T_{mm}}{T_i-T_{mm}}\right]_{\substack{semi-\inf inite\\ solid}} = .99$$

For the infinite Cylinder:

$$Bi^{-1} = \frac{k}{hr_o} = \frac{17W/mK}{11{,}600W/m^2K \cdot .0025m} = 2.07$$

$$Fo = \frac{at}{r_o^2} = \frac{18\times10^{-6}\frac{m^2}{\sec}\cdot .6\sec}{(.0025m)^2} = 1.728$$

referring to the provided chart

$$\left[\frac{T(r,t)-T_{mm}}{T_i-T_{mm}}\right]_{\substack{\inf inite\\ cylinder}} = .25$$

hence

$$\left[\frac{T(x,t)-T_{mm}}{T_i-T_{mm}}\right]_{\substack{semi-\inf inite\\ solid}} \cdot \left[\frac{T(r,t)-T_{mm}}{T_i-T_{mm}}\right]_{\substack{\inf inite\\ cylinder}} = .99\cdot .25 \cong .25$$

Because .25<.4111 t was chosen to be too large. One can see that the dominant heat transfer is in the radial direction and hence we can look for the Fo number that corresponds to:

$$\left[\frac{T(r,t)-T_{mm}}{T_i-T_{mm}}\right]_{\substack{\inf inite\\ cylinder}} = .411$$

we find Fo=1.1 which corresponds to a value for t of .38 seconds. The resulting mass transfer rate is calculated as follows

$$massflowrate = \pi r_o^2 \frac{H}{t} = \pi(.0025m)^2 \frac{.01m}{.38\sec} = 5.1\times10^{-7} m^3/\sec$$

The analysis for the Diameters of D=1 mm and D= 0.025mm were carried out in the same manner. Since the diameter is even smaller in these cases the semi-infinite solid solution becomes even less significant and one can solve the problem only accounting for the semi-infinite cylinder solution. Since the Biot number is fixed for a given diameter the problem comes down to finding the appropriate Fourier number. The mass flow rate for these two smaller diameters is given here:

$$massflowrate = \pi r_o^2 \frac{H}{t} = \pi(.0005m)^2 \frac{.01m}{.067\sec} = 1.17\times10^{-7} m^3/\sec$$

$$massflowrate = \pi r_o^2 \frac{H}{t} = \pi(.000125m)^2 \frac{.01m}{.016\sec} = 3.14\times10^{-8} m^3/\sec$$

Appendix E: Additional Analysis of Plant for Temperature Control System

The following symbols are used in this appendix:

T	- Temperature [K]
t	- Time [seconds]
P_{in}	- Power input from Hobart power supply [W]
ρ	- Density [Kg/m^3]
c	- Specific heat [J/KgK]
V	- Volume [m^3]
h_1	- Convective heat transfer coefficient from the molten metal to the crucible [W/m^2K]
h_2	- Heat transfer coefficient that accounts for convection and linearized radiation effects between crucible and surroundings [W/m^2K]
h_3	- Convective heat transfer coefficient from the crucible to the argon shielding flow [W/m^2K]
A_s	- Interface area between the molten metal and the crucible [m^2]
A_2	- Area of crucible exterior exposed to shielding flow [m^2]
K_a	- Steady state relationship between P_{in} and T_c [K/W]
τ_a	- Time constant for the first order approximation of plant [seconds]
$subscript_m$	- molten metal
$subscript_c$	- crucible
$subscript_{ar}$	- argon shielding flow
$subscript_{surr}$	- surroundings of exterior of the crucible

Although the temperature control system performs well, it may be beneficial to have a better knowledge of how K_a and τ_a vary under different operating conditions. Here a lumped parameter analysis is carried out that helps predict the effect of molten metal mass on the plant parameters τ_a and K_a. This analysis should help characterize the thermal characteristics of the furnace under different molten metal level operating conditions and perhaps lead to a more refined model of the plant dynamics.

A figure of the relevant system parameters is given below

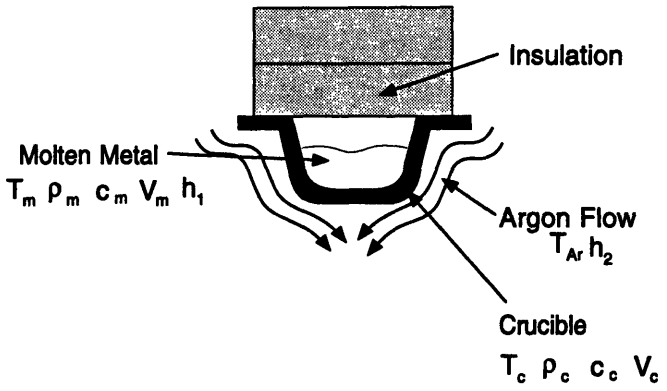

Figure E1: Relevant Parameters in Analysis

The equations approximating the heat transfer for the system shown above are as follows

$$\rho_m V_m c_m \frac{dT_m}{dt} = -h_1 A_s (Tm - Tc) + Pin$$

$$\rho_c V_c c_c \frac{dT_c}{dt} = h_1 A_s (T_m - T_c) - h_3 A_2 (T_c - T_{ar}) + K_3 (T_c^4 - T_{surr}^4)$$

Here the crucible is assumed to be at a uniform temperature T_C, and the molten metal is also at a uniform temperature T_m as implied by the 'lumped' analysis. The only mode of heat transfer considered, between the crucible and the molten metal, is convection. However, radiation heat transfer as well as convection are both important modes of heat transfer away from the exterior of the crucible. The convective coefficients h_1 and h_3 are treated as constants as are density, volume, and specific heat. Latent heat effects are also neglected. For different masses of molten metal the value of A_S, the interfacial area between the crucible and molten metal, changes accordingly. The value of A_S is related to the molten metal mass as follows

$$A_s = (Mass / \rho \pi r_0^2) 2\pi r_0 + \pi r_0^2$$

This lumped analysis is not altogether valid since there are considerable temperature gradients in both the molten metal and the crucible, but this lumped analysis should at least provide good qualitative results. A distributed parameter analysis would require lengthy numerical simulation as well as a number of assumptions as in this analysis.

To simplify the system of nonlinear differential equations above, the radiation heat transfer term is linearized and combined with the convective term h_3 to get h_2. In

comparing an actual response to the response predicted by this model, it is apparent that this linearized term is only valid over a limited operating range. The linearized heat transfer between the crucible, molten metal, and argon flow can be given by the following equations:

$$\rho_m V_{mCm}\frac{dTm}{dt} = -h_1 A_s(Tm - Tc) + Pin$$
$$\rho_c V_{cCc}\frac{dTc}{dt} = h_1 A_s(T_m - T_c) - h_2 A_2(T_c - T_{ar})$$

which can be put into the following form:

$$\begin{bmatrix} \frac{dTm}{dt} \\ \frac{dTc}{dt} \end{bmatrix} = \begin{bmatrix} \frac{-h_1 A_s}{\rho_m V_{mCm}} & \frac{h_1 A_s}{\rho_m V_{mCm}} \\ \frac{h_1 A_s}{\rho_c V_{cCc}} & \frac{-h_1 A_s - h_2 A_2}{\rho_c V_{cCc}} \end{bmatrix} \begin{bmatrix} Tm \\ Tc \end{bmatrix} + \begin{bmatrix} \frac{Pin}{\rho_m V_{mCm}} \\ \frac{h_2 A_2 T_{ar}}{\rho_c V_{cCc}} \end{bmatrix}$$

this system of ODE's can be solved using Laplace transforms and the solution is:

$$Tm = C_1 + C_2 e^{\lambda_1 t} + C_3 e^{\lambda_2 t}$$
$$Tc = C_4 + C_5 e^{\lambda_1 t} + C_6 e^{\lambda_2 t}$$

The eigen-values λ_1 and λ_2 and coefficients C_5 and C_6 determine the first order approximation of the time constant τ_a. Solving for the eigen-values and coefficients above turned out to be algebraically tedious to determine and are given below:

$$\lambda_1 = \frac{-h_1 A_s}{2\rho_m V_{mCm}} + \frac{-h_1 A_s - h_2 A_2}{2\rho_c V_{cCc}} + \frac{\sqrt{\left(\frac{h_1 A_s}{\rho_m V_{mCm}}\right)^2 - \frac{2h_1 A_s}{\rho_m V_{mCm}}\frac{(-h_1 A_s + h_2 A_2)}{\rho_c V_{cCc}} + \frac{(h_1 A_s + h_2 A_2)^2}{(\rho_c V_{cCc})^2}}}{2}$$

$$\lambda_2 = \frac{-h_1 A_s}{2\rho_m V_{mCm}} + \frac{-h_1 A_s - h_2 A_2}{2\rho_c V_{cCc}} - \frac{\sqrt{\left(\frac{h_1 A_s}{\rho_m V_{mCm}}\right)^2 - \frac{2h_1 A_s}{\rho_m V_{mCm}}\frac{(-h_1 A_s + h_2 A_2)}{\rho_c V_{cCc}} + \frac{(h_1 A_s + h_2 A_2)^2}{(\rho_c V_{cCc})^2}}}{2}$$

$$C_1 = T_{ar} - P_{in}\frac{(h_1A_s + h_2A_2)}{h_1A_sh_2A}$$

$$C_2 = \frac{\frac{P_{in}}{\rho_m V_{mCm}}\lambda_1 + (\frac{h_1A_s}{\rho_m V_{mCm}}\frac{h_2A_2T_{ar}}{\rho_c V_{cCc}}) - (\frac{-h_1A_s - h_2A_2}{\rho_c V_{cCc}}\frac{P_{in}}{\rho_m V_{mCm}})}{\lambda_1\sqrt{(\frac{-h_1A_s}{\rho_m V_{mCm}} + \frac{-h_1A_s - h_2A_2}{\rho_c V_{cCc}})^2 - 4(\frac{-h_1A_s}{\rho_m V_{mCm}}\frac{-h_1A_s - h_2A_2}{\rho_c V_{cCc}} - \frac{h_1A_s}{\rho_m V_{mCm}}\frac{h_1A_s}{\rho_c V_{cCc}})}}$$

$$C_3 = \frac{\frac{P_{in}}{\rho_m V_{mCm}}\lambda_2 + (\frac{h_1A_s}{\rho_m V_{mCm}}\frac{h_2A_2T_{ar}}{\rho_c V_{cCc}}) - (\frac{-h_1A_s - h_2A_2}{\rho_c V_{cCc}}\frac{P_{in}}{\rho_m V_{mCm}})}{-\lambda_2\sqrt{(\frac{-h_1A_s}{\rho_m V_{mCm}} + \frac{-h_1A_s - h_2A_2}{\rho_c V_{cCc}})^2 - 4(\frac{-h_1A_s}{\rho_m V_{mCm}}\frac{-h_1A_s - h_2A_2}{\rho_c V_{cCc}} - \frac{h_1A_s}{\rho_m V_{mCm}}\frac{h_1A_s}{\rho_c V_{cCc}})}}$$

$$C_4 = T_{ar} - \frac{P_{in}(h_1A_s + h_2A_2)}{h_1A_sh_2A_2}$$

$$C_5 = \frac{\frac{P_{in}}{\rho_m V_{mCm}}\lambda_1 + (\frac{h_1A_s}{\rho_c V_{cCc}}\frac{P_{in}}{\rho_m V_{mCm}}) - (\frac{-h_1A_s}{\rho_m V_{mCm}}\frac{h_2A_2T_{ar}}{\rho_c V_{cCc}})}{\lambda_1\sqrt{(\frac{-h_1A_s}{\rho_m V_{mCm}} + \frac{-h_1A_s - h_2A_2}{\rho_c V_{cCc}})^2 - 4(\frac{-h_1A_s}{\rho_m V_{mCm}}\frac{-h_1A_s - h_2A_2}{\rho_c V_{cCc}} - \frac{h_1A_s}{\rho_m V_{mCm}}\frac{h_1A_s}{\rho_c V_{cCc}})}}$$

$$C_6 = \frac{\frac{P_{in}}{\rho_m V_{mCm}}\lambda_1 + (\frac{h_1A_s}{\rho_c V_{cCc}}\frac{P_{in}}{\rho_m V_{mCm}}) - (\frac{-h_1A_s}{\rho_m V_{mCm}}\frac{h_2A_2T_{ar}}{\rho_c V_{cCc}})}{-\lambda_2\sqrt{(\frac{-h_1A_s}{\rho_m V_{mCm}} + \frac{-h_1A_s - h_2A_2}{\rho_c V_{cCc}})^2 - 4(\frac{-h_1A_s}{\rho_m V_{mCm}}\frac{-h_1A_s - h_2A_2}{\rho_c V_{cCc}} - \frac{h_1A_s}{\rho_m V_{mCm}}\frac{h_1A_s}{\rho_c V_{cCc}})}}$$

Results

The results given here are based on estimated values h=1700W/m^{2}C and h_2=250W/m^{2}C. The value of h_1 was chosen based on the convection coefficient of molten steel on solid steel which is on the order of 10^3-10^4 and the difference in temperature between the molten metal chamber and the crucible exterior (from chapter 2). The value of h_2 was chosen to closest match the actual open loop responses from weld617.dat.

Figure E2 and E3 show plots of T_m and T_c in response to multiple steps in P_{in}. The dashed lines represents T_m and the solid lines represent T_c. Figure E2 has a molten steel mass of 50g, an exponential curve was fitted to the response at t=250 seconds; here the first order approximation of the time constant, τ_a, is 50 seconds. In Figure E3 the molten steel mass is 80 g and the first order approximation of τ_a is 70 seconds. If it was desired to incorporate the effect of molten metal mass in the first order model of the plant, one could carry out this analysis for a full range of molten metal masses to get τ_a as a function of molten metal charge.

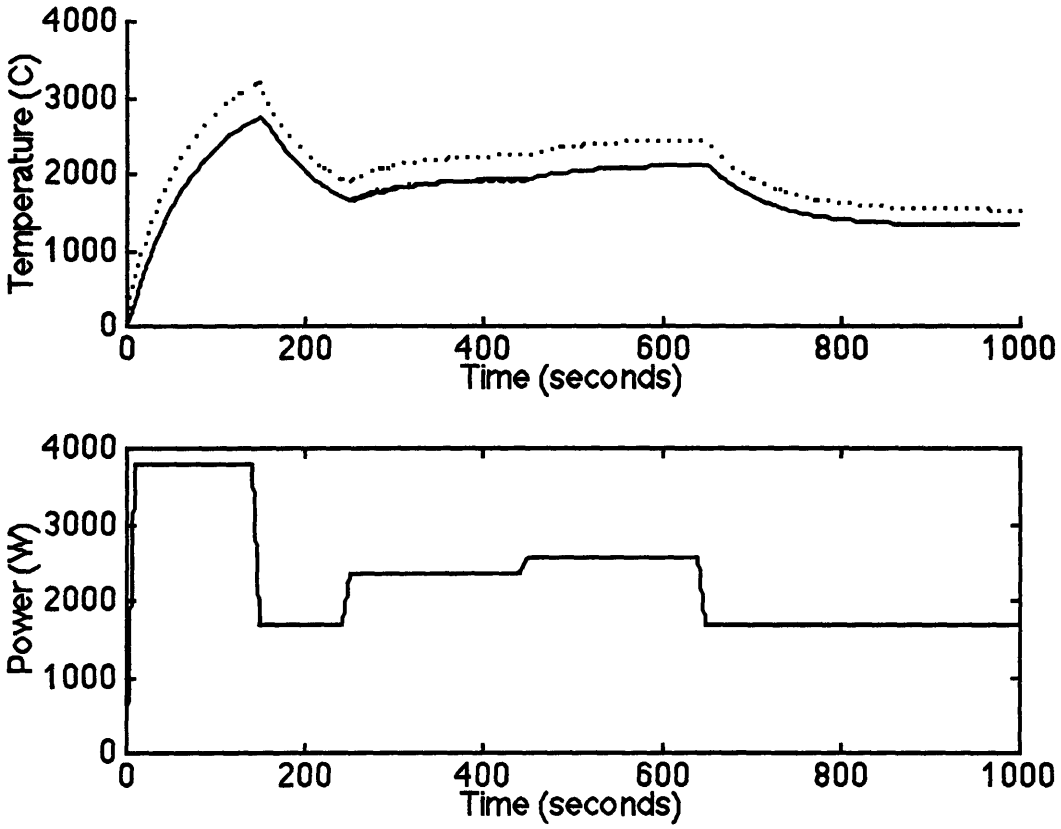

Figure E2: Temperature Response for Crucible and Molten Metal for a Molten Steel Mass of 50g

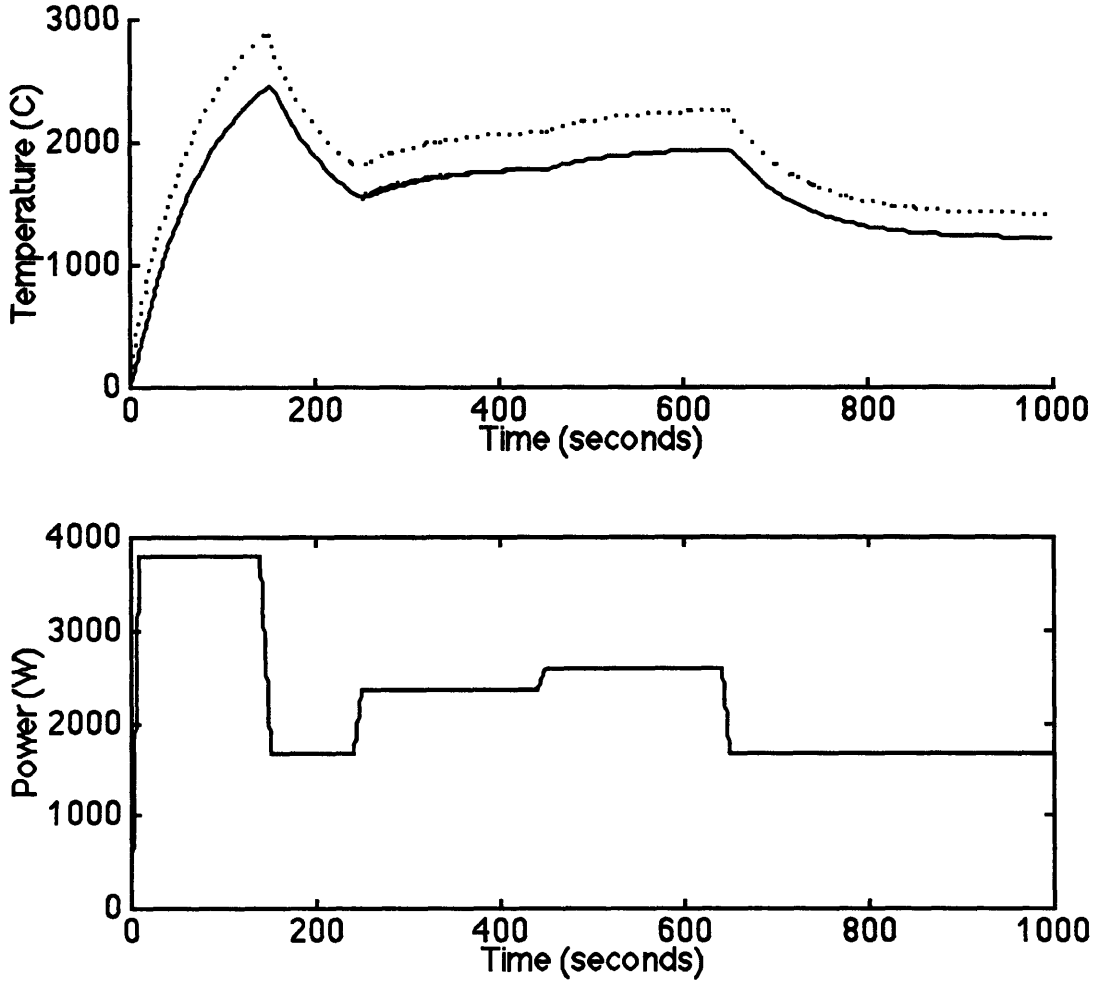

Figure E3: Temperature Response for Crucible and Molten Metal for a Molten Steel Mass of 80g

The value of K_a as a function of molten metal mass can be determined more easily with the coefficient C_4. The value of K_a is as follows:

$$K_a = \frac{h_1 A_s + h_2 A_2}{h_1 A_s h_2 A_2}$$

References

1 Avallone, E. A., Baumeister, I. Marks Standard Handbook for Mechanical Engineers, 9th Ed. McGraw-Hill, New York, NY. 1987.

2 Bowman, M. G. Fundamentals of Refractory Compounds. Plenum Press, New York, NY. 1968.

3 Campbell, I.E. High Temperature Materials and Technology. Wiley, New York, NY. 1967.

4 Data Translation. User Manual for DT2801. Data Translation Inc., Marlboro, MA. Document UM-00666-D-1855. 1985

5 Data Translation. PCLAB User Manual: Data Acquisition Subroutine Library. Data Translation Inc., Marlboro, MA. Document UM-02899-F. 1991.

6 Doumanidis, C.C. Modeling and Control of Thermal Phenomenon in Welding, PhD Thesis. Massachusettes Institute of Technology, February 1988.

7 Franklin, G. F., Powell, J.D., Workman M.L. Digital Control of Dynamic Systems, 2nd Ed. Addison-Wesley, Reading, MA. 1990.

8 Hale, M.B. Multivariable Dynamic Modeling and Control of GMAW Weld Pool Geometry Ph.D. Thesis. Massachusettes Institute of Technology, September 1989.

9 Horowitz, P., Hill, W. The Art of Electronics, 2nd Ed. Cambridge University Press, New York, NY. 1989.

10 Houldcroft, P.T. Welding Process Technology. Cambridge University Press, New York, NY. 1979.

11 Incropera, F. P., Dewitt, D.P. Introduction to Heat Transfer, 2nd Ed. Wiley, New York, NY. 1990.

12 Jones, L.A., Eagar, T.W., Lang, J.H., Investigations of Drop Detachment Control in Gas Metal Arc Welding. International Trends in Welding Science and Technology. ASM International, Materials Park, OH. 1993.

13 Kim, Y. Metal Transfer in Gas Metal Arc Welding Ph.D. Thesis. Massachusettes Institute of Technology, September 1989.

14 Lee, S. Development of a Continuous Flow Arc Furnace for Welding Applications, S. M. Thesis, Massachusettes Institute of Technology, September 1993.

15 Luxtron Corporation. Users Manual Accufiber Model 100C. Accufiber Division of the Luxtron Corporation, Beaverton, OR. 1990.

16 Masubuchi, K. Analysis of Welded Structures. Pergamon Press, New York, NY. 1980.

17 The Math Works. Simulink: Dynamic System Simulation Software. The Math Works Inc., Natick, MA. 1993.

18 Norrish, J. Advanced Welding Processes. IOP Publishing Ltd, New York, NY. 1992.

19 O'Brien, R. L. Welding Handbook, 8th Ed. American Welding Society, Miami, FL. 1991.

20 Ogata, K. Modern Control Engineering, 2nd Ed. Prentice Hall, Englewood Cliffs, NJ. 1990. pp. 595-598.

21 Samsonov, G. V. Plenum Press Handbook of High-Temperature Materials No. 2 Properties Index. Plenum Press, New York, NY. 1964.

22 Shaffer, P. T. Plenum Press Handbook of High-Temperature Materials No. 1 Materials Index. Plenum Press, New York, NY. 1964.

23 U.S. Department of Commerce. US Industrial Outlook . Bernam Press, Lanham, MD. 1993. pp. 16-8.